Ab Initio Calculations of Hydrocarbon Thermochemistry and Reaction Kinetics

Zur Erlangung des akademischen Grades eines

Doktors der Naturwissenschaften

(Dr. rer. nat.)

der Fakultät für Chemie und Biowissenschaften
der Universität Karlsruhe (TH)
vorgelegte

Dissertation

von
Licenciado en Ciencias Quimicas

Jorge Aguilera Iparraguirre

aus Zaragoza - Spanien

Dekan:
1. Gutachter: Prof. Dr. W. Klopper
2. Gutachter: Priv.-Doz. Dr. K. Fink
Tag der mündlichen Prüfung: 12/02/2009

I hear and I forget
I see and I remember
I do and I understand.

Confucius

I don't want to achieve immortality through my work
I want to achieve it through not dying.

Woody Allen

A mis padres, a mis madres, a mis hermanas y a mi hermano...

Contents

Chapter 1

Introduction

The present work has been carried out in the Sonderforschungsbereich (SFB) 551 "Carbon from the Gas Phase: Elementary Reactions, Structures, Materials" supported by the Deutsche Forschungsgemeinschaft (DFG). The idea of the full project is to be able to understand from the simplest chemical reaction of carbon in the gas phase until the last macroscopic property of the final solid product. In this context this work is just the first step in the process, being able to give plausible explanations for chemical reactions and at the same time provide data (usually in the form of reaction rate constants) for the next step to carry on. A good way to summarize the idea would be the question: How can we go from the most basic hydrocarbons to build complex polycyclic aromatic hydrocarbons (PAHs)? Many people have devoted many studies to answer this question, our task is to try to fill some of the gaps still remaining.

As the reader soon will see, very different techniques have been used in this work. The reason is simple, the questions being asked do not allow us to standardize. For example the size of the molecules involved varies dramatically, making impossible to use accurate methods when the molecule is too big, or from a different perspective, we can give highly accurate answers but then only for a few atoms.

We can divide the work in three main subjects. One deals with the exploration of different ways of building basic PAHs. For its very nature, relative big systems, density functional theory (DFT) has been used. In this case the problem

is not the size nor the technique, but the unknown space we are exploring, new reactions are proposed, calculated and discarded, in a process that ends up in the proposal of the most reasonable ones. The second topic would be, once that the reaction pathways are clear, to provide a reaction rate constant for the process. Finally, the determination of thermochemical properties at a very high accuracy for small hydrocarbons. All three steps get us closer to a better understanding of the overall process under study.

The content is organized as follows: Chapter 2 introduces the foundations of the theoretical tools employed while Chapter 3 tries to explain the transition state theory (TST) as a bridge between the raw theoretical data and the final rate constants. On the direct applications, Chapter 4 deals with the formation of naphthalene and phenanthrene in the way of PAH building. Chapter 5 presents the use of highly-accurate explicitly-correlated methodology on the calculation of atomization energies of different small hydrocarbons and Chapter 6 shows a detailed study for the kinetics of the hydroperoxyl radical in reaction with hydrocarbons. Finally, Chapter 7 extracts a few conclusions from the overall work.

Chapter 2

Foundations of Theoretical Chemistry

2.1 Introduction

During the development of this thesis we will encounter many problems, but all of them can be summarized in one: How can we obtain the properties of a given number of nuclei and the electrons associated with them? Around this simple question the field of quantum chemistry has grown. In 1926, Erwin Schrödinger suggested the equation that, with major or minor modifications, would allow us to answer the question. It is the non-relativistic time-independent Schrödinger equation[1]

$$\hat{H}\Psi = E\Psi \tag{2.1}$$

Where Ψ is the total wave function associated with our molecule, E is the total energy and $\hat{H}$ is the Hamiltonian, the operator that links both, having the following form

$$\hat{H} = \hat{T}_n + \hat{T}_e + \hat{V}_{ee} + \hat{V}_{nn} + \hat{V}_{ne} \tag{2.2}$$

Where $\hat{T}_n$ and $\hat{T}_e$ are the operators of kinetic energy of nuclei n and electron e, and $\hat{V}_{ee}$, $\hat{V}_{nn}$ and $\hat{V}_{ne}$ are the operators of potential energy for the electron-electron ee, nuclei-nuclei nn and nuclei-electron ne interactions. Here we can apply a vital simplification, the Born-Oppenheimer (BO) approximation,[2] that

suggests that the motions of nuclei are uncoupled with those of electrons. In a very visual analogy the system can be expressed as a cake with flies around. The flies would move so fast following a change in the position of the cake, that we can approximate this movement to be instantaneous. The assumption is reasonable due to the huge differences in mass between the cake and the flies, or between electrons and nuclei. The new formulation of the previous equations is now

$$\hat{H}_e \Psi_e = E_e \Psi_e \qquad \hat{H}_e = \hat{T}_e + \hat{V}_{ee} + \hat{V}_{ne} \tag{2.3}$$

The beauty of this approximation is clear, all the components in the Hamiltonian that depend only of the position of the nuclei, $\hat{T}_n$ and $\hat{V}_{nn}$, are not present here, and are treated as constants through integration. That is why now, after this step, we can rename our initial problem *the electron problem*. The BO approximation is particularly useful because it allows us to construct *potential energy surfaces*. As we will see in detail in the next chapter, they are energy surfaces whose only parameters are the coordinates of the nuclei, and include vital information on our system.

Now the bad news. Due to the presence of the element $\hat{V}_{ee}$ in our equations, which treats the interaction of electrons one with another at the same time interacting with the nuclei and the rest of electrons, the Schrödinger equation doesn't have an exact solution for systems with more than one electron.

2.2   Improving step by step

Since now we know that an exact solution for Eq. (2.3) is not possible, we face the choice of either approximating the wave function Ψ_e or the Hamiltonian $\hat{H}_e$. In this section we will deal with different approaches for the former solution.

First we should think how to construct the wave function. Since we are dealing with an N-electron wave function, we can define it to be the product of one-electron functions, known in this case as molecular orbitals ϕ_p, being the product of a spatial function $\varphi(r)$, depending on the three spatial coordinates, and a spin function $\sigma(s)$, that can be either α or β, corresponding to the two

orientations of the spin, up and down. With this we can construct the Slater Determinant (SD) of the form

$$
\text{SD} = \frac{1}{\sqrt{N!}}
\begin{vmatrix}
\phi_1(1) & \phi_2(1) & \cdots & \phi_N(1) \\
\phi_1(2) & \phi_2(2) & \cdots & \phi_N(2) \\
\vdots & \vdots & \ddots & \vdots \\
\phi_1(N) & \phi_2(N) & \cdots & \phi_N(N)
\end{vmatrix}
\tag{2.4}
$$

This formulation respects the antisymmetry of the wave function that corresponds to the fermionic nature of electrons, meaning that the sign of the function will change if we interchange two of them. On top of that, the antisymmetry produces the Pauli exclusion principle as a by product, two electrons cannot occupy the same spin orbital.

2.2.1 Hartree-Fock

The first step in our quest for a good solution of Eq. (2.3) is provided by the Hartree-Fock theory.[3–5] Our N-electron wave function has the shape of a SD and the energy associated will be the expectation value of the Hamiltonian, following

$$
E = \frac{\langle \Psi_e | \hat{H} | \Psi_e \rangle}{\langle \Psi_e | \Psi_e \rangle}
\tag{2.5}
$$

The solution for the Hartree-Fock wave function, known as Ψ_0, is the SD that minimizes the expectation value for the energy. A few consequences arise from the construction of our wave function. First, since Ψ_0 is an approximation to the real Ψ_e, the calculated value of the energy will always be higher, according to the variational principle, than the real one, forming an upper bound. Second, the construction of every molecular orbital in the SD depends on all the rest of them. This means that when one is modified to improve our result, the rest have to be modified as well to adapt. This happens in a iterative procedure, that only ends when all molecular orbitals are consistent with one another. That is why this method is known as *self-consistent-field* (SCF). The last consequence is related with the electron-electron interaction. In this method a single electron, will only modify its behavior against the average interaction with the rest. We know this to be untrue, electrons react to the close presence of others, making the average

distance between them much larger than calculated here. This effect, since it links the response of the electrons, is known as *correlation* and it is defined

$$E_{correlation} = E_{exact} - E_{SCF} \tag{2.6}$$

Our following step will be to try to recover part of this energy.

2.2.2   Configuration interaction (CI)

We can improve our wavefunction by expanding it using a linear combination of N-electron basis functions corresponding to different determinants. This procedure is known as Configuration Interaction.[6] The determinants are created taking as a starting point our Hartree-Fock determinant and exciting electrons into virtual orbitals. We can create new determinants with single (S), double (D), triple (T),... excitations, depending of the number of electrons promoted. We can then define the operator $\hat{T}$ that generates all the new N-basis functions as

$$\hat{T} = 1 + \hat{T}_1 + \hat{T}_2 + \cdots + \hat{T}_N \tag{2.7}$$

If we perform all possible excitations, the method is known as full-CI (FCI), but it is common to truncate our expansion at a certain number of electrons excited: S,D,T,... . This creates a family of methods depending of the extend of the truncation: CISD, CISDT,... . The higher the excitations, the lower the effect on the final result, so we will have to decide at what level of truncation we obtain the desired accuracy. Now that we have the approximate wave function of the form

$$\Psi = \hat{T}\Psi_0 \tag{2.8}$$

We can proceed with the variational minimization, has it has been shown before.

2.2.3 Coupled clusters (CC)

In principle the coupled cluster approach[7] does not look much different from the previous method, CI. We just change the expression of the operator that generates the new determinants, now in an exponential form

$$\exp(\hat{T}) = 1 + \hat{T}^1 + \frac{1}{2}\hat{T}^2 + \frac{1}{3!}\hat{T}^3 + \cdots \tag{2.9}$$

yielding our wave function

$$\Psi = \exp(\hat{T})\Psi_0 \tag{2.10}$$

In practice the differences are very important. For a given truncation of our expansion, for example including singles and doubles, in CC theory we will have factors like $\hat{T}_1\hat{T}_2$ or $\hat{T}_2\hat{T}_2$, that include, indirectly, higher excitations. These are known as disconnected clusters. We can see the difference between a connected cluster like $\hat{T}_4$ representing the simultaneous interaction of four electrons, and the disconnected term $\hat{T}_2\hat{T}_2$ representing the simultaneous excitation of two independent pairs of electrons. Unfortunately, a variational formulation is difficult in this case, so non-variational techniques are used instead. As in CI, a family of truncated methods are available: CCSD, CCSDT,.... Of particular interest is the method noted as CCSD(T) where the calculation of the triples, T, is not included in the normal CC procedure, but it is obtained instead using perturbation theory on the CCSD wave function.[8]

2.3 The last step. Basis set

Until now we have started all our discussions from the molecular orbitals φ_p, but now we should go back and see how these orbitals are constructed. The general approach is to construct them using atomic basis functions χ_μ

$$\varphi_p = \sum_\mu c_{\mu p}\chi_\mu \tag{2.11}$$

Where the index μ is summed over the number M of atomic basis functions and the prefactors $c_{\mu p}$ are called expansion coefficients. This strategy is known as linear combination of atomic orbitals (LCAO). Note that, since the number M

is in reality finite, we encounter here a second source of error in our development (the first being the different methods to approximate Ψ). Each basis function is composed of a radial part $R(r)$ and an angular part $Y(\theta, \phi)$, where r, θ and ϕ denote polar coordinates.

$$\chi_\mu = R(r)Y(\theta, \phi) \tag{2.12}$$

Two types of atomic basis functions have been used predominantly to describe the radial part $R(r)$: Slater type orbitals (STOs) and Gaussian type orbitals (GTOs)

$$f_{STO}(r) = \exp(-\xi r) \qquad f_{GTO}(r) = \exp(-\xi r^2) \tag{2.13}$$

It would appear that the STOs should be preferentially used, since they have the correct shape and behavior for both $r = 0$ and $r = \infty$ (with the exception of a too slow drop off if the exponent is too small), and in that direction were all the first developments. The big disadvantage is that STOs cannot be analytically integrated in many-center two-electron integrals, so they are very difficult to work with. On the other hand, a GTO doesn't have the proper behavior, but has the nice property that a product of two Gaussians is still a Gaussian function, and so they are the most commonly used basis functions nowadays. Nevertheless, since a single GTO doesn't reflect the right shape of the orbital we will need several to simulate the right function. The more functions there are, the better the similarity.

2.3.1   Extrapolation

The fact that the size of our basis set is finite opens up a dilemma. The bigger the number of basis functions, the closer to the basis set limit (that is the result that would be obtained with an infinite number of functions) we get. On the other hand the bigger the number of functions the greater our computational cost grows. Several families of basis sets have been designed trying to obtain a systematic behavior with respect to their size. Two features are desirable. One, that the convergence is smooth, that is, that we get closer and closer to the limit with corrections of the same sign, and second, that the first members of the family should recover the biggest part of the error, with the new functions

added recovering less and less. A good example of this concept is the cc-pVXZ (being X the cardinal number with values D, T, Q, 5, 6,...) basis set developed by Dunning.[9] We can see the amount of functions that form each level in Tab. 2.1

Table 2.1: Dunning-type correlation-consistent basis set cc-pVXZ. X goes from D to 6. Square brackets mean contracted functions.

Cardinal number	Functions
D	[3s,2p,1d]
T	[4s,3p,2d,1f]
Q	[5s,4p,3d,2f,1g]
5	[6s,5p,4d,3f,2g,1h]
6	[7s,6p,5d,4f,3g,2h,1i]

A very useful property of this basis set family is that the correlation energy that they recover not only converges smoothly but also follows approximately an X^{-3} dependence with respect to the cardinal number.[10,11] This allows us to perform two calculations in two consecutive cardinal numbers and approximate the basis set limit following the equation

$$E_\infty^{(X-1)X} = \frac{X^3 E^X - (X-1)^3 E^{(X-1)}}{X^3 - (X-1)^3} \tag{2.14}$$

2.3.2 Explicitly-correlated wave functions and R12 theory

Tricks like the one employed in the previous paragraph are very useful to solve the problem of the very slow convergence of correlation energy with the number of atomic basis function used. Now we should ask why this convergency is so slow? The problem is that we are trying to calculate the interaction between the electrons. For example, the probability for one of them to be in the vicinity of another will be low, it will be repelled, creating around it what is known as Coulomb hole. However, we attempt to describe it using functions centered at the atoms. For these functions it is very difficult to properly describe the shape of this non-atom centered hole, and thus we have to add many functions to get close to the limit. A possible solution would be to include directly in the wave

function a factor depending on the inter-electronic distance r_{12}, hoping that this will describe the shape of the Coulomb hole properly for a much smaller number of atomic functions, and thus recovering a given amount of correlation energy at less computational cost. In 1929, Hylleraas introduced this model successfully for the helium atom.[12] However the development of this methodology was slow due to several factors. First, due to the inclusion of the new factor, previous basic concepts in the field such as orbitals, had to be modified. Second and most important, the new three and more electron integrals made it computationally very difficult to handle. The first practical methods have been introduced in the last two decades, consisting on the inclusion of a linear factor r_{12} and therefore denoted R12 methods. Until now they have been extended in the framework of Mller-Plesset (MP, another post-Hartree-Fock methodology not detailed here) and CC, and a big part of the work was performed by Kutzelnigg, Klopper and Noga, among others.[13–17] The idea is to add to the conventional N-electron configuration space a supplementary set of functions Ω_{ij} of the form

$$\Omega_{ij}(1, 2, \ldots, N) = \hat{A}(\hat{Q}_{12} r_{12} \phi_i(1) \phi_j(2) \ldots \phi_l(N)) \tag{2.15}$$

Where $\hat{A}$ is an antisymmetrization operator. A projection operator $\hat{Q}_{12}$ is applied to remove all contributions to Ω_{ij} from singly excited determinants (within and beyond the finite basis set) and doubly excited determinants within the finite basis. If $\hat{F}_2$ represents the operator that creates the set of the new r_{12} dependent terms, the cluster operator, analog to Eq. (2.7), is

$$\hat{T} = 1 + \hat{T}_1 + \hat{T}_2 + \hat{F}_2 + \hat{T}_3 + \cdots + \hat{T}_N \tag{2.16}$$

The great achievement of this procedure was the inclusion of the resolution of the identity to reduce the difficult three-and-more-electron integrals to simple products of two-electron integrals. This requires a basis set close to completeness to be valid, but the great advantage is that all integrals can readily be solved analytically.

2.4 Anything else?

There are a few subjects that should not be forgotten. Even though they make the standard theory a bit more complicated, they are indispensable when

dealing with real molecules to high accuracy.

2.4.1 An odd number of electrons

Until now we have not specified whether our orbitals are filled with two electrons with an identical spatial function, and that differ only in the spin direction. It is true that a large number of molecules have an even number of electrons in a singlet occupation, but when dealing with reactions we encounter all kinds of molecules with an even or odd number of electrons, in singlet, doublet, triplet,... occupations. We have to find a way to deal with all of them. The first approach is the one we already know. Two electrons that share the spatial part and have opposite spins (denoted α and β). This is known as *Restricted* (R) method.

$$\varphi_k^\alpha = \varphi_k(r)\alpha \tag{2.17}$$

$$\varphi_k^\beta = \varphi_k(r)\beta \tag{2.18}$$

The interesting thing is that this method satisfies the two following relations

$$\hat{S}^2\Psi = S(S+1)\Psi \tag{2.19}$$

$$\hat{S}_z\Psi = M_s\Psi \tag{2.20}$$

That is, the wave function is an eigenfunction of the spin operators, $\hat{S}^2$ and $\hat{S}_z$, as an exact wave function for a many-electron system must. When an odd number of electrons is treated, an orbital will be filled with an α electron, without the β counterpart. This includes some mathematical problems, but the principles, and more important the properties, remain. The method is known as *Restricted Open* (RO). Another possibility is to allow the orbitals with different spins to have different spatial parts, leading to the following equations, analogous to Eq. (2.17) and Eq. (2.18)

$$\varphi_k^\alpha = \varphi_k^\alpha(r)\alpha \tag{2.21}$$

$$\varphi_k^\beta = \varphi_k^\beta(r)\beta \tag{2.22}$$

This is known as *Unrestricted Open* (U), since now the spatial part of the α and β electron in one orbital is not forced to be the same. This method

doesn't fulfill Eq. (2.19) anymore, and therefore lacks desirable properties in the wave function, on the other hand its flexibility allows us to treat bond-breaking problems, even if the underlying physics are dubious.

2.4.2 Core correlation

In all our previous methodologies, only the electrons that belong to the valence space have been included for correlation treatments. It is a very sensible approximation since one would assume that the electrons in the core would be unaffected through all our processes, indeed that is why we call them core! Only when we intend to achieve high accuracy does this core-valence correlation (CV) play an important role. We will then have to include all the electrons in our molecule in the correlation treatment with a large computational cost associated. An important note is that usual basis sets are designed for valence correlation only treatments, and are commonly not suitable for an all-electron one, making the choice of a suitable basis a very important task.

2.4.3 Relativistic effects

Another effect that has been conscientiously ignored since line 1 in this chapter is the effect of relativity in our wave function, beyond that of the presence of electron spin coordinates. We have assumed that the electrons in our molecules are going slowly enough to be treated non-relativistically. This assumption has two major exceptions. First, when we deal with transition metals the inclusion of some sort of relativistic treatment is a must. Second, when the level of accuracy is so high that even the small effects in light elements cannot be neglected. The problem is that Dirac's relativistic formulation of the Schrödinger equation transforms a simple one component wave function into a four component beast. Several approaches have been proposed, and it is important to see what the physical effects they try to describe are. The three most important terms are: The *mass-velocity*, is the affect on the mass of the particle due to its speed. The *spin-orbit coupling*, that takes into account the interaction between the orbital magnetic moment, coming from the orbital motion of the charge, and the spin magnetic moment of the electron, and finally the *Darwin* term, that can be considered as the change in the effective potential at the nucleus, due to the effect on

the electrostatic interaction between the electron and nucleus produced by rapid quantum oscillations of the electron in the relativistic framework.

2.5   Density functional theory (DFT)

In every attempt to explain the fundamental developments in quantum chemistry there is always a part dedicated to Density Functional Theory. It is interesting to observe that, unlike with the Hartree-Fock and its posterior developments seen in the previous sections, different authors find different places to explain it. It seems there is no consensus according where to put it, and that is explained with its particular history. It is a difficult relationship, people doubt about the accuracy, inability to check that accuracy, theoretical foundations,... but we massively, more than with any other method, use it. We will try to explain the basic ideas.

The main concept is: Why use the wave function as a base for our calculations, that depends on 4N variables and not use the electron density $\rho(r)$ that has both the advantages of being an observable and depending only on three spatial variables?

$$\rho(r) = N \int \ldots \int |\Psi|^2 ds_1 dx_2 \ldots dx_N \qquad (2.23)$$

The beauty of the idea was already seen and used in the 20's by Thomas and Fermi,[18,19] but it was not until the 60's when it got a major push.

2.5.1   Hohenberg-Kohn theorems

In 1964, two theorems built the foundations of the theory.[20] The first one says

"The external potential $v_{ext}(r)$ is a unique functional of $\rho(r)$. Since, in turn $v_{ext}(r)$ fixes $\hat{H}$, we see that the full many particle ground state is a unique functional of $\rho(r)$".

In other words, the density $\rho(r)$ determines every property of the system, including the total energy. In the case of a molecule, the external potential $v_{ext}(r)$

is determined by the positions and charges of the nuclei, so the total energy can be written

$$E_0[\rho] = T[\rho] + V_{ee}[\rho] + V_{Ne}[\rho] = F_{HK}[\rho] + \int \rho(r)v_{ext}(r)d^3r \tag{2.24}$$

Where $F_{HK}[\rho]$ contains the electronic kinetic energy $T[\rho]$ and the potential energy due to the repulsion between electrons, while the nuclei-electron attraction $V_{Ne}[\rho]$ is expressed in terms of $v_{ext}(r)$. The functional $V_{ee}[\rho]$ can be divided into two contributions. The first being the classical Coulomb energy of a charge distribution with itself $J[\rho]$, and the second containing the non-classical exchange-correlation energy $E'_{xc}[\rho]$. The second theorem is analogous to the variational principle seen before, and goes

"For a trial density $\tilde{\rho}$, such that $\tilde{\rho} \geq 0$ and $\int \tilde{\rho} \, d^3r = N$, $E_0 \leq E[\tilde{\rho}]$, where $E[\tilde{\rho}]$ is the energy functional of Eq. (2.24)".

These two theorems, while providing very important foundations for the theory, don't give us any information about the functional itself, or how it should be constructed.

2.5.2   Kohn-Sham equations

The basic concept, introduced in 1965,[21] is that we can construct a model with N non interacting electrons in N orbitals ϕ_i to built a Slater determinant with a kinetic energy associated

$$T_s = -\frac{1}{2}\sum_i^N \left\langle \phi_i | \nabla^2 | \phi_i \right\rangle \tag{2.25}$$

The functional $F_{HK}[\rho]$ is

$$F_{HK}[\rho] = T_s[\rho] + J[\rho] + E_{xc}[\rho] \tag{2.26}$$

Where $E_{xc}[\rho]$ includes all non-classical effects and the difference in kinetic energy between the real and the reference system. Finally, we can construct the Kohn-Sham equations

$$[-\frac{1}{2}\nabla^2 + \int \frac{\rho(r')}{|r - r'|}d^3r' + V_{xc} + V_{ext}]\phi_i = \varepsilon_i\phi_i \qquad (2.27)$$

And in these equations lies the success of the method. They necessarily resemble the previously seen Hartree-Fock equation, so all the machinery already available could be easily modified to be used with the new theory.

2.5.3   Functionals

It should be clear by now, that the main problem in the quest for a reasonable functional is located in the exchange-correlation term $E_{xc}[\rho]$. This is not surprising since we have thrown in it all the problematic parts. During the last decades several attempts to give a form to this functional have been tried. The first, called *local density approximation* (LDA), based on a model system composed of the uniform electron gas, leads to the following expression

$$E_{xc}^{LDA} = \int \rho(r)\varepsilon(\rho(r))d^3r \qquad (2.28)$$

Even though a very interesting first attempt, still widely used nowadays, for example with transition metals, it is clear that the uniform electron gas is just a very raw and unrealistic approximation since in molecules electrons experience a varying density. The next step to improve upon LDA functionals, was to include a dependency on the gradient of $\rho(r)$ leading to the *generalized gradient approximation* (GGA)

$$E_{xc}^{GGA} = \int f(\rho(r), \nabla\rho(r))d^3r \qquad (2.29)$$

The final, until now, step in the ladder is to include the kinetic energy density in the expression of E_{xc}. This has created the family of the *meta-generalized gradient approximation* (meta-GGA) functionals. Outside this traditional ladder a very successful group of functionals, called *hybrid*, include a certain amount of exact Hartree-Fock exchange. Since the amount of exchange to be included is arbitrary, it requires an *a priori* tuning. All together DFT has proven to be a very successful technique, and several different functionals have been created, some using *a priori* knowledge in form of exact constrains to determine coefficients, and some with different fittings to reproduce satisfactorily several molecular properties.

2.6   Software

At the beginning of every chapter, the methodology and the program packages used to apply that methodology will be specified in large detail. Nevertheless this section shall show the guidelines of the software usage.

All DFT calculations have been performed using the Turbomole package,[22] with special attention to the Freeh module for thermochemical properties. Post-Hartree-Fock calculations were carried out with help of the Mainz-Austin-Budapest version of Aces II[23] and Molpro,[24] with Dirccr12-os[25] for the explicitly-correlated problems. Gaussian[26] has been run for literature comparison as it will be later detailed. Other minor contributions will be specified when needed.

Chapter 3

Potential Energy Surfaces (PES)

In the previous chapter we have shown different approaches to obtain the energy value associated to a given point in the coordinate space, but if we plan to study in detail a given molecule and its reactivity, this is not enough, and we will have to explore a broader spectrum of the full space. The function that links the energy of our system with the spatial coordinates of its parts is known as *Potential Energy Hypersurface*. This surface gives us all the information about our system, under the Born-Oppenheimer approximation, for example we can locate points of special interest or find the path that links different points.

3.1 The optimization problem

The first important data that we can extract are the locations of the minima on the surface, this will give us the information about what are the geometry parameters of our molecule, or in case of a chemical reaction, where are located reactants and products. We can define our potential energy surface (PES) as a function $f(\mathbf{x})$, so for a given point $\mathbf{x}_p$ to be a minimum the following conditions have to be fulfilled: The first derivative of the function, known as gradient $(\mathbf{g}_p)$ has to be zero and the second derivative, known as Hessian $(\mathbf{H}_p)$ must have only positive eigenvalues. They are defined by

$$\mathbf{g}_p = \nabla f(\mathbf{x}_p) = \begin{bmatrix} \frac{\partial f}{\partial x_1} \\ \vdots \\ \frac{\partial f}{\partial x_n} \end{bmatrix} \tag{3.1}$$

$$\mathbf{H}_p = \nabla^2 f(\mathbf{x}_p) = \begin{bmatrix} \frac{\partial^2 f}{\partial x_1 \partial x_1} & \cdots & \frac{\partial^2 f}{\partial x_1 \partial x_n} \\ \vdots & \ddots & \vdots \\ \frac{\partial^2 f}{\partial x_n \partial x_1} & \cdots & \frac{\partial^2 f}{\partial x_n \partial x_n} \end{bmatrix} \tag{3.2}$$

Now that we know the properties that define a minimum we can take advantage of them and devise strategies to find it from a given point. Before going into detail we should note a few things: Only for the simplest cases we will have a single minimum, for systems with several atoms the number of minima corresponding to the different conformations of the system can be very big. This is important because the methods that we will now discuss are designed to find a minimum when the starting point is reasonably close to the final one. However, if several minima are present, we will need different methods to obtain them all, in case we are interested in them. Applying the common analogy of the *"mountain-valley"* to describe our PES, we will find the closest lowest point of a valley from every place of that valley, but we cannot expect the same result if we start in the next valley. Another important point is that, since we don't have an analytical expression for the function defining our surface, the stopping point, the decision about what we call a minimum will be based on a numerical threshold, so we will have to decide at what accuracy we want to obtain it.

3.1.1   Linear model

The simplest model is not particular useful, but will allow us to show the steps that a minimization has to follow. The idea is that wherever we are on the PES, we check in which direction the energy decreases faster, that is to say, in which direction the gradient is bigger, and will follow that direction, repeating the procedure at certain steps. The mathematical formulation is

$$M_L(\mathbf{x_p} + \mathbf{s}) = f(\mathbf{x}_p) + \mathbf{g}_p^T \mathbf{s} \tag{3.3}$$

where the step $\mathbf{s}$ is defined by

$$\mathbf{s} = \mathbf{x} - \mathbf{x}_p \tag{3.4}$$

and $\mathbf{g}_p$ is the gradient of the function at a given point as we have defined before. So the overall procedure will look like this

1. Calculate the energy E_p of the starting point $\mathbf{x}_p$.

2. Compute the first derivative, $\mathbf{g}_p$ for the given point.

3. Get the next point $\mathbf{x}_{p+1}$. In this case, we will have to decide how big our step is going to be.

4. Calculate the energy for the new point E_{p+1}.

5. Have we reached convergence? (We can define it with respect to the gradient, energy, coordinate,...). When no, go back to 2.

3.1.2 Quadratic model

The biggest problem with the linear model is that it does not use any information about the curvature of the function $f(\mathbf{x}_p)$. This information is contained in the Hessian-matrix $\mathbf{H}_p$. In this case, the minimization function can be formulated in this way

$$M_Q(\mathbf{x}_p + \mathbf{s}) = f(\mathbf{x}_p) + \mathbf{g}_p^T \mathbf{s} + \frac{1}{2}\mathbf{s}^T \mathbf{H}_p \mathbf{s} \tag{3.5}$$

We solve this equation to find the stationary points and obtain

$$\mathbf{H}_p \mathbf{s} = -\mathbf{g}_p \tag{3.6}$$

which leads to a unique solution

$$\mathbf{s} = -\mathbf{H}_p^{-1}\mathbf{g}_p \tag{3.7}$$

If the exact Hessian has been used, the method is known as *second-order model* since it is the second-order Taylor expansion of the function around $\mathbf{x}_p$.

The step $\mathbf{s}$ is then known as *Newton-Raphson* step. The advantages are clear. First, $\mathbf{s}$ is defined *a priori*, we don't have to provide it. Second, the convergence is quadratic. On the other hand to compute the exact Hessian in every step is computationally very demanding. For this reason, there is a variety of the *Newton-Raphson* method which uses an approximate Hessian. They are known as *quasi-Newton* methods. There are several ways to construct the approximate Hessian depending on the properties that we want from it. One problem of all these methods is that they are unbounded, that is that $\mathbf{s}$ can take any value. Since our model is just an approximation, we can expect that it is only good sufficiently close to our point $\mathbf{x}_p$. To force that we don't go to far away from it, we can impose a so called *trust region* in this way

$$\mathbf{s}^T\mathbf{s} \leq h^2 \tag{3.8}$$

This procedure is particularly useful when we are dealing with complicated surfaces (very shallow).

3.1.3   Trust region image minimization

Until now we have focused on the location of minima on the PES, but as we will see in the next section, there are other points of interest. They are the ones where the gradient is zero and in which the eigenvalues of the Hessian-matrix one and only one has a negative curvature, that is, this point is a minimum in all coordinates except in one, in the case of our molecule reacting, that coordinate is the reaction coordinate that links the reactants with the products. This point is know as first order saddle point for a general function, and transition state for our PES.

We can easily see that to find a first order saddle point has to be more complicated than a minimum. First of all, it is not easy to find a good starting point, sufficiently close to the final one. Most of the time this requires a lot of chemical intuition about the properties of our system, only acquired with experience, that is why it has been said, that the finding of transition states is more an art than a technique.

A beautiful approach, called trust region image minimization (TRIM),[27, 28] has been devised using the following procedure. If we have a function $f(\mathbf{x})$ with the gradient $\mathbf{g}(\mathbf{x})$ and the eigenvalues of the Hessian-matrix $\boldsymbol{\lambda}(\mathbf{x})$ at a certain point $\mathbf{x}$ of the form

$$\mathbf{g}(\mathbf{x}) = \begin{bmatrix} \phi_1(\mathbf{x}) \\ \phi_2(\mathbf{x}) \\ \vdots \\ \phi_n(\mathbf{x}) \end{bmatrix} \qquad \boldsymbol{\lambda}(\mathbf{x}) = \begin{bmatrix} \lambda_1(\mathbf{x}) \\ \lambda_2(\mathbf{x}) \\ \vdots \\ \lambda_n(\mathbf{x}) \end{bmatrix} \tag{3.9}$$

Then we can create an image function $\bar{f}(\mathbf{x})$ that will have the following gradient and eigenvalues

$$\bar{\mathbf{g}}(\mathbf{x}) = \begin{bmatrix} -\phi_1(\mathbf{x}) \\ \phi_2(\mathbf{x}) \\ \vdots \\ \phi_n(\mathbf{x}) \end{bmatrix} \qquad \bar{\boldsymbol{\lambda}}(\mathbf{x}) = \begin{bmatrix} -\lambda_1(\mathbf{x}) \\ \lambda_2(\mathbf{x}) \\ \vdots \\ \lambda_n(\mathbf{x}) \end{bmatrix} \tag{3.10}$$

Now we see that in this diagonal representation, the image function $\bar{f}(\mathbf{x})$ is equal to $f(\mathbf{x})$ except for the sign of the first mode. This implies that the first order saddle point that we are looking for is just the minimum for the image function. We can apply now the quadratic model to obtain that minimum.

3.2   Transition state theory

Until now it has been shown how to obtain the energies associated to a molecule in a certain configuration and how to obtain the minima and saddle points that are present in the coordinate space of that molecule. But our final goal would be to finally produce an expression showing reaction rates of conversion from reactant to product. The classical form of the Arrhenius expression is widely used as a way to present these data, since the plot of $k(T)$ vs. $1/T$ is usually linear, and it is purely empirically derived.

$$k(T) = A \cdot \exp(-E_a/RT) \tag{3.11}$$

Or the more recent form including T^n dependence on the temperature, known as pseudo-Arrhenius expression

$$k(T) = A \cdot T^n \cdot \exp(-E_a/RT) \tag{3.12}$$

Where E_a is know as the activation energy and A as pre-exponential factor. These expressions were derived experimentally and are the common way to express reaction constants for example when they are used in the construction of complex chemical models.

To obtain the reaction constants we will introduce the Transition State Theory (TST). Proposed in the early 30s by Eyring and Polyani[29,30] it introduces the key concept of Transition State (TS). The basic idea is that there is a point in the PES called TS, which is in quasi-equilibrium with the reactants and its formation limits the reaction rate. In other words, the amount of energy needed to reach the highest point on the lowest path between two valleys would give us the speed for going from one to the other. This theory is not only extremely simple, but also very useful since it uses the well know equilibrium thermodynamics and it reduces our work on the PES to just two areas: Our minimum for the reactants and the Transition State. To obtain this simplicity we must do some assumptions that may, or may not, represent the reality.[31–33]

- There is a Transition State in our PES that divides the space in two regions, reactants and products, and the trajectories that cross it in one direction they do it only once. For obvious reasons it is known as *not-recrossing* postulate.

- The degree of freedom corresponding to the reaction coordinate (the one that links reactants and products trough the Transition State) can be separated from the rest and be treated as a classical translation.

The expression for a bimolecular reaction $X + Y \rightarrow XY^{\ddagger}$ is

$$k(T) = \kappa \cdot V_m \cdot \frac{k_B T}{h} \cdot \frac{Q^{XY^{\ddagger}}}{Q^X Q^Y} \cdot \exp\left(\frac{-\Delta E_{B,0}}{RT}\right) \tag{3.13}$$

Where $Q^{XY^{\ddagger}}$, Q^X and Q^Y are the dimensionless partition functions (including translational, vibrational and rotational contributions) of the TS (the corresponding degree of freedom of the reaction coordinate has been removed) and the reactants, respectively. R is the gas constant, k_B is the Boltzmann constant, h is

the Planck constant, and V_m is the molar volume of an ideal gas at temperature T. $\Delta E_{B,0}$ is the barrier height. κ is the transmission coefficient accounting for tunneling effects. We will analyze now some of the terms included.

3.2.1 Zero point vibrational energy

If we were treating our molecule as an oscillator with classical mechanics we could have it at perfect rest. Since we use quantum-mechanics to get a closer picture of reality, our oscillator is always in motion. The small residual motion at absolute zero temperature is the *zero-point vibrational energy* (ZPVE). For a simple harmonic oscillator the ZPVE is half the vibrational frequency, giving the overall expression

$$\text{ZPVE} = \frac{1}{2} \sum_{i=1}^{3N-6} h v_i \tag{3.14}$$

Where N is the number of atoms in the molecule and v_i the fundamental vibrational frequencies. There are $3N - 6$ vibrations in a non-linear molecule and $3N - 5$ in a linear one, so the previous equation is valid for the non-linear. In the case of a TS, one of the fundamental modes have been removed, leaving only $3N - 7$ vibrations, for a non-linear case, to be included. This treatment uses harmonic oscillators, the real molecular vibration are slightly anharmonic, but are approximated as harmonic. There are several approaches to take into account these anharmonic effects.

Finally, the ZPVE is added to the energy obtained from some *ab initio* method, to obtain the energy corresponding to absolute zero. In the case of our TST formulation we have that the barrier height is defined by

$$\begin{aligned}\Delta E_{B,0} &= \Delta E_{B,e} + \text{ZPVE}_{Total} \\ &= E_{XY^{\ddagger},e} - E_{X,e} - E_{Y,e} + \text{ZPVE}_{XY^{\ddagger}} - \text{ZPVE}_{X} - \text{ZPVE}_{Y}\end{aligned} \tag{3.15}$$

Where $\Delta E_{B,e}$ is the *electronic* barrier.

3.2.2   Partition functions

The problem we are facing is how to convert our molecular energy levels ε_i into macromolecular thermodynamic properties that, starting with the pseudo-equilibrium between our reactants and the transition state, would lead to the reaction rate. We can achieve that with help of the *partition functions*. A simple, but precise, definition is that these functions determine how particles distribute themselves over accessible quantum states, hence the name. The general formulation is

$$q = \sum_i \exp\left(\frac{-\varepsilon_i}{RT}\right) \tag{3.16}$$

Now we have to turn to our molecule and see in which way can it distribute energy. There are four: Translational, rotational, vibrational motions and electronic excitation. It would be very desirable if we could assume that the energy modes are separable meaning that each one is independent of the others, so we could write the expression

$$q_{tot} = q_{trans} \cdot q_{rot} \cdot q_{vib} \cdot q_{elec} \tag{3.17}$$

This is true for the translational mode, and it can also be applied to the rest under some assumptions. The rotational modes are independent from the vibrational modes under the rigid rotor assumption, and are also independent of the electronic ones under the Born-Oppenheimer approximation, described in the previous chapter. All together this means that a molecule that moves very fast, doesn't have, as a consequence, to rotate or vibrate rapidly. This means that we can treat them separately.

3.2.2.1   Translational partition function

In classical mechanics, all kinetic energies are allowed in a system for a fixed volume and temperature T. When quantum mechanics is used, some restrictions appear to the possible kinetic energies. Using the simple model of a particle in a box, we end up with the approximate equation

$$q_{trans} = \left(\frac{2\pi m k_B T}{h^2}\right)^{\frac{3}{2}} \cdot V \tag{3.18}$$

where m is the mass of the particle and V the volume of the box.

3.2.2.2 Rotational partition function

The rotation of a rigid molecule is also quantized, so the rotational energy is restricted to certain discrete levels. We can define the characteristic rotational constants of the system A, B and C of the form

$$A = \frac{h}{8\pi^2 I_A} \qquad B = \dots \qquad (3.19)$$

Being I_A, I_B and I_C the principal moments of inertia with respect to the axes $\vec{A}, \vec{B}$ and $\vec{C}$, respectively. Leading to the final expression

$$q_{rot} = \left(\frac{k_B T}{h}\right)^{\frac{3}{2}} \cdot \left(\frac{\pi}{A \cdot B \cdot C}\right)^{\frac{1}{2}} \qquad (3.20)$$

Note that the usual reference to the symmetry number σ has been omitted since it will be treated in further detail when the appropriate examples are brought into play.

3.2.2.3 Vibrational partition function

The energy level spacing in the vibrational modes are larger by, at least, an order of magnitude than those in rotational modes, that means that they cannot be simplified in a continuum treatment. The value of the partition function is then the product of all the vibrational frequencies v_i to get the expression

$$q_{vib} = \prod_i \frac{1}{1 - \exp\left(\frac{-hv_i}{k_B T}\right)} \qquad (3.21)$$

3.2.2.4 Electronic partition function

The electronic partition function only plays a role through degeneracy of the ground state or when an electronic first excited state is close enough to the ground state to have a representative level of population. In our case this will take place only with the presence of doublets. Since, then, they will be present both in a reactant and in the TS they cancel out, so q_{elec} will not be considered any further.

3.2.3   Internal rotations

Until now, the degrees of freedom corresponding to vibrational modes have been included in the respective partition function using the harmonic approximation. This may be reasonable most of the times, but it causes discrepancies especially when weak torsional modes take place, leading to some extremely low vibrational modes that, when treated as harmonic oscillator, induce a big error in the final partition function. Several approaches have been adopted to correct this problem depending on the value of the barrier for the given rotation. If the value of the barrier is particularly small we can substitute the vibrational mode by a free rotor without inducing a big error. There is, nevertheless a big range where the mode is not completely a free rotor but is not an harmonic oscillator either. That is why these modes are called *Hindered Internal Rotations* (HIR).

A possible way to treat these rotations, developed by Vansteenkiste *et al.*[34] would follow, for a corrected q_{vib}, the equation

$$q_{vib,corr} = \underbrace{\prod_{i=1}^{N(harm)} q_{i,harm}}_{q_{vib,harm}} \cdot \prod_{j=1}^{M(HIR)} \frac{q_{j,HIR}}{q_{j,harm\ 1-D}} \tag{3.22}$$

Where N is the number of vibrational modes and M the number of hindered rotations that we want to include. To obtain $q_{j,HIR}$, potential energy curves are computed for the hindered rotations, then a one-dimensional Schrödinger equation is solved to obtain the eigenstates needed to compute the partition function. The term $q_{j,harm\ 1-D}$ is the harmonic oscillator value from these one-dimensional curves. The big advantage of this approach is that the corrected partition function q_{corr} is just the standard one $q_{vib,harm}$, with a multiplying factor. This allows us to use the output of available codes.

3.2.4   Tunneling

We have kept improving our original expression for the rate constant, first including the quantum expression for the partition functions, later we have corrected the modes that are not properly represented by an harmonic oscillator. Finally we should not forget that in all these treatments the movement along the

reaction coordinate has been treated classically. As we know in the non-classic approach, our particle will have a wave behavior associated, this implies that sometimes even if our molecule has an energy lower than the one corresponding to the barrier it can cross to the product side of the PES. This effect is known as tunneling since our particle seems to "tunnel" through the barrier and appear in the other side. Since the effect becomes bigger the lighter the particle is, this effect is particularly important when a hydrogen is involved in the reaction, *i.e.*, hydrogen abstractions. A straightforward approximation, introduced by Wigner,[35] is to include a correction factor that takes into account this deficiency of the form

$$\kappa = 1 - \frac{1}{24}\left(\frac{hv^{\ddagger}}{k_B T}\right)^2\left(1 + \frac{RT}{\Delta E_{B,0}}\right) \tag{3.23}$$

Where only the frequency $v^{\ddagger}$, associated with the reaction coordinate and the reaction barrier $\Delta E_{B,0}$ are required to calculate the correction factor κ. Notice that the minus sign of the second term on the right-hand side of the equation is canceled by the square of the imaginary frequency $v^{\ddagger}$, such that $\kappa > 1$. We should also note that this approach has some limitations, including the fact that it does not take into account the curvature of the PES, that drastically affects the amount of tunneling. It works very well at high temperatures, where κ is close to one and the correction is therefore small. When the temperature is low this expression underestimates the value of the correction factor in orders of magnitude, so more sophisticated treatments, like the ones developed by Skodje and Truhlar,[36,37] are needed.

Chapter 4

Formation of Naphthalene and Phenanthrene from Phenyl with Vinyl- and Phenylacetylene

4.1 Building polycyclic aromatic hydrocarbons (PAH)

We will try to explain, why these two particular reactions, the formation of naphthalene and phenanthrene from phenyl with vinyl- and phenylacetylene, among the huge number of possibilities are in the focus of our efforts. Chemical vapor deposition (CVD) of carbon from light hydrocarbons involves a large and complex set of homogeneous gas phase reactions leading to various products including polycyclic aromatic hydrocarbons (PAHs) and heterogeneous surface reactions leading to the deposition of pyrolytic carbon on the substrate.[38–40] In an attempt to understand this process, Norinaga *et al.* studied the product distributions in the CVD of carbon from acetylene at 8 kPa and 900 °C and found that the major products formed under these conditions are benzene, dihydrogen, vinylacetylene, naphthalene, ethylene, and methane.[41] Benzene and vinylacetylene are known to be formed in acetylene pyrolysis, and in [Ref. 41], it was suggested that vinylacetylene is formed by dimerization of acetylene while benzene is formed by combination of acetylene and vinylacetylene. Possible reactions for benzene formation from small aliphatics are:

$$n\text{-}C_4H_3 + C_2H_2 \quad \rightarrow \quad \text{phenyl} \tag{4.1}$$

$$n\text{-}C_4H_5 + C_2H_2 \quad \rightarrow \quad \text{benzene} + H \tag{4.2}$$

$$C_3H_3 + C_3H_3 \quad \rightarrow \quad \text{benzene} \tag{4.3}$$
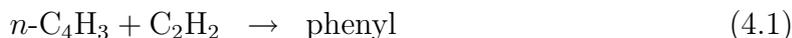
Although still under debate (cf. [Ref. 42–44] for a review of the literature), we shall not be concerned with the formation of benzene but rather with the formation of larger PAHs such as naphthalene and phenanthrene. This is explained by the results of the sensitivity analysis performed in the kinetic model of Noringa and Deutschmann,[41,45] that points directly to the formation of naphthalene and phenanthrene from phenyl with vinyl- and phenylacetylene as the main sources of uncertainty in the model. This does not mean that these two reactions are the most important on a quantitative basis, but that small effects in their rate constant values have big effects in the overall product behavior. That explains that a deep understanding and a meaningful value are needed. It is, therefore, necessary to provide new and reliable data to substitute the one used at present. In this case modeling was performed with a mechanism involving 227 species and 827 reactions.[45]

Table 4.1: Parameters used in the kinetic modeling in [Ref. 45]

Reaction (Number)	A $(\text{cm}^3\,\text{mol}^{-1}\,\text{s}^{-1})$	n	E_a $(\text{kJ}\,\text{mol}^{-1})$	Ref.
phenyl + vinylacetylene → naphthalene + H (Nr. 454)	9.900×10^{30}	-5.07	88.29	[Ref. 46]
phenyl + phenylacetylene → phenanthrene + H (Nr. 537)	9.550×10^{11}	0.0	18.03	[Ref. 43]

The two reactions have been previously looked at. Addition of vinylacetylene to benzene (or more precisely phenyl) is a possible route to naphthalene formation:[46]
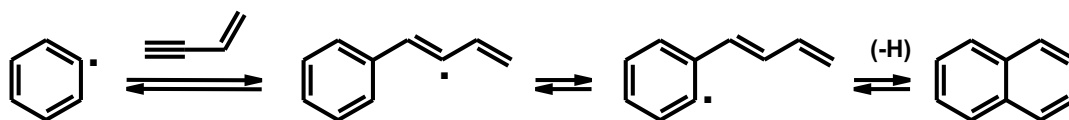
While Appel and co-workers have reported that in their kinetic modeling, the vinylacetylene addition channel contributed the most to the naphthalene production,[46] Frenklach and others have argued that this chanel may be ineffective due to the large barrier to rotation about the C=C double bond in the last step.[42,47,48]

Appel and co-workers have furthermore suggested that phenanthrene is formed primarily via ring-ring condensation reactions.
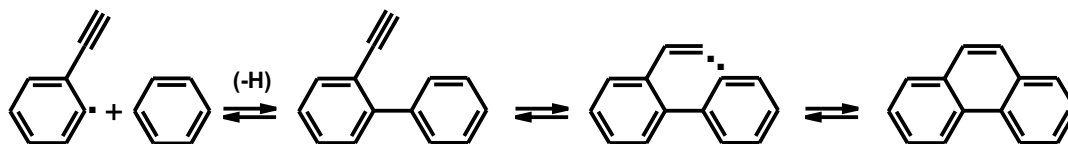
Alternatively, the growth of phenanthrene could be initiated by the formation of biphenyl from benzene, then yielding phenanthrene via the HACA mechanism (hydrogen-abstraction-C_2H_2-addition) of Frenklach and Wang.[42, 49, 50]

In their kinetic modeling of acetylene pyrolysis (900 °C, 8 kPa, 0.5 s), Norinaga and Deutschmann[51] find that 68% of acetylene is consumed by dimerization to form vinylacetylene ($2C_2H_2 \rightarrow C_4H_4$), 17% by diacetylene formation ($2C_2H_2 \rightarrow C_4H_2 + H_2$), and 7% by benzene formation from vinylacetylene and acetylene ($C_4H_4 + C_2H_2 \rightarrow$ benzene). From the viewpoint of the products, 98% of vinylacetylene is formed by dimerization of acetylene, and 95% of benzene is formed by the combination of vinylacetylene and acetylene.

In [Ref. 41], for example, yields (based on C_1) of ca. 2% of naphthalene and ca. 1% of phenanthrene were observed in acetylene pyrolysis after about 1.0 s under the aforementioned conditions.

The kinetic modeling of [Ref. 51] and [Ref. 45] was based on Arrhenius-like rate expressions:

$$k(T) = AT^n \exp\left(-E_a/RT\right) \tag{4.4}$$

with the kinetic parameters (pre-exponential A, temperature exponent n, activation energy E_a) taken from the literature (R is the gas constant, T is the temperature). Since the modeling of the formation of naphthalene and phenanthrene appeared to be difficult, we decided to reinvestigate — by means of density functional theory (DFT) — the two sets of parameters shown in Table 4.1. We shall show that very different parameters can be derived from a reaction mechanism that involves a cis-trans isomerization via a radicalic 4-membered ring, which has so far not been considered in the literature.

This chapter describes the DFT investigations of the reactions of phenyl with vinylacetylene and phenylacetylene via this type of 4-membered intermediate.
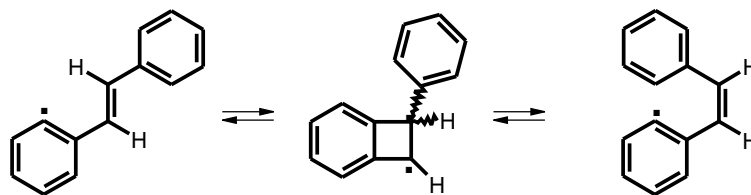
4.2 Computational details

The basic concepts of the methodology employed have been already introduced in Chapter 2. Here we shall deal with the particular details of the tools employed here.

Density Functional Theory has been used through the whole study as implemented in TURBOMOLE.[52–54] At the initial stage of our work, we used the SV(P) basis[55] (split-valence basis with a set of d-type polarization functions on C) and the BP86 functional[56–58] in combination with the RI-J approximation[59,60] to explore possible pathways at a very low computational cost. The RI-J approximation reduces the computing time to about 10% of the time needed for the corresponding calculation without this approximation. This overall procedure provides us with an easy way to tackle the big amount of different molecules and, while quantitatively incorrect, provide us a with good understanding of the qualitatively shape of our problem potential energy surface.

Subsequently, the final results were obtained by locating the minima and saddle points using the TZVP basis[61] (triple ξ valence plus polarization) and the B3LYP functional.[57,62,63] Moreover, single-point calculations were carried out in the same TZVP basis using the BMK functional,[64] which has been designed specifically for accurate calculations of barrier heights. With this new, and much bigger basis, the problem of the basis-set superposition error (BSSE) is reduced to insignificance and will not be treated any more. The harmonic frequencies were calculated for all species at the B3LYP/TZVP level,[65,66] scaled by a factor of 0.9 and used to compute the zero-point vibrational energies (ZPVE) and the vibrational partition functions.

Simple Transition State Theory (TST) was used to compute reaction rate

constants. Since it has been explained in detail in Chapter 3, it will not be repeated here. The final expression for the reaction rate constant of a unimolecular reaction is

$$k = \kappa \cdot \frac{k_B T}{h} \cdot \frac{q^{X\ddagger}}{q^X} \cdot \exp\left(\frac{-\Delta E_{B,0}}{RT}\right) \qquad (4.5)$$

Where in the case of this study the temperature has been varied from 300 to 1.300 K. This range of temperatures is not totally arbitrary, it is a compromise between being useful for combustion chemistry, that tends to higher temperatures, and being reasonably accurate in application of TST, tending itself to lower temperatures. For the bimolecular reactions, the analog to Eq (4.5) is

$$k = \kappa \cdot V_m \cdot \frac{k_B T}{h} \cdot \frac{q^{XY\ddagger}}{q^X q^Y} \cdot \exp\left(\frac{-\Delta E_{B,0}}{RT}\right) \qquad (4.6)$$

Now the molecular volume has to be included, and the partition functions of both reactants. In both cases tunneling effects have been taken into account using the Wigner formula as described in Chapter 3. Finally, Arrhenius-like expressions are fitted to the computed rate constants for our temperature interval (in 100 K steps), using A and n as fitting parameters, and leaving E_a to be substituted for the corresponding value of $\Delta E_{B,0}$ for both functionals, leaving room in the future to be substituted by more accurate estimations of the reaction barrier. This procedure makes, in principle, the fitting less accurate, but in the case of this study this devaluation did not play a significant role. Therefore we decided to keep the value of the barrier height intact, keeping a significant meaning that is usually distorted in the fitting procedure.

During the course of this study, the important role of the four-membered ring intermediates became clear. Since this type of compounds had not been suggested before, we performed a detailed study of them. Single-point calculations (at the B3LYP-TZVP geometries) were performed with the functionals BLYP,[63] TPSS,[67,68] TPSSh[67–69] and B97-K.[64] It turned out that the energies were quite different among them, so a study case was built, using the penta-1,3-dien-1-yl radical, and calculated using the MP2,[70] CC2[71] and RCCSD(T)[72–74] methods. The former two as implemented in TURBOMOLE, the latter in MOLPRO. The innershell electrons (carbon 1s) were not correlated (frozen core, FC, approxima-

tion) in any of the correlation treatments.

4.3   Formation of naphthalene
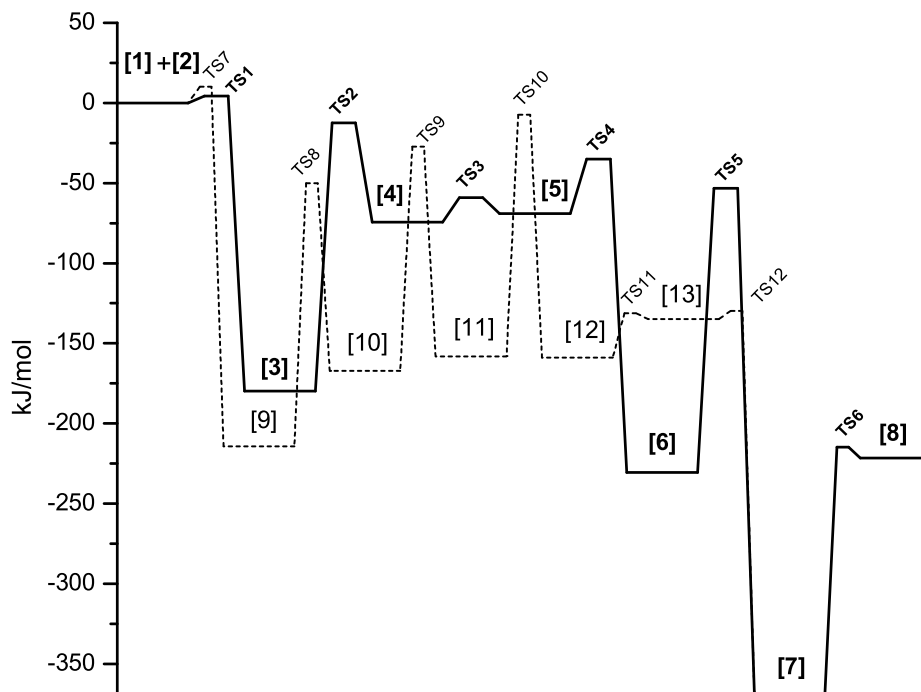
Figure 4.1: Formation of naphthalene, C_6H_5**[1]** $+$ C_4H_4**[2]** $\rightarrow$ $C_{10}H_8$**[8]**, calculated at the B3LYP/TZVP level.

We have computed two pathways for the formation of naphthalene from phenyl and vinylacetylene. On one pathway, the phenyl radical attacks the vinylacetylene at its double bond (solid line in Fig. 4.1, see also Fig. 4.2), and on the other pathway, the phenyl radical attacks the vinylacetylene at its triple bond (dashed line in Fig. 4.1, see also Fig. 4.2). The attack at the double bond yields **[3]** and is followed by a 1,4 hydrogen shift bringing the radical center back to the ring (**[4]**). Then, further reactions to naphthalene (**[8]**) are straightforward. The other possible pathway occurs after the phenyl's attack to the triple bond of vinylacetylene, yielding **[9]**. Here also, a 1,4 hydrogen shift brings the radical center back to the ring (**[10]**). To proceed further, a rotation about a double bond
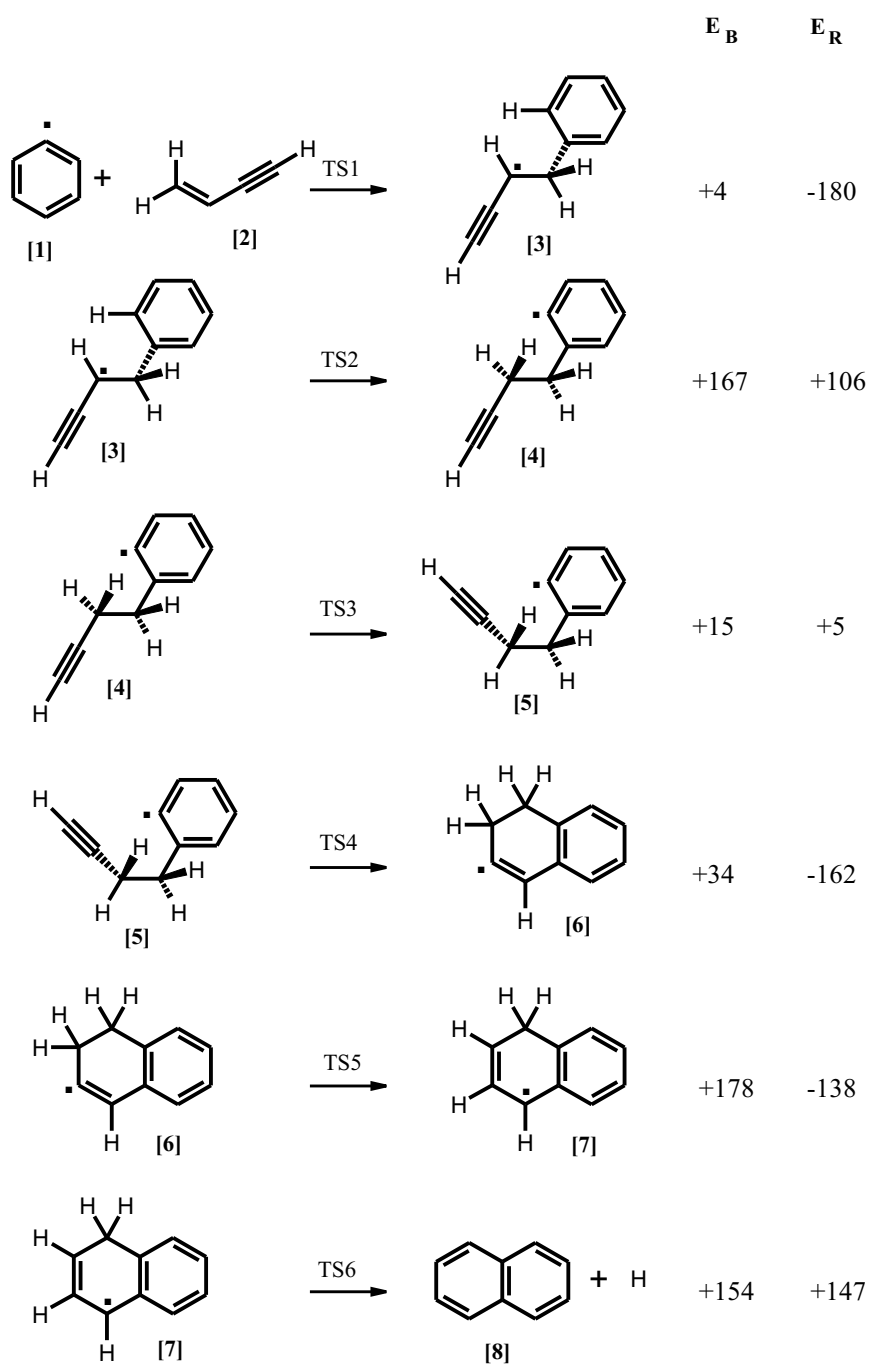
Figure 4.2: Intermediates and transition states on the first reaction path (solid line in Fig. 4.1) towards the formation of naphthalene, $C_6H_5[1] + C_4H_4[2] \rightarrow C_{10}H_8[8]$, calculated at the B3LYP/TZVP level (electronic energies in kJ/mol).
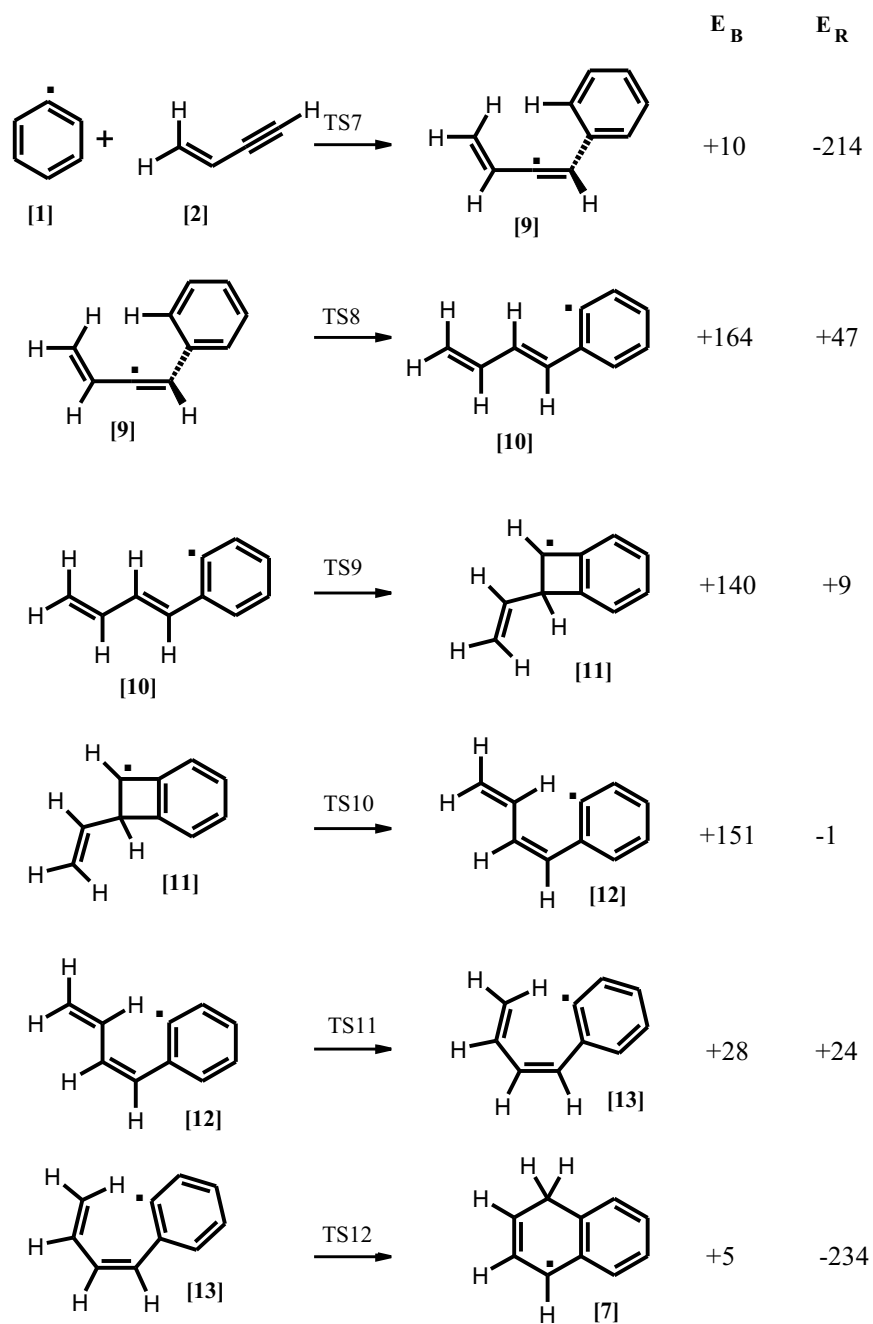
Figure 4.3: Intermediates and transition states on the second reaction path (dashed line in Fig. 4.1) towards the formation of naphthalene, $C_6H_5[1] + C_4H_4[2] \rightarrow C_{10}H_8[8]$, calculated at the B3LYP/TZVP level (electronic energies in kJ/mol).

seems required to prepare for the closure of the second 6-ring of naphthalene, and it was this rotation about a double bond that, in previous work, let the second pathway seem inefficient, because barriers to rotation about a double bond are usually very high.[42, 47, 48]

In our study, however, this rotation takes place in a two-step reaction via the intermediate **[11]**. This 4-membered ring helps to decrease the barrier to "rotation" about the double bond significantly. From **[12]** onwards, the ring-closure to yield naphthalene is straightforward. We stress that, in contrast with the work by Moriarty *et al.*,[47] we do not find any structure (minimum or saddle point) with an electronic energy above the transition state of the first, bimolecular reaction step (TS1 or TS7, cf. Fig. 4.1).

In Table 4.2, we provide the reaction rates obtained from TST for all of the steps of the two pathways in the temperature range 300–1300 K, along with the fitted Arrhenius parameters A and n and computed values of E_a (including ZPVE). We give the activation energies obtained from calculations with the density functionals B3LYP and BMK and recommend the latter for use in the mechanisms on which pyrolysis simulations such as those of Norinaga and co-workers are based.[41, 45]

4.4   Formation of phenanthrene

In Table 4.3, we provide the reaction rates obtained from TST for all of the steps of the reaction (cf. Fig. 4.4 and Fig. 4.5) in the temperature range 300–1300 K, along with the fitted Arrhenius parameters A and n and computed values of E_a (including ZPVE). Not only for the formation of naphthalene but also for the formation of phenanthrene, we recommend the BMK activation energies for modeling purposes.

In the case of vinylacetylene, the phenyl radical can be added to both ends of the molecule, but in the case of phenylacetylene, the phenyl can only react with the triple bond. The addition of the phenyl radical is followed by a 1,4 hydrogen shift to yield the *trans* isomer **[16]**, which isomerizes to the *cis* isomer **[18]** via the 4-membered ring intermediate **[17]**. The electronic energy of the transition structure TS16 (10 kJ/mol, cf. Fig. 4.4) lies just below the barrier (TS13, 11 kJ/mol) of the first, bimolecular reaction step. A new 6-ring is formed in **[18]** to

Table 4.2: Calculated TST rate constants for the formation of Naphthalene

Reaction	T											Fit: $AT^n\exp(-E_a/RT)$			
	300	400	500	600	700	800	900	1000	1100	1200	1300	A	n	E_a^{B3LYP}	E_a^{BMK}[a]
$1+2\rightarrow3$[b]	5.94×10^{-15}	2.08×10^{-14}	5.23×10^{-14}	1.06×10^{-13}	1.90×10^{-13}	3.12×10^{-13}	4.73×10^{-13}	6.93×10^{-13}	9.71×10^{-13}	1.28×10^{-12}	1.70×10^{-12}	2.09×10^{-20}	2.61	6.0	6.9
$3\rightarrow4$[c]	4.16×10^{-16}	2.34×10^{-9}	2.58×10^{-5}	1.07×10^{-2}	1.31×10^{0}	3.03×10^{1}	4.13×10^{2}	3.32×10^{3}	1.86×10^{4}	7.82×10^{4}	2.62×10^{5}	2.53×10^{13}	-0.55	157.0	157.4
$4\rightarrow5$[c]	1.28×10^{10}	5.95×10^{10}	1.52×10^{11}	2.79×10^{11}	4.33×10^{11}	6.04×10^{11}	7.80×10^{11}	9.57×10^{11}	1.13×10^{12}	1.33×10^{12}	1.49×10^{12}	2.71×10^{12}	0.11	14.8	15.3
$5\rightarrow6$[c]	8.43×10^{5}	2.11×10^{7}	1.43×10^{8}	5.32×10^{8}	1.32×10^{9}	2.66×10^{9}	4.60×10^{9}	7.13×10^{9}	1.00×10^{10}	1.34×10^{10}	1.72×10^{10}	6.85×10^{11}	-0.10	32.5	34.2
$6\rightarrow7$[c]	8.81×10^{-16}	1.06×10^{-8}	1.91×10^{-4}	1.32×10^{-1}	1.45×10^{1}	4.94×10^{2}	7.86×10^{3}	7.13×10^{4}	4.43×10^{5}	2.04×10^{6}	7.38×10^{6}	1.05×10^{13}	0.10	162.1	170.9
$7\rightarrow8+H$[c]	8.74×10^{-12}	1.06×10^{-5}	5.32×10^{-2}	1.45×10^{1}	7.86×10^{2}	1.70×10^{4}	1.87×10^{5}	1.31×10^{6}	6.31×10^{6}	2.37×10^{7}	7.40×10^{7}	1.97×10^{10}	0.97	135.8	146.3
$1+2\rightarrow9$[b]	8.02×10^{-15}	4.87×10^{-14}	1.68×10^{-13}	4.25×10^{-13}	8.72×10^{-13}	1.62×10^{-12}	2.68×10^{-12}	4.23×10^{-12}	6.18×10^{-12}	8.62×10^{-12}	1.19×10^{-11}	1.07×10^{-19}	2.72	10.7	13.4
$9\rightarrow10$[c]	1.28×10^{-14}	5.06×10^{-8}	4.38×10^{-4}	1.85×10^{-1}	1.40×10^{1}	4.51×10^{2}	4.51×10^{3}	3.49×10^{4}	1.84×10^{5}	7.48×10^{5}	2.46×10^{6}	1.19×10^{14}	-0.51	152.8	157.7
$10\rightarrow11$[c]	6.55×10^{-12}	5.36×10^{-6}	1.91×10^{-2}	4.47×10^{0}	2.29×10^{2}	4.34×10^{3}	4.26×10^{4}	2.66×10^{5}	1.20×10^{6}	4.23×10^{6}	1.21×10^{7}	5.54×10^{11}	0.23	134.4	135.9
$11\rightarrow12$[c]	2.18×10^{-13}	6.29×10^{-7}	4.78×10^{-3}	1.84×10^{0}	1.30×10^{2}	3.25×10^{3}	3.97×10^{4}	2.88×10^{5}	1.48×10^{6}	5.75×10^{6}	1.82×10^{7}	7.00×10^{11}	0.41	145.7	177.3
$12\rightarrow13$[c]	8.54×10^{7}	1.23×10^{9}	6.28×10^{9}	1.82×10^{10}	3.92×10^{10}	7.00×10^{10}	1.09×10^{11}	1.60×10^{11}	2.13×10^{11}	2.72×10^{11}	3.38×10^{11}	8.85×10^{11}	0.20	25.7	22.5
$13\rightarrow7$[c]	5.23×10^{11}	9.74×10^{11}	1.53×10^{12}	2.13×10^{12}	2.79×10^{12}	3.48×10^{12}	4.19×10^{12}	4.92×10^{12}	5.65×10^{12}	6.47×10^{12}	7.23×10^{12}	1.49×10^{10}	0.91	4.2	4.0

[a]This value includes a ZPVE correction calculated at the B3LYP level.
[b]In cm^{3}s^{-1}molecule^{-1}, with T in K and E_a in kJ/mol.
[c]In s^{-1}, with T in K and E_a in kJ/mol.

Table 4.3: Calculated TST rate constants for the formation of Phenanthrene

Reaction	T											Fit: $AT^n\exp(-E_a/RT)$			
	300	400	500	600	700	800	900	1000	1100	1200	1300	A	n	E_a^{B3LYP}	E_a^{BMK}[a]
$1+14\rightarrow15$[b]	3.83×10^{-15}	2.65×10^{-14}	9.87×10^{-14}	2.61×10^{-13}	5.57×10^{-13}	1.06×10^{-12}	1.79×10^{-12}	2.80×10^{-12}	4.27×10^{-12}	6.02×10^{-12}	8.30×10^{-12}	6.96×10^{-20}	2.74	11.8	14.7
$15\rightarrow16$[c]	8.02×10^{-13}	1.00×10^{-6}	4.49×10^{-3}	1.21×10^{0}	6.59×10^{1}	1.35×10^{3}	1.43×10^{4}	9.51×10^{4}	4.51×10^{5}	1.63×10^{6}	4.89×10^{6}	8.82×10^{13}	-0.51	141.8	142.8
$16\rightarrow17$[c]	1.11×10^{-10}	3.23×10^{-5}	6.18×10^{-2}	9.57×10^{0}	3.55×10^{2}	5.39×10^{3}	4.45×10^{4}	2.46×10^{5}	9.67×10^{5}	3.12×10^{6}	8.32×10^{6}	3.34×10^{11}	0.13	124.5	126.9
$17\rightarrow18$[c]	1.80×10^{-15}	1.65×10^{-8}	2.49×10^{-4}	1.53×10^{-1}	1.43×10^{1}	4.45×10^{2}	7.17×10^{3}	6.18×10^{4}	3.59×10^{5}	1.56×10^{6}	5.50×10^{6}	3.60×10^{11}	0.48	156.9	190.6
$18\rightarrow19$[c]	6.17×10^{8}	2.80×10^{9}	7.07×10^{9}	1.31×10^{10}	2.02×10^{10}	2.87×10^{10}	3.73×10^{10}	4.64×10^{10}	5.46×10^{10}	6.32×10^{10}	7.18×10^{10}	2.71×10^{11}	0.01	15.3	17.5
$19\rightarrow20+H$[c]	5.70×10^{-2}	2.03×10^{2}	2.91×10^{4}	8.36×10^{5}	9.50×10^{6}	5.85×10^{7}	2.49×10^{8}	7.96×10^{8}	2.08×10^{9}	4.62×10^{9}	9.05×10^{9}	1.38×10^{11}	0.65	80.1	89.3

[a]This value includes a ZPVE correction calculated at the B3LYP level.
[b]In cm^{3}s^{-1}molecule^{-1}, with T in K and E_a in kJ/mol.
[c]In s^{-1}, with T in K and E_a in kJ/mol.
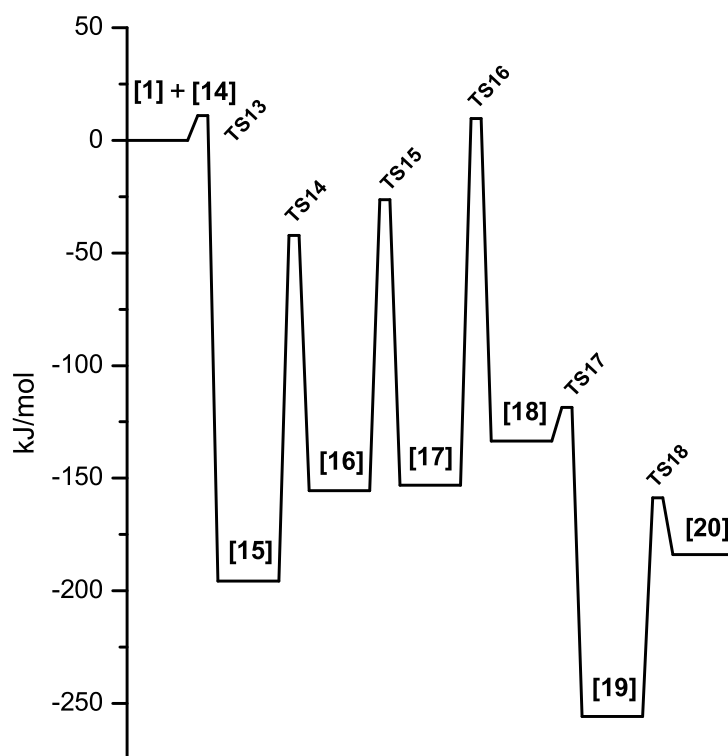
Figure 4.4: Formation of phenanthrene, C_6H_5[1] + C_8H_6[14] $\rightarrow$ $C_{14}H_{10}$[20], calculated at the B3LYP/TZVP level.

give phenanthrene [20].

4.5 Four-membered ring intermediates

The radicalic intermediates [11] and [17] with a 4-membered ring play a key role in the proposed reaction mechanisms for the formations of naphthalene and phenanthrene from reactions of phenyl with vinylacetylene and phenylacetylene, respectively. Unfortunately, we observe large discrepancies between the B3LYP and BMK results for the barriers between the 4-membered ring intermediates and the *cis* isomers. For example, the BMK barrier (177.3 kJ/mol, including ZPVE) for the step [11] $\rightarrow$ [12] is more than 30 kJ/mol higher than the corresponding B3LYP barrier (145.7 kJ/mol, cf. Table 4.2). Also for the formation of
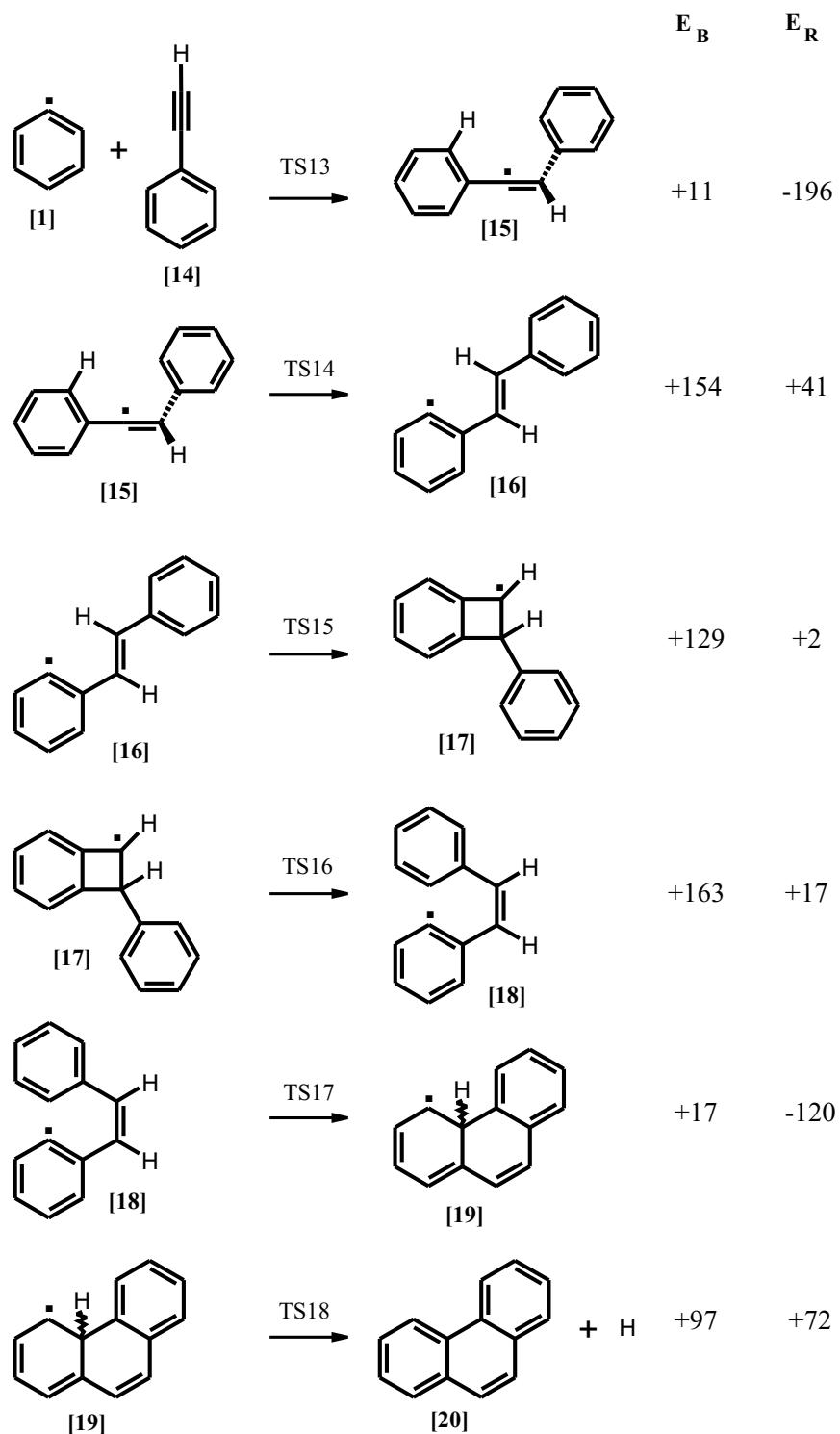
Figure 4.5: Intermediates and transition states on the reaction path (Fig. 4.4) towards the formation of phenanthrene, C_6H_5[1] + C_8H_6[14] → $C_{14}H_{10}$[20], calculated at the B3LYP/TZVP level (electronic energies in kJ/mol).

phenanthrene, the BMK barrier (190.6 kJ/mol) for the step **[17]** → **[18]** is more than 30 kJ/mol higher than the corresponding B3LYP barrier (156.9 kJ/mol, cf. Table 4.3).

Similar data for the functionals BP86, BLYP, TPSS, TPSSh, and B97-K are collected in Table 4.4, showing that it is mainly the energy of the intermediates **[11]** and **[17]** that causes the large variations in computed activation energies for the **[11]** → **[12]** and **[17]** → **[18]** steps.
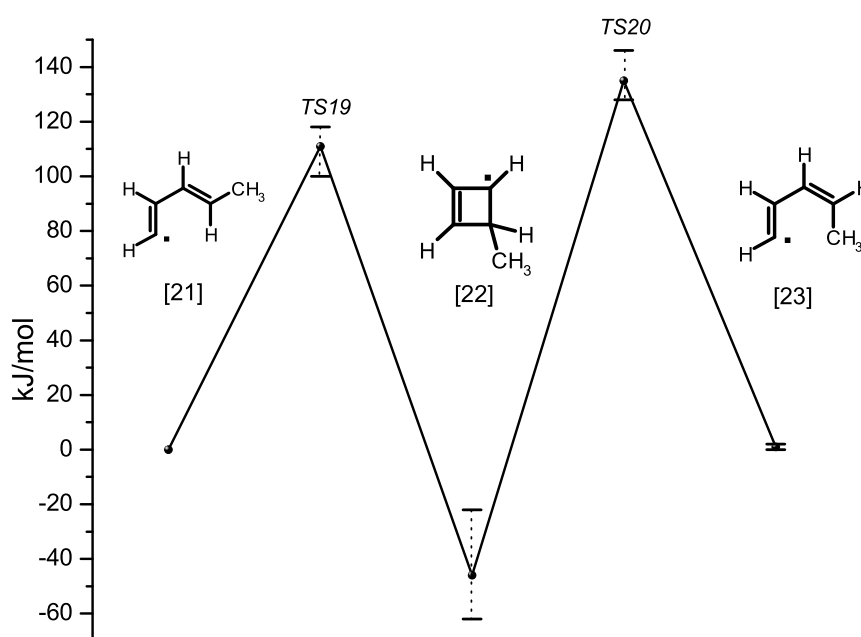
Figure 4.6: Energy profile of the isomerization of penta-1,3-dien-1-yl **[21]**, (see Table 4.5). The range of calculated DFT energies is indicated by error bars.

In an attempt to understand the different behavior of various exchange–correlation functionals, we have investigated the isomerization of the penta-1,3-dien-1-yl radical **[21]** as a model system (cf. Fig. 4.6). For this model system, we have performed single-point RCCSD(T)(FC) calculations at the B3LYP/TZVP geometries with a restricted open-shell Hartree–Fock reference state (ROHF) using the correlation-consistent cc-pVTZ basis. According to the T1 diagnostic criteria, the RCCSD(T) results do not suffer from a strong multireference character and represent a reliable set of reference data. The equilibrium and transition

Table 4.4: Calculated (in the TZVP basis) relative energies (in kJ/mol, with respect to **[10]** and **[16]**, respectively) for the formation of the 4-membered ring intermediates **[11]** and **[17]**

Method	TS9	[11]	TS10	TS15	[17]	TS16
BP86	122	−1	141	111	−8	146
BLYP	129	18	149	118	11	154
TPSS	125	0	144	115	−7	149
B3LYP	140	9	160	129	2	165
TPSSh	130	−4	149	119	−11	154
B97-K	142	−10	162	132	−16	169
BMK	141	−21	162	132	−29	168

Table 4.5: Calculated (in the TZVP basis) relative energies (in kJ/mol, with respect to [**21**]) of the model reaction with penta-1,3-dien-1-yl (cf. Fig. 4.6) at the B3LYP/TZVP geometries. A cc-pVTZ basis was used for the ROHF-RCCSD(T)(FC) calculations.

Method	TS19	$\delta_{\text{TS19}}{}^{a}$	[22]	$\delta_{[22]}{}^{a}$	TS20	$\delta_{\text{TS20}}{}^{a}$	[23]	$\delta_{[23]}{}^{a}$
BP86	100	−11	−43	3	128	−7	0	−1
BLYP	110	−1	−22	24	136	1	2	1
TPSS	102	−9	−45	1	128	−7	1	0
B3LYP	117	6	−32	14	145	10	2	1
TPSSh	105	−6	−49	−3	132	−3	1	0
B97-K	118	7	−49	−3	146	11	2	1
BMK	116	5	−62	−16	144	9	0	−1
ROHF	182	71	5	51	211	76	6	5
UHF	137	26	−15	31	155	20	7	6
ROHF-UMP2(FC)	103	−8	−65	−19	129	−6	1	0
UHF-UMP2(FC)	124	13	−86	−40	152	17	0	−1
ROHF-UCC2(FC)	100	−11	−54	−8	124	−11	0	−1
UHF-UCC2(FC)	115	4	−67	−21	143	8	0	−1
ROHF-RCCSD(T)(FC)	111	0	−46	0	135	0	1	0

[a]Deviation from the ROHF-RCCSD(T)(FC) result.

structures were determined at the B3LYP/TZVP level (Fig. 4.6), and the results from various single-point calculations are shown in Table 4.5. All of the DFT and coupled-cluster calculations indicate that the energy of the 4-membered ring seems to be the most difficult to compute accurately. For the 4-membered ring [22], the deviations of the results from the ROHF-CCSD(T)(FC) results vary between 51 (ROHF) and -40 kJ/mol (UHF-UMP2(FC)). The corresponding deviations of the B3LYP (14 kJ/mol) and BMK (-16 kJ/mol) results are not so large, but have different signs.

Spin contamination of the doublet states may be a reason for the differences between the DFT results. Indeed, the spin-unrestricted Hartree–Fock (UHF) expectation values of $\hat{S}^2$ amount to 1.30, 0.97, and 1.28 for the minima [21], [22], and [23], respectively, and as much as 1.45 and 1.53 for the transition structures TS19 and TS20. The UHF and UHF-based values seem not reliable. On the other hand, all of the DFT values are much closer to 0.75 and in good mutual agreement. For all of the minima, the DFT values range from 0.76 to 0.78 for all of the functionals studied, and the values for TS19 and TS20 vary between 0.77 and 0.81 and between 0.77 and 0.83, respectively. Overall, the DFT values agree to within 25 kJ/mol with the ROHF-CCSD(T)(FC) results, as can be seen from the error bars on Fig. 4.6.

4.6 Conclusions

We have proposed three reaction pathways for PAH growth from reactions of either vinyl- or phenylacetylene with a phenyl radical. We have found pathways via 4-membered ring intermediates that enable a *cis–trans* isomerization. These intermediates have so far not been investigated in the literature.

Arrhenius parameters (pre-exponential A, temperature exponent n, and activation energy E_a) have been derived for all of the reaction steps on the three different pathways. We suggest to use Arrhenius-like rate expressions such as Eq. ((3.11)) with our parameters for the first bimolecular steps in the kinetic modeling of [Ref. 51] and [Ref. 45].

Chapter 5

Thermochemical Data for $C_3H_x(x = 0, \cdots , 4)$ Species

5.1 Introduction

C_3H_x species with x = 0, ..., 4 play an important role in the formation and growth of polycyclic aromatic hydrocarbons (PAHs), in particular of small PAHs such as benzene and naphthalene, during combustion or pyrolysis.[42–44, 75–79] The self reaction of the propargyl radical (2-propynyl, CH_2CCH), for example, is thought to be the dominant reaction leading to the formation of benzene.[76, 78] Reactions of phenyl radicals with propyne[80] or vinyl acetylene[81] may lead to naphthalene, and so on. Since many C_3H_3 and C_3H_x isomers are involved in the formation of PAHs and soot, the modeling of their formation under pyrolysis conditions requires the accurate knowledge of thermochemical data and rate constants of hundreds of species and elementary reactions.[41, 45]

Furthermore, C_3H_x species have been observed in interstellar space.[82] Examples are tricarbon (C_3),[83] linear[84] and cyclic C_3H,[85] propadienylidene and cyclopropenylidene.[86, 87]

Ab initio quantum chemical calculations can provide very accurate structural, spectroscopic and energetic data of small polyatomic molecules, radicals and carbenes of relevance to interstellar cloud chemistry and combustion processes. Particularly successful have been calculations employing the coupled-cluster method that includes single and double excitations (CCSD, cf. [Ref. 88, 89]) as well as a perturbative treatment of triple excitations [CCSD(T), cf. [Ref. 8, 74, 90–92]].

Examples of such successes can be found in [Ref. 93–96].

This chapter is concerned with the highly accurate calculation of the equilibrium structures and ground-state energies of the C_3H_x species with x = 0, ..., 4. In the present work, the same set of molecules and radicals as studied by Vereecken and co-workers[97] at the level of density-functional theory will be investigated at the CCSD(T) level. Corrections for core–core and core–valence correlation effects, anharmonic zero-point vibrational energies and relativistic effects (both scalar and spin–orbit effects) will be taken into account in an attempt to compute the atomization energies of the species studied with chemical accuracy, that is, accurate to within 1 kcal/mol ($\approx$ 4 kJ/mol). Here, accuracy refers to a 95% confidence limit. This means that atomization energies must be calculated with a mean absolute deviation of 1–2 kJ/mol from experimental data (*vide infra*). Such accuracy can only be achieved by performing the CCSD(T) calculations in very large and nearly complete one-electron basis sets, followed by basis-set extrapolation,[10,98,99] or by expanding the coupled-cluster wavefunction in a many-electron basis that contains terms that depend explicitly on the interelectronic distances in the system,[16,100,101] applying the techniques explained in detail in Chapter 2.

Recently, Wheeler and co-workers published very accurate calculations of the enthalpies of formation of the following four key intermediates in soot formation: propargyl, 1-propynyl, cycloprop-1-enyl, and cycloprop-2-enyl.[79] These authors used the CCSD(T) method in conjunction with basis-set extrapolation techniques, that is, in the framework of the focal-point analysis,[102,103] and also added corrections for core–core and core–valence correlation effects, anharmonic zero-point vibrational energies and relativistic effects. They even added diagonal Born–Oppenheimer corrections and correlation effects from triple excitations beyond the CCSD(T) level as obtained at the full CCSDT model, and from quadruple excitations as described at the CCSDT(Q) level.[104]

The purpose of the present work is to provide highly accurate thermochemical data (*i.e.*, atomization energies) for the above four key intermediates as well as for a number of other C_3H_x species from explicitly-correlated coupled-cluster calculations, that is, without resorting to basis-set extrapolation techniques,[10,98,99] and to obtain the equilibrium geometries at a CCSD(T) coupled-cluster level at the limits of what is technically feasible today (*i.e.*, CCSD(T) calculations correlating all electrons in a correlation-consistent polarized core–valence quadruple-zeta

basis).

The explicitly-correlated coupled electron-pair approximation and coupled-cluster methods were developed in the early 1990s for closed-shell atoms and molecules.[105–109] The general theory of the explicitly-correlated coupled-cluster theory is described in detail in [Ref. 107] and a number of review articles exist.[16,100,101] In 2000, the theory was extended to single-reference open-shell cases with unrestricted Hartree–Fock (UHF) and restricted open-shell Hartree–Fock (ROHF) reference determinants.[17,100]

5.2   Computational details

The backbone of our computational procedure is based on the calculation of the CCSD(T)(FC)-R12 energy in a very large basis described in detail in Section 5.2.1 at CCSD(T)(Full)/cc-pCVQZ$'$ optimized geometries. Here, (FC) indicates that the core orbitals ($1s$ on C) were kept frozen, whereas (Full) indicates that all orbitals were included in the correlation treatment.

Several corrections were added to these values. These corrections are: (i) Energy corrections due to including core orbitals in the correlation treatment (denoted CV); (ii) Corrections due to zero-point vibrational energy (E_{ZPVE}), which consists of harmonic (Harm.) and anharmonic (Anharm.) contributions; (iii) First-order spin–orbit contributions (E_{SO}), which arise from the atomic states involved; (iv) First-order scalar relativistic effects (E_{SR}) due to the one-electron Darwin and mass–velocity (Ms.–Vel.) operators.

5.2.1   Basis sets

The standard CCSD(T) coupled-cluster calculations were performed using correlation-consistent polarized core-valence basis sets of triple- (cc-pCVTZ$'$) and quadruple-zeta (cc-pCVQZ$'$) quality.[9,110] We have attached a prime to these sets to indicate that cc-pCVTZ$'$ refers to the basis cc-pCVTZ for C, but only cc-pVDZ for H. Similarly, the cc-pCVQZ$'$ refers to the basis cc-pCVQZ for C, but only cc-pVTZ for H.

The effect of using the "primed" basis sets in place of the full basis sets, that is, the effect of using basis sets with a smaller cardinal number for H than for C, has been investigated in detail for the molecules CH ($^2\Pi$ state), CH$_2$ ($^3B_1$ state)

and CH_4 ($^1A_1$). Concerning the equilibrium geometries of these molecules, we find that in the cc-pCVQZ$'$ basis, the C-H bond lengths are 0.1 pm longer than in the full cc-pCVQZ basis (in CH_2, the H-C-H angle is reduced by 0.06° in the full cc-pCVQZ basis). Moreover, we can compare our cc-pCVQZ$'$ geometry of singlet propadienylidene with the equilibrium geometry obtained by Gauss and Stanton in the full cc-pCVQZ basis.[111] The only significant difference between the two geometries is the C-H distance, which is 0.1 pm longer in the cc-pCVQZ$'$ basis (see also Section 5.3.2.6).

The effect of the cc-pCVQZ$'$ basis on the correction for core–core and core–valence (CV) correlation effects (*vide infra*) is almost negligible. For CH, the "primed" basis yields a CV correction to the atomization energy that is 0.03 kJ/mol smaller than in the full cc-pCVQZ basis. For triplet methylene and methane, the corresponding reductions are 0.06 and 0.13 kJ/mol, respectively. Hence, we expect that the effect on the CV correction will be of the order of 0.1 kJ/mol for most of the molecules studied (ca. 0.03 kJ/mol per H atom).

The impact of the "primed" basis on the zero-point vibrational energy is more important than on the CV correction. This is not surprising, because only a small cc-pVDZ basis is used for H in the cc-pCVTZ$'$ basis. In the "primed" basis, the zero-point vibrational energies of CH, CH_2 and CH_4 are 0.28, 0.55 and 1.6 kJ/mol, respectively, smaller than in the full basis. Hence, the effect may be of the order of 1–2 kJ/mol for molecules with up to four C-H bonds.

The explicitly-correlated CCSD(T)-R12 calculations were carried out in the basis $19s14p8d6f4g3h$ for C and $9s6p4d3f$ for H, taken from [Ref. 112]. For a molecule such as C_3H_4, this basis comprises 908 spherical Gaussian orbitals. For CH, triplet CH_2 and CH_4, we computed their CCSD(T)-R12 energies at the cc-pCVQZ$'$ and cc-pCVQZ equilibrium geometries. The energy differences were below 0.02 kJ/mol and can be neglected.

5.2.2 Methods and programs

In the CCSD(T)(Full)/cc-pCVQZ$'$ geometry optimizations as well as in the CCSD(T)(FC)-R12 single-point energy calculations, we have used restricted (open-shell) Hartree–Fock reference wave functions (RHF or ROHF) and semicanonical orbitals for the (T) triples correction.[74]

Due to hardware restrictions, although we used the improved algorithm for

triple-excitation contributions of Noga and Valiron,[113] the contribution from the valence-shell (T) connected triples could not always be computed using the previous CCSD(T)(FC)-R12 level in the large C=$19s14p8d6f4g3h$/H=$9s6p4d3f$ basis. In cases where this calculation was impossible, the triples correction was computed at the conventional CCSD(T)(FC) level in the cc-pCVQZ$'$ basis. A comparison of the (T) values from both types of calculations (where available) showed that the CCSD(T)(FC)-R12 triples correction adds about 0.36 kJ/mol per C atom to the atomization energy more than the conventional CCSD(T)(FC) correction. Hence, we have added an empirical 0.36 kJ/mol per C atom to the atomization energy on the occasions where the triples corrections were computed at the CCSD(T)(FC)/cc-pCVQZ$'$ level.

The CV correction was obtained from the difference between the all-electron correlated, CCSD(T)(Full)/cc-pCVQZ$'$ and the only-valence-electron correlated, CCSD(T)(FC)/cc-pCVQZ$'$ energies at the CCSD(T)(Full)/cc-pCVQZ$'$ optimized geometries.

The harmonic ZPVE was computed at the CCSD(T)(Full)/cc-pCVTZ$'$ level using RHF reference wave functions for closed–shell and UHF reference wave functions for open-shell molecules.[114, 115]

The anharmonic correction to the zero-point energies were calculated at the DFT (density-functional theory) level. Concerning the force field, we followed the approach proposed by Schneider and Thiel,[116] in which a full cubic and a semidiagonal quartic force field are obtained by central numerical differentiation (in rectilinear normal coordinates about the equilibrium geometry) of analytical second derivatives. The latter were obtained by means of locally modified versions of GAUSSIAN. Modified routines from CADPAC[117] were used as the driver for the numerical differentiation routine.[118, 119] These calculations have been performed with the B97-1 functional[120] and the TZ2P basis sets.[121] These are Dunning[122] contractions of Huzinaga primitive sets. For C, it is a $11s6p$ to $5s4p$ contraction with two sets of polarization functions with exponents 1.2 and 0.4. For H the contraction is $5s$ to $3s$ and the two sets of polarization functions have exponents 1.5 and 0.5. All of the force fields were analyzed by means of the SPECTRO[123] and POLYAD[124] rovibrational perturbation theory programs. In this way, the G_0 term has been included into the calculation of the anharmonic correction to the ZPVE.

For a test set of 15 closed-shell molecules plus CH_2 and NH_2, we obtained a root-mean-square error of 0.2 kJ/mol for the anharmonic correction employing this scheme.[118] In some cases, the anharmonicity constants of the lowest torsion modes were physically unrealistic when determined by second-order perturbation theory. We therefore decoupled these modes by zeroing all off-diagonal anharmonicity constants involving them. For six molecules (CH, CH_3, C_2, C_3, triplet cyclopropenylidene, and singlet propadienylidene) the anharmonic correction to the zero-point vibrational energy was computed from third and fourth derivatives of the UHF-CCSD(T)(Full)/cc-pCVTZ$'$ energy by numerical differentiation of analytically calculated second derivatives,[114,115] as implemented in the Mainz–Austin–Budapest version of the program system ACES II.

The spin–orbit contributions (E_{SO}) were obtained from experimental atomic levels while the Darwin and mass–velocity energy corrections were computed analytically as a first-order molecular property at the CCSD(T)(Full)/cc-pCVQZ$'$ level using the ACES II program.

All coupled-cluster calculations except for the CCSD(T)-R12 calculations were performed with the Mainz–Austin–Budapest version of the ACES II package of programs.[125] The CCSD(T)-R12 calculations were done with the DIRCCR12-OS program.

Finally, we note that not all equilibrium geometries could be determined at the CCSD(T)(Full)/cc-pCVQZ$'$ level using an ROHF reference determinant, partly for technical reasons and partly due to convergence problems. In particular, we did not succeed for the ^3A state of cyclopropenylidene (c-C_3H_2), the ^3B state of prop-2-ynylidene (HCCCH), and the $^2A''$ states of 1- and 2-propene-1-yl-3-ylidene. For these four systems, we used the UHF-CCSD(T)/cc-pCVTZ$'$ equilibrium geometries. Furthermore, with the DIRCCR12-OS program, we could not converge the $^2A''$ ROHF wave function in the large C=$19s14p8d6f4g3h$ H=$9s6p4d3f$ Gaussian basis of Section 5.2.1 for 1-propene-1-yl-3-ylidene. We used an UHF reference instead for this system.

5.2.3   Active thermochemical tables

Active thermochemical tables (ATcT) are a new paradigm of how to obtain accurate, reliable, and internally consistent thermochemical values by using all available knowledge[126–128] and overcome the limitations that are deeply engrained

in the traditional approach to thermochemistry, such as that used in all traditional thermochemical compilations. As opposed to the traditional sequential approach, ATcT derives its results from a Thermochemical Network (TN). The thermochemical values used in the present work for the purpose of benchmarking the current method have been obtained from the latest version of the Core (Argonne) Thermochemical Network, C(A)TN, that is currently under development and describes ca. 800 species interconnected by ca. 8000 experimental and theoretical determinations. For the species of interest here, the current version of C(A)TN includes all available experimental results and also considers a selection of prior highly accurate theoretical results, such as those by Karton *et al.*[99] (with weights proportional to the expected uncertainties), but does not include the present computational results.

5.3   Results and discussion

5.3.1 CH_x and C_2H_x species

Accurate atomization energies, that is, the sum of all of the bond dissociation enthalpies at zero kelvin, $\sum D_0$ (0 K), are available for the small CH_x and C_2H_x species from the Active Thermochemical Tables (ATcT, cf. Section 5.2.3). The atomization energies are known with an accuracy of about ± 0.3 kJ/mol or better. Only for the dicarbon molecule and the vinyl radical, the ATcT uncertainty is slightly larger (± 0.6 and ± 0.9 kJ/mol, respectively). The ATcT values are presented in Table 5.1, together with other experimental and computational data from the literature.[129–136] The ATcT uncertainties correspond to 95% confidence limits, as expected in thermochemistry (approximately equal to two standard deviations). Please note that, in general, before directly comparing the 95% confidence limits, which are the generally accepted measure of uncertainty in thermochemistry, with the mean absolute deviation (which is the prevailing measure of fidelity in electronic-structure theory), one of the two needs to be rescaled: either the 95% confidence limits need to be divided by a factor between two and three (2.5 if the distribution of errors is normal) or the mean absolute deviation needs to be multiplied by the same factor.

For these small molecules and radicals, the CCSD(T) level of theory as applied in the present work—including core-correlation, relativistic and anharmonic
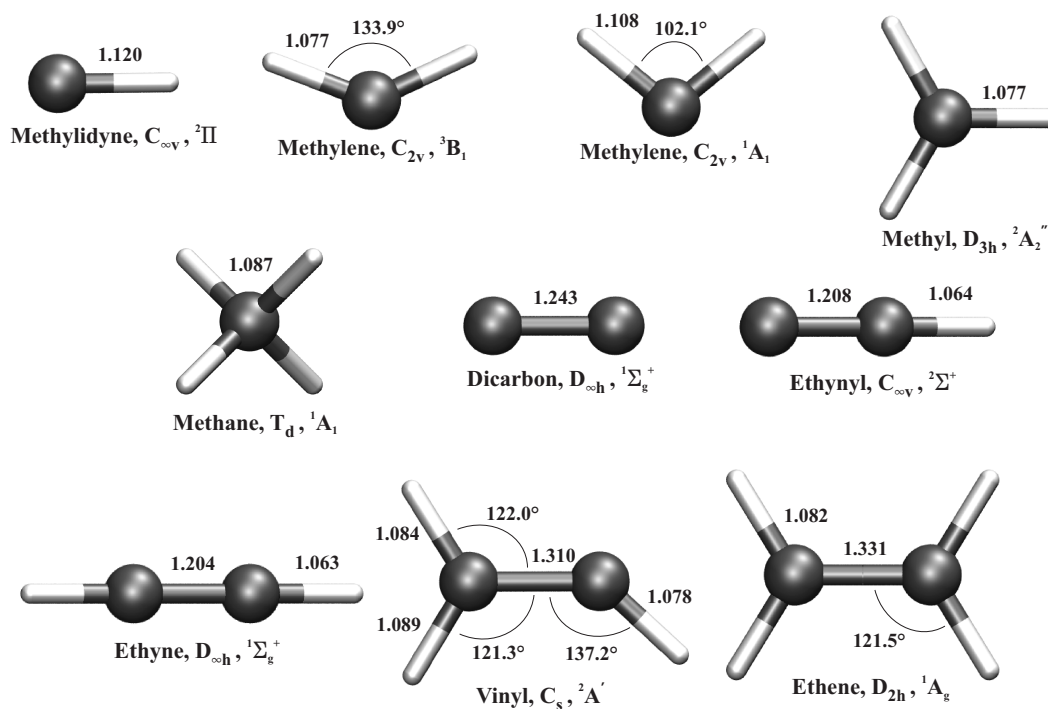
Figure 5.1: ROHF-CCSD(T)(Full)/cc-pCVQZ′ optimized geometries of the CH_x and C_2H_x (x = 0 . . . 4) species of Table 5.1. All bond lengths in Å.

vibrational corrections—provides atomization energies (column "Calc." in Table 5.1) with a mean absolute deviation of 1.4 kJ/mol from the ATcT values (1 kcal/mol 95% confidence limit or 1–2 kJ/mol mean absolute deviation may be regarded as chemical accuracy). The CCSD(T) calculations of the C_2 molecule and the C_2H radical exhibit the largest errors (−4.2 and −3.8 kJ/mol, respectively).

We have included the small CH_x and C_2H_x species in the present study to test the accuracy of the applied computational approach. For example, ZPVEs of diatomic molecules are accurately known from experiment. Concerning our systems, the experimental ZPVEs (including the often forgotten Dunham[137,138] Y_{00} term and spin–orbit coupling in form of a correction for the lowest *existing* rovibrational level) of CH and C_2 amount to 1416.2 cm^{-1} = 16.942 kJ/mol and 924.0 cm^{-1} = 11.053 kJ/mol, respectively. They agree with the calculated values (16.56 kJ/mol and 11.06 kJ/mol) to within 0.4 kJ/mol.

The electronic structures of (some of) the C_3H_x species are significantly more complex than those of the small C_1 and C_2 systems. Therefore, we may not expect that the computational data presented in Section 5.3.2 are accurate to

Table 5.1: CH$_x$ and C$_2$H$_x$ ($x = 0 \ldots 4$) isomers: Frozen-core (FC) and core–valence (CV) contributions to the equilibrium atomization energy D_e (0 K), harmonic (Harm.) and anharmonic (Anharm.) zero-point vibrational energy contributions E_{ZPVE}, spin–orbit energy contributions E_{SO}, first-order Darwin (Darwin) and mass–velocity (Ms.–Vel.) scalar relativistic energy contributions E_{SR}, and calculated (Calc.) and experimental or previous theoretical (Exptl./Theor.) atomization energy $\sum D_0$ (0 K). All values in kJ/mol.

Species	State	D_e(0 K)		E_{ZPVE}		E_{SO}	E_{SR}			$\sum D_0$ (0 K)	
		FC	CV	Harm.	Anharm.		Darwin	Ms.-Vel.	Calc.	ATcT	Exptl./Theor.
Methylidyne, CH	$^2\Pi$	350.93	0.61	-16.74	0.18^a	-0.35	0.38	-0.55	334.45	334.65±0.23	$334.74^{+0.13}_{-0.34}$ [Ref. 129]
Methylene, CH$_2$	$^3B_1$	794.15	3.15	-45.05	0.57	-0.35	1.68	-2.30	751.85	752.68±0.26	$753.03^{+0.43}_{-0.62}$ [Ref. 130]
	$^1A_1$	755.72	1.56	-43.16	0.46	-0.35	0.88	-1.24	713.86	715.02±0.26	$715.38^{+0.43}_{-0.62}$ [Ref. 130]
											713±2 [Ref. 131]
Methyl, CH$_3$	$^2A_2''$	1282.98	4.16	-77.32	0.90^a	-0.35	1.89	-2.61	1209.64	1209.66±0.14	1210.3±0.9 [Ref. 132]
Methane, CH$_4$	$^1A_1$	1753.10	4.88	-116.25	1.41	-0.35	2.08	-2.89	1641.97	1642.24±0.12	1642.2±0.6 [Ref. 132]
Dicarbon, C$_2$	$^1\Sigma_g^+$	606.96	3.96	-11.10	0.04^a	-0.71	2.17	-2.91	598.42	602.60±0.57	593±4 [Ref. 132]
											601.2±1.3 [Ref. 133]
											603.0±0.7 [Ref. 139]
Ethynyl, C$_2$H	$^2\Sigma^+$	1102.25	8.23	-38.15	0.75	-0.71	3.45	-4.61	1071.20	1074.99±0.29	1075.1±1.5 [Ref. 134]
Ethyne, C$_2$H$_2$	$^1\Sigma_g^+$	1684.92	9.62	-69.17	0.77	-0.71	3.46	-4.63	1624.27	1626.10±0.29	1619±1 [Ref. 132]
											1627±1 [Ref. 135]
Vinyl, C$_2$H$_3$	$^2A'$	1855.21^b	8.56	-95.49	1.24	-0.71	3.57	-4.86	1767.53	1768.24±0.88	
Ethene, C$_2$H$_4$	^1A_g	2349.01	9.24	-132.58	1.54	-0.71	3.78	-5.17	2225.11	2225.96±0.26	2225.5±0.7 [Ref. 132]

[a]UHF-CCSD(T)(Full)/cc-pCVTZ′

[b]Valence-shell triples correction (T) computed in the cc-pCVQZ′ basis

within a mean absolute deviation of 1.4 kJ/mol. Nevertheless, we believe that an accuracy very close to chemical accuracy is a realistic assumption.

In the following section, we shall discuss all of the nineteen C_3H_x species in great detail. All of these species have already been investigated on several occasions by other researchers and we shall compare our results with the corresponding data from the literature. These comparisons also reassure us that we have optimized the appropriate equilibrium structures (point-group symmetries) and electronic states (cf. Fig. 5.2).

5.3.2 C_3H_x species

In the following subsections, we discuss each of the nineteen C_3H_x species in some detail. Their equilibrium geometries are depicted in Fig. 5.2 and Fig. 5.3.

5.3.2.1   Tricarbon, C_3

Tricarbon was investigated in great detail and accuracy at the CCSD(T) level by Mladenović *et al.* in 1994.[141] These authors obtained an equilibrium C-C distance of 129.45 pm for the $^1\Sigma_g^+$ state in $D_{\infty h}$ symmetry. This is in full agreement with the CCSD(T)(Full)/cc-pCVQZ′ value of $r_e = 129.46$ pm obtained in the present work, which is however slightly larger than the B3LYP/6-311G(d,p) value of 129.1 pm.[142,143] Botschwina has argued that CCSD(T) calculations tend to overestimate the bond length of multiple CC bonds slightly (*e.g.*, by 0.1 pm) and therefore has reported a recommended value for the CC bond length of C_3 of 129.36±0.04 pm.[144]

Our best estimate of the atomization energy amounts to 1316 kJ/mol, which is in agreement with the NIST-JANAF value of 1323 ± 17 kJ/mol to within the experimental uncertainty. It is furthermore noteworthy that we have been able to compute the anharmonic correction to the ZPVE (0.13 kJ/mol) at the UHF-CCSD(T)(Full)/cc-pCVTZ′ level and that the basis-set incompleteness correction to the atomization energy amounts to 14.5 kJ/mol. The latter correction is defined as the difference between the frozen-core CCSD(T)-R12 and CCSD(T)(FC)/cc-pCVQZ′ results, that is, it corrects for the basis-set incompleteness error of the cc-pCVQZ′ basis.

Table 5.2: C_3H_x (x = 0...2) isomers: Frozen-core (FC) and core–valence (CV) contributions to the equilibrium atomization energy D_e (0 K), harmonic (Harm.) and anharmonic (Anharm.) zero-point vibrational energy contributions E_{ZPVE}, spin–orbit energy contributions E_{SO}, first-order Darwin (Darwin) and mass-velocity (Ms.–Vel.) scalar relativistic energy contributions E_{SR}, and calculated (Calc.) and experimental or previous theoretical (Exptl./Theor.) atomization energy $\sum D_0$ (0 K). All values in kJ/mol.

Species	State	D_e(0 K) FC	CV	E_{ZPVE} Harm.	Anharm.	E_{SO}	E_{SR} Darwin	Ms.-Vel.	$\sum D_0$ (0 K) Calc.	Exptl./Theor.
Tricarbon, C_3	$^1\Sigma_g^+$	1330.93	7.86	−20.78	0.13[a]	−1.06	2.48	−3.29	1316.27	1323±17 [Ref. 132]
Cyclopropynylidyne, c-C_3H	$^2B_2$	1678.46[b]	10.88	−49.94	0.38	−1.06	4.39	−5.93	1637.17	
Propynylidyne, l-C_3H	$^2\Pi$	1663.95[b]	10.75	−43.98	0.40[c]	−1.06	3.92	−5.25	1628.73	
Cyclopropenylidene, c-C_3H_2	$^1A_1$	2142.16	11.93	−84.28	0.82	−1.06	4.72	−6.39	2067.90	2064±10 [Ref. 140]
	$^3A^d$	1915.59[b]	11.43	−78.94	1.18[a]	−1.06	5.05	−6.86	1846.38	
Propadienylidene, CH_2CC	$^1A_1$	2079.53	11.01	−80.18	0.83[a]	−1.06	4.11	−5.55	2008.70	
	$^1A_1$	1952.98[b]	12.72	−78.89	0.73	−1.06	5.53	−7.47	1884.54	
Prop-2-ynylidene, HCCCH	$^1A'$	2029.99	11.93	−72.64	0.78	−1.06	4.57	−6.16	1967.41	
	$^3B^d$	2077.03[b]	13.60	−67.09	0.60	−1.06	5.41	−7.28	2021.22	
Propenediylidene,[e] HCCHC	$^3A''$	1831.01[b]	9.99	−71.87	0.16	−1.06	4.13	−5.60	1767.44	
Cyclopropene-1,2-diyl, c-CH_2CC	$^3B_1$	1846.61[b]	10.22	−82.94	0.80[c]	−1.06	4.61	−6.29	1771.95	

[a] UHF-CCSD(T)(Full)/cc-pCVTZ' value.
[b] Valence-shell triples correction (T) computed in the cc-pCVQZ' basis.
[c] Estimated.
[d] UHF-CCSD(T)/cc-pCVTZ' optimized geometry.
[e] Trans isomer.
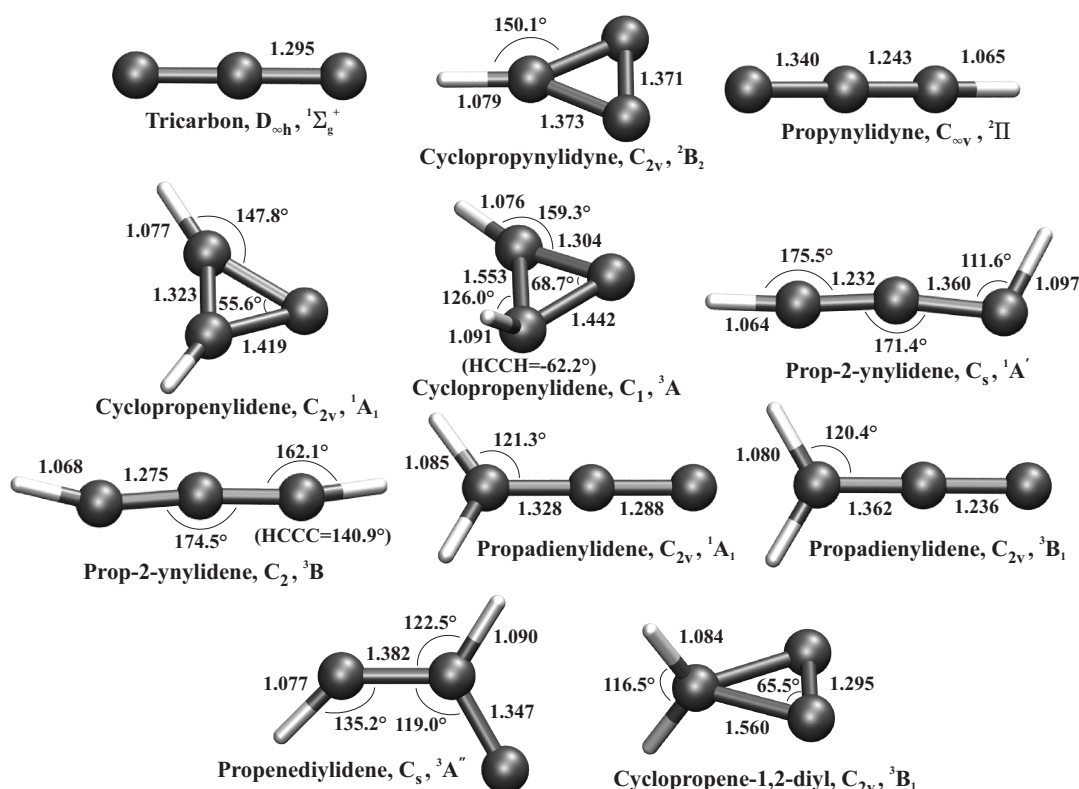
Figure 5.2: ROHF-CCSD(T)(Full)/cc-pCVQZ′ optimized geometries of the C_3H_x (x = 0 . . . 2) species of Table 5.2. All bond lengths in Å. The ^3A state of cyclopropenylidene and the ^3B state of prop-2-ynylidene were optimized at the UHF-CCSD(T)(Full)/cc-pCVTZ′ level.

Table 5.3: Literature comparison of the Tricarbon, C_3

Reference	Geometry	State	Symmetry	r(C-C)
Kaiser *et al.*[143]	B3LYP/6-311G(d,p)	$^1\Sigma_g^+$	$D_{\infty h}$	129.1
Schmatz *et al.*[141]	CCSD(T)/177 cGTOs	$^1\Sigma_g^+$	$D_{\infty h}$	129.45
This work	CCSD(T)/cc-pCVQZ′	$^1\Sigma_g^+$	$D_{\infty h}$	129.46

5.3.2.2   Cyclopropynylidyne, *c*-C_3H

We have computed the atomization energy of the cyclopropynylidyne radical in its $^2B_2$ ground state in C_{2v} symmetry,[145] with the molecule in the yz plane (concerning the symmetry conventions, see [Ref. 146]). We have optimized the geometry in C_{2v} symmetry at the CCSD(T)(Full)/cc-pCVQZ′ level but use the

accurate harmonic ZPVE of Stanton[147] obtained at the EOMIP-CCSD level to circumvent the problems related to the strong pseudo Jahn–Teller effects in the c-C_3H radical (note that the *anharmonic* contribution was obtained from DFT calculations). The CCSD(T)(Full)/cc-pCVQZ′ equilibrium distances (r_e(C-H) = 107.9 pm, r_e(C-CH) = 137.3 pm, and r_e(C-C) = 137.1 pm) compare to within 0.6 pm with the experimental r_s values of Yamamoto and Saito (107.6, 137.4, and 137.7 pm, respectively).[145]

Table 5.4: Literature comparison of the Cyclopropynylidyne, c-C_3H

Reference	Geometry	State	Symmetry	r(C-H)	r(C-CH)	r(C-C)
Kaiser *et al.*[143]	B3LYP/6-311G(d,p)	$^2B_2$	C_{2v}	108.2	137.3	136.8
Nguyen *et al.*[148]	MP2/6-311G(d,p)	$^2B_2$	C_{2v}	108.2	137.9	138.8
Yamamoto and Saito[145]	Exp.	$^2B_2$	C_{2v}	107.6	137.4	137.7
This work	CCSD(T)/cc-pCVQZ′	$^2B_2$	C_{2v}	107.9	137.3	137.1

We find the cyclopropynylidyne radical 8.4 kJ/mol below the linear isomer (*vide infra*). This is in line with the coupled-cluster results of other researchers,[148, 149] who report the cyclic isomer 6.7–7.1 kJ/mol below the linear form.

5.3.2.3 Propynylidyne, l-C_3H

Three isomers of C_3H are discussed in the literature; a cyclic c-C_3H (C_{2v} symmetry, *vide supra*), a linear l-C_3H ($C_{\infty v}$), and a bent b-C_3H (*trans*) form with C_s symmetry (cf. [Ref. 149]). The two linear structures l-C_3H and b-C_3H are virtually isoenergetic with the l-C_3H radical ca. 0.8 kJ/mol below b-C_3H at the CCSD(T)/cc-pVQZ level.[149] Hence, we have restricted our CCSD(T)(Full)/cc-pCVQZ′ geometry optimization to the linear l-C_3H isomer (for technical reasons, the calculation was performed in C_{2v} symmetry). It is difficult to compute the vibrational frequencies and the ZPVE for the linear l-C_3H radical in its $^2\Pi$ state because no stable wave function can be determined with the correct symmetry restrictions. Therefore, we follow the approach chosen by Ochsenfeld *et al.*[149] and adopt their CCSD(T)/TZP value for the b-C_3H isomer (43.98 kJ/mol). The anharmonic correction is crudely estimated to be of the same order of magnitude (0.4 kJ/mol) as for c-C_3H, which is sufficiently accurate in view of our target accuracy of ca. 4 kJ/mol and the remaining errors in the calculations. Our final atomization energy amounts to 1629 kJ/mol and contains a basis-set incompleteness correction of 18.8 kJ/mol.

Table 5.5: Literature comparison of the Propynylidyne, l-C_3H

Reference	Geometry	State	Symmetry	r(C-H)	r(C-CH)	r(C-C)
Kaiser *et al.*[143]	B3LYP/6-311G(d,p)	$^2\Pi$	$C_{\infty v}$	106.5	124.2	133.6
Takahashi *et al.*[150]	MP2/6-31G(d,p)	$^2\Pi$	$C_{\infty v}$	106.3	120.0	136.4
This work	CCSD(T)/cc-pCVQZ$'$	$^2\Pi$	$C_{\infty v}$	106.5	124.3	134.0

5.3.2.4   Singlet cyclopropenylidene, c-C_3H_2

We have optimized the $^1A_1$ ground state of c-C_3H_2 in C_{2v} symmetry at the CCSD(T)(Full)/cc-pCVQZ$'$ level. The internuclear distances agree to within 0.7 pm with the coupled-cluster results of Sherill *et al.*[151] and to within 0.5 pm with those of Seburg *et al.*[152] Furthermore, we obtain virtually the same harmonic ZPVE (84.3 kJ/mol) as in [Ref. 152] (85.1 kJ/mol). Calculations of the $^1A_1$ state of cyclopropenylidene appear to be straightforward, and our final atomization energy of 2068 kJ/mol may be regarded as a reliable value. The correction for basis-set incompleteness contributes 25.4 kJ/mol to this atomization energy. Concerning the reaction

$$C_2H_3(^2A') + C(^3P) \rightarrow c\text{-}C_3H_2(^1A_1) + H(^2S) \,, \tag{5.1}$$
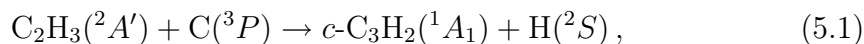
Nguyen *et al.* report an exothermic energy of reaction (at 0 K) of -69.5 kcal/mol (-291 kJ/mol) at the CCSD(T)/6-311+G(3df,2p) level. We obtain -300 kJ/mol for this reaction energy (cf. Table 5.2 and Table 5.15). The difference of 9 kJ/mol between both results can largely be traced back to the basis-set incompleteness and CV corrections (-5.5 and -3.4 kJ/mol) that are taken into account in the present work.

Clauberg *et al.* have reported an experimentally derived heat of formation of $\Delta_f H^0$ (298.15 K) = 114 ± 4 kcal/mol.[153] This value corresponds to a heat of reaction for the complete dissociation of $\Delta_r H^0$ (298.15 K) = 2109 ± 17 kJ/mol. Correcting for the difference $\Delta_r H^0$ (298.15 K) $- \Delta_r H^0$ (0 K) = 21.6 kJ/mol, which is estimated from the UHF-CCSD(T)/cc-pCVTZ$'$ harmonic vibrational frequencies and the experimental electronic energy levels of the C atom, the value of Clauberg *et al.*[153] yields an experimentally derived estimate of the atomization energy of singlet cyclopropenylidene of 2087 ± 17 kJ/mol. Our computed value is almost within the experimental uncertainty. Furthermore, Chyall and Squires have reported an experimentally derived $\Delta_f H^0$ (298.15 K) of 119.5 ± 2.2 kcal/mol.[140]

This value leads to an experimentally derived estimate of the atomization energy of 2064 ± 10 kJ/mol, in agreement with our CCSD(T)-R12 value of 2068 kJ/mol.

Table 5.6: Literature comparison of the Singlet cyclopropenylidene, c-C_3H_2

Reference	Geometry	State	Symmetry	r(C-H)	r(C-CH)	r(HC-CH)
Kaiser *et al.*[143]	B3LYP/6-311G(d,p)	$^1A_1$	C_{2v}	108.0	142.3	132.3
Takahashi *et al.*[150]	MP2/6-31G(d,p)	$^1A_1$	C_{2v}	107.6	143.0	133.1
Sherill *et al.*[151]	CCSD(T)/TZ(2df/2pd)	$^1A_1$	C_{2v}	107.6	142.7	132.8
This work	CCSD(T)/cc-pCVQZ$'$	$^1A_1$	C_{2v}	107.7	141.9	132.3

5.3.2.5   Triplet cyclopropenylidene, c-C_3H_2

Triplet cyclopropenylidene displays C_1 symmetry and a ^3A state.[148,149] CC calculations on this system are unproblematic and we were able to compute the anharmonic correction to the ZPVE at the UHF-CCSD(T)(Full)/cc-pCVTZ$'$ level. In our calculations, the triplet state of cyclopropenylidene lies 222 kJ/mol above the singlet ground state, and the energy of reaction (at 0 K) of the reaction

$$C_2H_3(^2A') + C(^3P) \rightarrow c\text{-}C_3H_2(^3A) + H(^2S) \tag{5.2}$$
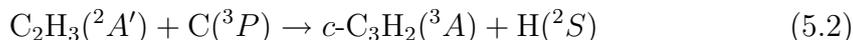
hence amounts to -79 kJ/mol. Nguyen *et al.*[148] have reported -71 kJ/mol for this reaction and the difference between their value and ours can again largely be explained by the basis-set incompleteness and CV corrections, which contribute -3.7 and -2.9 kJ/mol, respectively, to the reaction energy of (5.2).

Table 5.7: Literature comparison of the Triplet cyclopropenylidene, c-C_3H_2

Reference	Geometry	State	Symmetry	r(C-H$_1$)	r(C-H$_2$)	r(HC-CH)
Nguyen *et al.*[148]	B3LYP/6-311G(d,p)	^3A	C_1	107.3	109.0	156.6
Jonas *et al.*[154]	MP2/6-31G(d)	^3A	C_1	107.7	109.1	153.5
Ochsenfeld *et al.*[149]	CCSD(T)/TZP	^3A	C_1	107.3	108.8	155.1
This work	CCSD(T)/cc-pCVQZ$'$	^3A	C_1	107.6	109.1	155.3

5.3.2.6   Singlet propadienylidene, CH_2CC

Propadienylidene has a $^1A_1$ ground state in C_{2v} symmetry.[111,155] Our geometry optimization using CCSD(T)(Full)/cc-pCVQZ$'$ of this state is identical with the optimization carried out by Gauss and Stanton in 1999,[111] except that

we have used the slightly smaller cc-pCVQZ′ basis instead of the full cc-pCVQZ basis, and except that nine years after their work it is technically feasible to compute the gradient analytically.

Table 5.8: Literature comparison of the Singlet propadienylidene, CH_2CC

Reference	Geometry	State	Symmetry	r(C-H)	r(C-CH)	r(C-C)
Kaiser *et al.*[143]	B3LYP/6-311G(d,p)	$^1A_1$	C_{2v}	108.9	132.3	128.5
Jonas *et al.*[154]	MP2/6-31G(d)	$^1A_1$	C_{2v}	108.9	133.4	129.1
Gauss and Stanton[111]	CCSD(T)/cc-pCVQZ	$^1A_1$	C_{2v}	108.4	132.8	128.8
This work	CCSD(T)/cc-pCVQZ′	$^1A_1$	C_{2v}	108.5	132.8	128.8

Our analytical results are virtually in full agreement with the numerical results of [Ref. 111] (only the C-H distance is 0.1 pm longer in our optimization). We have computed the harmonic and anharmonic ZPVE at the CCSD(T)(Full)/cc-pCVTZ′ level, and our final atomization energy (2009 kJ/mol) is probably very reliable. This translates into a reaction energy of -241 kJ/mol for the reaction

$$C_2H_3(^2A') + C(^3P) \rightarrow CH_2CC(^1A_1) + H(^2S). \tag{5.3}$$
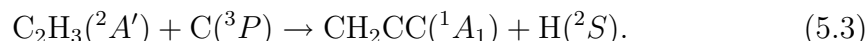
The corresponding frozen-core value in the 6-311+G(3df,2p) basis is -234 kJ/mol,[148] which seems reasonable in view of the basis-set incompleteness and CV corrections (-2.6 and -2.5 kJ/mol).

5.3.2.7   Triplet propadienylidene, $\mathbf{CH_2CC}$

In agreement with the works of Ochsenfeld *et al.*[149] and Rubio *et al.*,[156] we find a $^3B_1$ state in C_{2v} symmetry for the lowest triplet state of propadienylidene (with the molecule in the yz plane). At the CCSD(T)/TZP level, Ochsenfeld *et al.*[149] find C-C equilibrium distances of 123.8 and 136.9 pm and a C-H distance of 108.1 pm. Their H-C-H angle amounts to 119.0°. At the CCSD(T)/cc-pCVQZ′ level applied in the present work, the corresponding structural data are 123.6 pm, 136.2 pm, 108.0 pm and 119.2°, respectively. The adiabatic singlet–triplet splitting of the propadienylidene diradical has been reported to 29.7 kcal/mol (124 kJ/mol) by Robinson *et al.*, obtained from the photoelectron spectrum of the propadienylidene anion.[157] The difference between the atomization energies of the singlet and triplet species in Table 5.2 amounts to 124.2 kJ/mol (29.7 kcal/mol), which is in full agreement with the experimentally derived value.

Table 5.9: Literature comparison of the Triplet propadienylidene, CH_2CC

Reference	Geometry	State	Symmetry	r(C-H)	r(C-CH)	r(C-C)
Nguyen *et al.*[148]	B3LYP/6-311G(d,p)	$^3A''$	C_s	-	-	-
Jonas *et al.*[154]	MP2/6-31G(d)	$^3B_1$	C_{2v}	108.2	136.4	121.5
Ochsenfeld *et al.*[149]	CCSD(T)/TZP	$^3B_1$	C_{2v}	108.1	136.9	123.8
Rubio *et al.*[156]	CCSD(T)/TZ(2df,2pd)	$^3B_1$	C_{2v}	108.2	136.4	123.8
This work	CCSD(T)/cc-pCVQZ′	$^3B_1$	C_{2v}	108.0	136.2	123.6

5.3.2.8 Singlet prop-2-ynylidene, HCCCH

Although the triplet is the ground state of prop-2-ynylidene (propargylene), the singlet has been studied in great detail in the literature because of the competition between two possible structures that lie very close in energy.[158] Furthermore, the singlet state can of course occur as initial product in (photo)chemical reactions. The two possible structures display C_{2v} and C_s symmetry and can be characterized as a 1,3-diradical and a classical carbene, respectively. In the latter, the two C-C bonds differ by ca. 13 pm. In 1999, Stanton and Byun found that at the CCSD(T) level in a $5s4p3d2f/4s3p2d$ atomic natural orbital basis set for C/H, the C_s structure lies 437 cm^{-1} (ca. 5 kJ/mol) below the C_{2v} structure. At the CCSDT level with full triples (but in a small 6-31G* basis) this difference is reduced to only 25 cm^{-1}. Similar results are obtained by Nguyen *et al.*[148] from CCSD(T)/6-311+G(3df,2p) calculations that predict the C_s structure 1.7 kJ/mol below the C_{2v} structure.[148]

Table 5.10: Literature comparison of the Singlet prop-2-ynylidene, HCCCH

Reference	Geometry	State	Symmetry	r(C$_1$-C$_2$)	r(C$_2$-C$_3$)	A(C$_1$-C$_2$-C$_3$)
Nguyen *et al.*[148]	B3LYP/6-311G(d,p)	$^1A'$	C_s	-	-	-
Jonas *et al.*[154]	MP2/6-31G(d)	$^1A_1$	C_{2v}	123.7	137.0	168.2
This work	CCSD(T)/cc-pCVQZ′	$^1A_1$	C_{2v}	123.2	136.0	171.4

We note, however, that B3LYP/6-311G(d,p) calculations yield the opposite result with the 1,3-diradical C_{2v} structure 2.5 kJ/mol below the C_s carbene. Moreover, Rubio *et al.*[156] report that CASSCF geometry optimizations locate the C_s structure below the C_{2v} but that CASPT2 single-point calculations (performed at the CASSCF geometries) locate the C_{2v} structure 0.9 kJ/mol below the C_s structure. In any case, the C_{2v} and C_s structures are almost degenerate and for the present CCSD(T)-R12 calculations, we have decided to carry out calculations

for the C_s structure, which is favored by CCSD(T) theory.[158]

For the reaction

$$C_2H_3(^2A') + C(^3P) \rightarrow HCCCH(^1A') + H(^2S) , \tag{5.4}$$
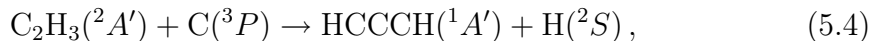
we obtain an energy of reaction of -200 kJ/mol, which is 10 kJ/mol more exothermic than at the CCSD(T)/6-311+G(3df,2p) level.[148] In our calculations, the basis-set incompleteness and core–valence correlation corrections both amount to -3.4 kJ/mol.

5.3.2.9   Triplet prop-2-ynylidene, HCCCH

We locate the ^3B ground state of prop-2-ynylidene 53.8 kJ/mol below the singlet C_s structure (Table 5.2). This value compares well with the CCSD(T)/6-311G+(3df,2p) value of Nguyen *et al.*[148] of 48.1 kJ/mol. In its ground state, prop-2-ynylidene displays C_2 symmetry.[148, 149, 156] On the triplet potential energy hypersurface calculated at the CCSD(T)/TZP level,[149] stationary points with Hessian index 1 (C_s symmetry) and 2 (C_{2v} symmetry) are found 0.5 and 0.7 kJ/mol, respectively above the C_2 minimum. It is noted, however, that single-point coupled-cluster calculations in the larger QZ2P basis set, carried out at the CCSD(T)/TZP geometries, located the C_s triplet 0.3 kJ/mol below the C_2 structure. At the CASPT2 level, Rubio *et al.*[156] have found the C_2 structure ca. 0.8 kJ/mol below the C_s structure. Since all of the above energy differences are below 1 kJ/mol, we have decided to concentrate our calculations on the C_2 structure, which is regarded as the global minimum on the triplet surface.[148, 149, 156]

Table 5.11: Literature comparison of the Triplet prop-2-ynylidene, HCCCH

Reference	Geometry	State	Symmetry	r(C-H)	r(C-CH)	A(C-C-C)
Nguyen *et al.*[148]	B3LYP/6-311G(d,p)	^3B	C_2	106.4	127.0	175.8
Jonas *et al.*[154]	MP2/6-31G(d)	^3B	C_2	106.7	126.6	174.9
Ochsenfeld *et al.*[149]	CCSD(T)/TZP	^3B	C_2	106.7	127.9	171.9
This work	CCSD(T)/cc-pCVQZ′	^3B	C_2	106.8	127.5	174.5

5.3.2.10   *Trans*-Propenediylidene, HCCHC

Trans-propenediylidene (*trans* with respect to the H atoms) shows C_s symmetry and is 254 kJ/mol less stable than triplet prop-2-ynylidene (Table 5.2).

This value is consistent with the energy difference of 251 kJ/mol reported by Ochsenfeld *et al.*[149] at the CCSD(T)/QZ2P level (including ZPVE). Also their C-C bond lengths (134.9 and 139.2 pm) compare well with ours (134.7 and 138.2 pm). Nguyen *et al.*[148] report a slightly smaller relative energy (246 kJ/mol) from CCSD(T)/6-311+G(3df,2p) single-point calculations at B3LYP/6-311G(d,p) geometries, in which the C-C bond lengths are 135.4 and 137.4 pm.

Table 5.12: Literature comparison of the *Trans*-Propenediylidene, HCCHC

Reference	Geometry	State	Symmetry	r(C-H$_1$)	r(C-CH)	r(HC-CH)
Nguyen *et al.*[148]	B3LYP/6-311G(d,p)	$^3A''$	C_s	109.3	135.4	137.4
Ochsenfeld *et al.*[149]	CCSD(T)/QZ2P	$^3A''$	C_s	109.2	134.9	139.2
This work	CCSD(T)/cc-pCVQZ′	$^3A''$	C_s	109.0	134.7	138.2

5.3.2.11 Cyclopropene-1,2-diyl, *c*-CH$_2$CC

Cyclopropene-1,2-diyl (cyclopropyne) has C_{2v} symmetry (nonplanar, perpendicular structure) and a $^3B_1$ ground state when the C atoms are chosen to lie in the xz plane and the H atoms in the yz plane.[146] In the CCSD(T)(Full)/cc-pCVQZ′ equilibrium structure, the two equivalent C-C bonds are 156.0 pm and the unique C-C bond is 129.5 pm long. Other researchers have found the corresponding values 155.6/130.0 pm (CISD/DZP),[151] and 156.7/128.9 pm [B3LYP/6-311G(d,p)].[148] We find triplet cyclopropyne 249 kJ/mol above triplet prop-2-ynylidene, the global minimum on the triplet surface (*vide supra*). This value can be compared with the CCSD(T)/6-311+G(3df,2p) value of Nguyen *et al.*,[148] which amounts to 238 kJ/mol.

Table 5.13: Literature comparison of the Cyclopropene-1,2-diyl, *c*-CH$_2$CC

Reference	Geometry	State	Symmetry	r(C-H)	r(C-CH)	r(C-C)
Nguyen *et al.*[148]	B3LYP/6-311G(d,p)	$^3B_1$	C_{2v}	108.8	156.7	128.9
Jonas *et al.*[154]	MP2/6-31G(d)	$^3B_1$	C_{2v}	108.9	155.6	130.7
Rubio *et al.*[156]	CISD/DZP	$^3B_1$	C_{2v}	108.9	155.6	130.0
This work	CCSD(T)/cc-pCVQZ′	$^3B_1$	C_{2v}	108.4	156.0	129.5

Table 5.14: Literature comparison of the 2-Propynyl, CH_2CCH

Reference	Geometry	State	Symmetry	$r(C-H_1)$	$r(C-CH_1)$	$r(H_2C-C)$
Nguyen *et al.*[148]	B3LYP/6-311G(d,p)	$^2B_1$	C_{2v}	106.2	122.2	136.7
This work	CCSD(T)/cc-pCVQZ′	$^2B_1$	C_{2v}	106.3	122.3	137.5

5.3.2.12   2-Propynyl, CH_2CCH

2-Propynyl (propargyl) is the most stable C_3H_3 isomer on the doublet surface. The planar radical shows C_{2v} symmetry and has a $^2B_1$ ground state (with the molecule in the yz plane).

In 1970, Walsh reported an experimental value for the heat of formation of $\Delta_f H^0$ (298.15 K) = 360.5 ± 5 kJ/mol,[159] which gives $\Delta_r H^0$ (298.15 K) = 2443.5 kJ/mol for the atomization reaction.
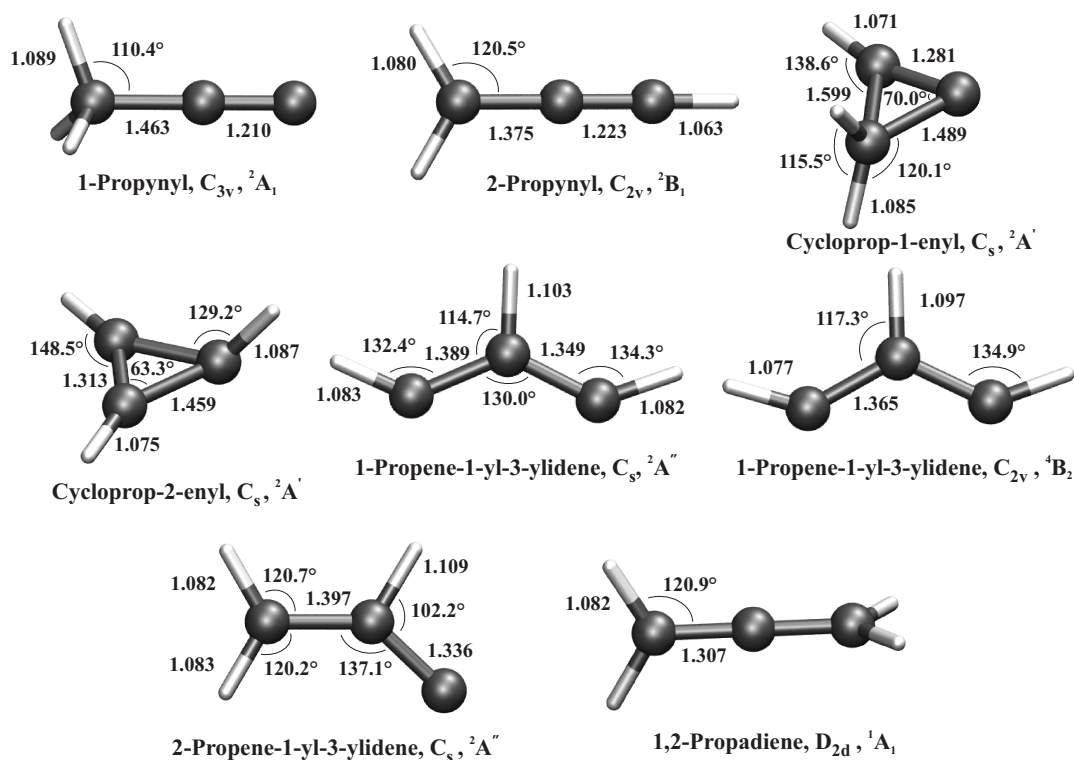
Figure 5.3: ROHF-CCSD(T)(Full)/cc-pCVQZ′ optimized geometries of the C_3H_x (x = 3, 4) species of Table 5.15. All bond lengths in Å. The $^2A''$ states of 1-propene-1-yl-3-ylidene and 2-propene-1-yl-3-ylidene were optimized at the UHF-CCSD(T)(Full)/cc-pCVTZ′ level.

Correcting for the difference $\Delta_r H^0$ (298.15 K) $- \Delta_r H^0$ (0 K) = 25.2 kJ/mol, which is estimated from the UHF-CCSD(T)/cc-pCVTZ' harmonic vibrational frequencies and the experimental electronic energy levels of the C atom, we obtain an experimentally derived estimate for the atomization energy of 2418±5 kJ/mol, in reasonable agreement with our theoretical value (2424 kJ/mol). More recently, Robinson et al.[157] experimentally derived the value $\Delta_f H^0$ (298.15 K) = 345 ± 13 kJ/mol, which yields an atomization energy of $\sum D_0$ (0 K) = 2434 ± 13 kJ/mol. The heat of formation of Robinson et al.[157] has been confirmed by Harkless and Lester by means of diffusion Monte Carlo (DMC) calculations.[160] These authors report $\Delta_f H^0$ (298.15 K) = 345.2 ± 2.5 kJ/mol in full agreement with the experimental value of Robinson et al.[157] However, the two DMC values for the atomization energy of propargyl reported in [Ref. 160] (without ZPVE, that is, $\sum D_e$ = 607.6 and 608.6 kcal/mol) are ca. 3–4 kcal/mol larger than our value (2530.4 kJ/mol or 604.8 kcal/mol).

Very recently, Wheeler and co-workers[79] reported the theoretically determined value $\Delta_f H^0$ (0 K) = 84.76 kcal/mol (354.6 kJ/mol) with an error not larger than 0.3 kcal/mol. This value translates into an atomization energy of $\sum D_0$ (0 K) = 2427 ± 1 kJ/mol, only 3 kJ/mol larger than our value. The value of Wheeler et al.[79] was obtained via the reactions

$$CH_2CCH_2(^1A_1) + CH_3(^2A_2'') \rightarrow CH_2CCH(^2B_1) + CH_4(^1A_1) \qquad (5.5)$$

and

$$CH_3CCH(^1A_1) + CH_3(^2A_2'') \rightarrow CH_2CCH(^2B_1) + CH_4(^1A_1) \qquad (5.6)$$

using accurate heats of formation for 1,2-propadiene (allene) and propyne, respectively. Our $\Delta_r H^0$ (0 K) value for reaction (5.5) amounts to -57.9 kJ/mol while at the focal-point extrapolated CCSD(T) level of Wheeler et al. the corresponding value is -59.5 kJ/mol. Changing the correlation treatment to the CCSDT(Q) approach (full triples with corrections for quadruples) changed this value by -0.7 kJ/mol to -60.2 kJ/mol.[79]

5.3.2.13   1-Propynyl, CH$_3$CC

1-Propynyl exhibits a $^2A_1$ ground state in C_{3v} symmetry. Our calculations locate 1-propynyl 174.0 kJ/mol above 2-propynyl while Nguyen et al.[148] report an energy difference of 168 kJ/mol at the CCSD(T)/6-311+G(3df,2p) level. At

Table 5.15: C_3H_3 isomers and 1,2-Propadiene: Frozen-core (FC) and core–valence (CV) contributions to the equilibrium atomization energy D_e (0 K), harmonic (Harm.) and anharmonic (Anharm.) zero-point vibrational energy contributions E_{ZPVE}, spin–orbit energy contributions E_{SO}, first-order Darwin (Darwin) and mass–velocity (Ms.–Vel.) scalar relativistic energy contributions E_{SR}, and calculated (Calc.) and experimental or previous theoretical (Exptl./Theor.) atomization energy $\sum D_0$ (0 K). All values in kJ/mol.

Species	State	D_e(0 K) FC	CV	E_{ZPVE} Harm.	Anharm.	E_{SO}	E_{SR} Darwin	Ms.–Vel.	$\sum D_0$ (0 K) Calc.	Exptl./Theor.
2-Propynyl, CH₂CCH	²B₁	2519.18[a]	14.18	−106.82	0.73	−1.06	5.53	−7.46	2424.28	2427±1 [Ref. 159]
										2434±13 [Ref. 157]
1-Propynyl, CH₃CC	²A₁	2352.87[a]	13.22	−114.73	1.97	−1.06	5.69	−7.70	2250.26	2252±1 [Ref. 79]
Cycloprop-1-enyl, c-CH₂CHC	²A'	2354.21[a]	12.45	−112.86	1.53	−1.06	5.40	−7.36	2252.31	2253±1 [Ref. 79]
Cycloprop-2-enyl, c-CHCHCH	²A'	2389.48[a]	13.50	−112.48	1.55	−1.06	5.85	−7.95	2288.88	2291±1 [Ref. 79]
1-Propene-1-yl-3-ylidene	²A''[b,c]	2182.01[a]	11.34	−101.27	1.52[d]	−1.06	5.31	−7.24	2090.69	
	⁴B₂	2216.26[a]	12.13	−103.19	1.40	−1.06	5.37	−7.31	2123.61	
2-Propene-1-yl-3-ylidene	²A''[b]	2315.89[a]	11.00	−107.80	2.13[d]	−1.06	4.42	−6.02	2218.56	
1,2-Propadiene, CH₂CCH₂	¹A₁	2929.00	14.32	−143.21	1.66	−1.06	5.60	−7.59	2798.71	2799.3±1.3 [Ref. 136]

[a]Valence-shell triples correction (T) computed in the cc-pCVQZ' basis.
[b]UHF-CCSD(T)/cc-pCVTZ' optimized geometry.
[c]UHF reference was used.
[d]B97-1/6-31+G**.

the frozen-core CCSD(T) level, without ZPVE and other corrections, the energy difference between 1-propynyl and 2-propynyl amounts to 166.3 kJ/mol in our calculations (with an basis-set incompleteness correction of only 0.3 kJ/mol), whereas Nguyen *et al.*[148] report 163.4 kJ/mol.

Table 5.16: Literature comparison of the 1-Propynyl, CH_3CC

Reference	Geometry	State	Symmetry	r(C-H)	r(C-CH)	r(C-C)
Nguyen *et al.*[148]	B3LYP/6-311G(d,p)	$^2A'$	C_s		-	-
This work	CCSD(T)/cc-pCVQZ′	$^2A_1$	C_{3v}	108.9	146.3	121.0

Our value is in agreement with the value reported by Wheeler *et al.*, who obtained $\Delta_r H^0$ (0 K) = 175 kJ/mol for the reaction

$$CH_2CCH(^2B_1) \rightarrow CH_3CC(^2A_1). \tag{5.7}$$
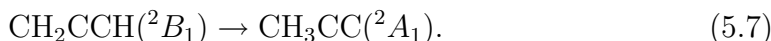
5.3.2.14 Cycloprop-1-enyl, *c*-CH$_2$CHC

Concerning the reaction

$$C_2H_3(^2A') + C(^3P) \rightarrow c\text{-}CH_2CHC(^2A'), \tag{5.8}$$

Nguyen *et al.* report an exothermic energy of reaction (at 0 K) of -111.8 kcal/mol (-468 kJ/mol) at the CCSD(T)/6-311+G(3df,2p) level. We obtain -485 kJ/mol for this reaction energy (cf. Table 5.2 and Table 5.15). Again, the difference between the two coupled-cluster results can be traced back partly to the basis-set incompleteness and CV corrections (-7.5 and -3.9 kJ/mol) that are taken into account in the present work. Taking the atomization energy (2253 kJ/mol) determined by Wheeler *et al.*[79] and the ATcT value for the vinyl radical from Table 5.1 also yields a reaction enthalpy of -485 kJ/mol.

Table 5.17: Literature comparison of the Cycloprop-1-enyl, *c*-CH$_2$CHC

Reference	Geometry	State	Symmetry	r(H$_1$C-CH$_2$)	r(C-CH$_1$)	r(C-CH$_2$)
Nguyen *et al.*[148]	B3LYP/6-311G(d,p)	$^2A'$	C_s	161.1	127.6	149.1
Nguyen *et al.*[148]	MP2/6-311G(d,p)	$^2A'$	C_s	162.7	125.6	149.6
This work	CCSD(T)/cc-pCVQZ′	$^2A'$	C_s	159.9	128.1	148.9

5.3.2.15 Cycloprop-2-enyl, c-CHCHCH

Nguyen *et al.* have found the $^2A'$ state of cycloprop-2-enyl at 8.8 kcal/mol (37 kJ/mol) below the $^2A'$ state of cycloprop-1-enyl, in agreement with our results. Table 5.15 reports a difference between the atomization energies of 36.6 kJ/mol. The value obtained by Wheeler *et al.*[79] amounts to 37.3 kJ/mol. All of these values mutually agree to within 1 kJ/mol.

Table 5.18: Literature comparison of the Cycloprop-2-enyl, c-CHCHC

Reference	Geometry	State	Symmetry	r(HC-C$_1$)	r(C$_1$-C$_2$)	r(C$_2$-C$_3$)
Nguyen *et al.*[148]	B3LYP/6-311G(d,p)	$^2A'$	C_s	109.2	146.2	131.1
This work	CCSD(T)/cc-pCVQZ′	$^2A'$	C_s	108.7	145.9	131.3

5.3.2.16 Doublet 1-Propene-1-yl-3-ylidene, CHCHCH

Le *et al.*[161] have performed CCSD(T)/6-311G(d,p)//B3LYP/6-311G(d,p) calculations of the reaction

$$C_2H_4(^1A_g) + C(^3P) \rightarrow CHCHCH(^2A'') + H(^2S) \qquad (5.9)$$

and obtained an endothermic reaction energy of 142 kJ/mol (at 0 K, including ZPVE). Our best estimate amounts to 134 kJ/mol.

Table 5.19: Literature comparison of the Doublet 1-Propene-1-yl-3-ylidene, CHCHCH

Reference	Geometry	State	Symmetry	r(H-C$_1$)	r(C$_1$-C$_2$)	r(C$_1$-C$_3$)
Nguyen *et al.*[148]	B3LYP/6-311G(d,p)	$^2A''$	C_s	110.4	138.0	134.6
This work	CCSD(T)/cc-pCVQZ′	$^2A''$	C_s	110.3	138.9	134.9

5.3.2.17 Quartet 1-Propene-1-yl-3-ylidene, CHCHCH

Vereecken *et al.*[97] found the $^4B_2$ state of 1-propene-1-yl-3-ylidene about 26 kJ/mol below the doublet state (ZPVE included) at the level of B3LYP-DFT/6-31G** level. The corresponding value obtained in the present work is 33 kJ/mol.

5.3.2.18   2-Propene-1-yl-3-ylidene

The planar 2-propene-1-yl-3-ylidene radical has a $^2A''$ ground state in C_s symmetry. We obtain an exothermic energy of reaction (at 0 K) of -451 kJ/mol for the reaction

$$C_2H_3(^2A') + C(^3P) \rightarrow CH_2CHC(^2A''), \qquad (5.10)$$

whereas Nguyen *et al.* report -105.0 kcal/mol (-439 kJ/mol) at the CCSD(T)/6-311+G(3df,2p) level.

Table 5.20: Literature comparison of the 2-Propene-1-yl-3-ylidene

Reference	Geometry	State	Symmetry	r(H-C$_1$)	r(C$_1$-CH)	r(C$_1$-C)
Nguyen *et al.*[148]	B3LYP/6-311G(d,p)	$^2A''$	C_s	112.3	132.3	139.0
This work	CCSD(T)/cc-pCVQZ′	$^2A''$	C_s	110.9	133.6	139.7

5.3.2.19   1,2-Propadiene, CH$_2$CCH$_2$

The experimentally derived atomization energy of 1,2-propadiene (or allene) amounts to $2\,799.3 \pm 1.3$ kJ/mol. Our computed value ($2\,798.7$ kJ/mol) agrees with this value to within the experimental error bar. The agreement between the calculated and experimental numbers highlights the accuracy of our computational approach based on the CCSD(T)-R12 method. Note, however, that 1,2-propadiene is a simple closed-shell molecule and single-reference case. The accuracy for the radicals and open-shell systems may be somewhat lower.

5.4   Conclusions

We have performed explicitly-correlated coupled-cluster calculations at the level of CCSD(T)-R12 theory on nineteen molecules and radicals of the type C$_3$H$_x$. Spin-restricted Hartree–Fock reference wave functions were used in conjunction with very large basis sets ($19s14p8d6f4g3h$ for C and $9s6p4d3f$ for H). CCSD-R12 calculations could be carried out with as many as 840 (C$_3$H$_3$) or 908 (C$_3$H$_4$) basis functions, but the (T) triples correction had to be computed in a smaller quadruple-zeta basis set on a few occasions.

It was demonstrated by similar calculations on selected CH$_x$ and C$_2$H$_x$ species that the CCSD(T)-R12 approach has the potential to yield very accurate atom-

ization energies. For these species, the calculated atomization energies agreed with the ATcT values to within 1.4 kJ/mol (mean absolute deviation), more or less within chemical accuracy (1 kcal/mol).

The atomization energies presented here may serve as benchmark data for future explicitly-correlated coupled-cluster calculations using STGs in the place of the linear r_{12} terms, as suggested by Ten-no.[162] At the level of CCSD(T) theory, the use of STGs makes possible calculations in (augmented) triple-zeta basis sets that are as accurate as those in (augmented) quintuple-zeta basis sets.[163, 164] Hence, much smaller basis sets than those used in the present work may be used and much larger systems may be treated in the future.

Chapter 6

Hydrogen Abstraction by the Hydroperoxyl Radical from Methane

6.1 Introduction

In the detailed chemical kinetic modeling of hydrocarbon[165] and oxygenated fuels, hydrogen atom abstraction by the hydroperoxyl radical, $HO_2^\bullet$, is an important reaction class in the autoignition of fuels, particularly at low to intermediate temperatures in the range 600 to 1,300 K. At these temperatures most of the hydroperoxyl radicals are generated either by abstraction of a hydrogen atom by molecular oxygen, or by the reaction of atomic hydrogen with molecular oxygen:

$$RH + O_2 \rightarrow R^\bullet + HO_2^\bullet$$
$$H^\bullet + O_2 + M \rightarrow HO_2^\bullet + M$$
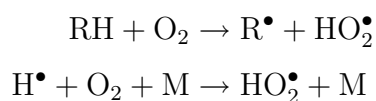
The hydroperoxyl radical produced in the above sequence can either self react or abstract a hydrogen atom generating hydrogen peroxide, which subsequently decomposes to produce two reactive hydroxyl radicals:

$$RH + HO_2^\bullet \rightarrow R^\bullet + H_2O_2$$
$$HO_2^\bullet + HO_2^\bullet \rightarrow H_2O_2 + O_2$$
$$H_2O_2 + M \rightarrow HO^\bullet + HO^\bullet + M$$
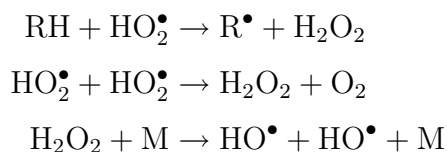
It has been shown[166,167] that changing the relative rates of (i) abstraction by the hydroperoxyl radical and (ii) its self reaction either promotes in (i) or inhibits in (ii) the reactivity of a fuel. The self reaction of hydroperoxyl radicals inhibit fuel reactivity as this reaction consumes hydroperoxyl radicals, which could otherwise abstract a hydrogen atom from a stable species to ultimately produce two hydroxyl radicals from one hydroperoxyl radical, as depicted in the reactions above. As the temperature increases, the reaction of a hydrogen atom with molecular oxygen produces a hydroxyl radical via $H^\bullet + O_2 \rightarrow O^\bullet + HO^\bullet$, becoming the most dominant chain branching reaction at higher temperatures.[168]

Despite this there are very few reliable determinations of the rates of hydrogen atom abstraction from hydrocarbons by the hydroperoxyl radical; all of these were obtained from measurements in boric acid-coated static reactors by an indirect technique over a quite narrow range of temperatures;[169–173] most values have been estimated.[174–178]

Quantum chemical calculation can provide accurate structural and energetic data of small polyatomic molecules of relevance to *inter alia* combustion chemistry. Concerning reaction barriers for hydrogen abstractions, an overview of the performance of density functionals has been recently presented by Sousa *et al.*[179] The authors conclude that B3LYP performs poorly for such reactions. Vandeputte *et al.*[180] extensively studied the behavior of CBS-QB3[181] calculating reaction barriers and reaction rates for hydrogen abstractions. They found very good agreement for the barrier height for the abstraction by methyl from methane, in comparison with a high-level W1 calculation. A much poorer result was found for the abstraction by methyl from ethene. In all the cases treated the calculated reaction rate computed with CBS-QB3 was satisfactory in comparison with experimental reaction rates.

Our goal in this work is to compute the reaction barriers for the series of reaction of $HO_2^\bullet$ with methane, ethane, propane, n-butane and iso-butane, see Fig. 6.1, as studied by Carstensen and co-workers[182] at the CBS-QB3 level of theory. In our work we use the CCSD(T) level in an attempt to obtain reaction barriers with chemical accuracy, that is within ~ 4 kJ mol^{-1}, and obtain from them the reaction rates. Such accuracy can only be achieved by performing the CCSD(T) calculations in very large and nearly complete one-electron basis sets, followed by basis-set extrapolation, or by expanding the coupled-cluster wavefunction in a
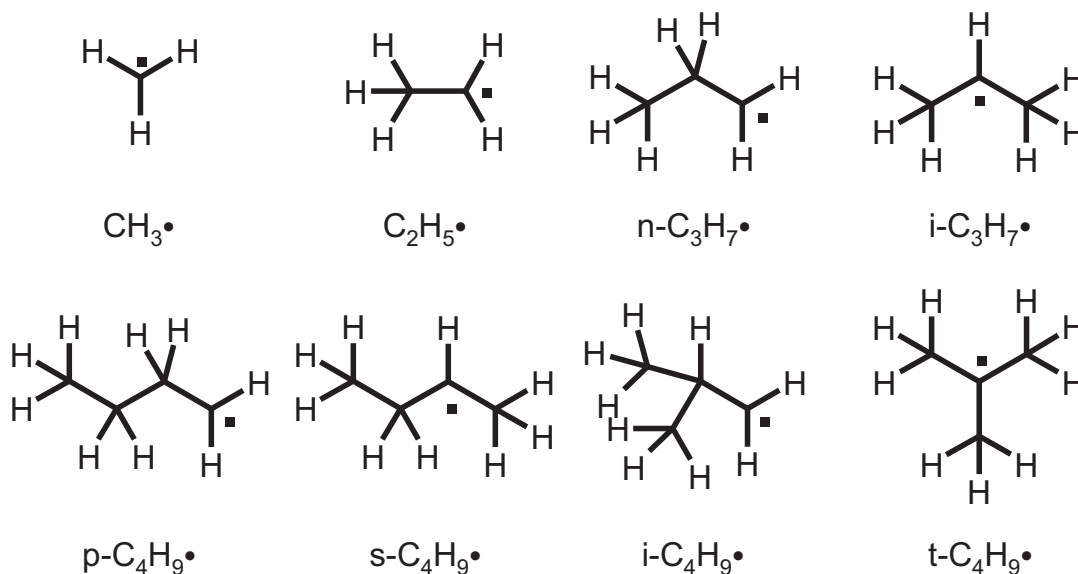
Figure 6.1: Set of radicals formed in $RH + HO_2^\bullet \rightarrow R^\bullet + H_2O_2$

many-electron basis that contains terms that depend explicitly on the interelectronic distances in the system.[106]

The general theory of the explicitly-correlated coupled-cluster approach is described in detail by Noga *et al.*[107] and a number of review articles exist.[16, 100, 183] In 2000, the theory was extended to single-reference open-shell cases with unrestricted Hartree-Fock (UHF) and restricted open-shell Hartree-Fock (ROHF) reference determinants[17, 184] and illustrative applications of explicitly-correlated coupled-cluster theory have been reported recently.[101, 163, 185, 186]

6.2   Computational details

Reaction barriers

Geometry optimizations utilizing analytical nuclear gradients are carried out to locate minima and saddle points at the level of density functional theory (DFT), using the B3LYP exchange-correlation functional[62, 63, 187] in combination with the def2-TZVP basis[188] as has been implemented in the TURBOMOLE program.[52, 54, 59, 60, 65, 66, 189] Redundant internal coordinates are used for the geometry optimizations and the search for saddle points is performed using the trust radius image minimization approach (TRIM).[28] Harmonic frequencies are calculated an-

alytically for all species at the B3LYP/def2-TZVP level and are used unscaled throughout the work. The frequencies of the minima are all real, and the saddle points exhibit only one imaginary frequency.

Moreover, single-point energy calculations are carried out in the same basis using the functionals BP86,[57,58] TPSS,[68] TPSSh,[69] BMK[64] and B97K;[64] the compound methods CBS-QB3 and CBS-APNO[190] calculated with GAUSSIAN; and conventional spin-restricted coupled-cluster theory in the correlation-consistent triple-zeta basis (cc-pVTZ) of Dunning.[9] These spin-restricted coupled-cluster calculations are based on a spin-restricted Hartree-Fock reference (restricted Hartree-Fock, RHF, or restricted open-shell Hartree-Fock, ROHF) and are carried out with MOLPRO. The coupled-cluster calculations include singles and doubles (RCCSD)[191] as well as perturbative triples [RCCSD(T)][192] and are performed in the frozen core approximation.

In the detailed study of the $CH_4 + HO_2^\bullet$ system the conventional coupled-cluster method with the family of n-tuple-zeta basis sets (cc-pVnZ) with n=2,3,4 and 5 is used.[9] In this system, integral-direct explicitly-correlated CCSD-R12 calculations are performed with the DIRCCR12-OS program[101] using a spin-restricted Hartree-Fock reference wave function (RHF or ROHF). A spin-restricted coupled-cluster calculation is performed for the closed-shell systems while the open-shell systems are treated at the spin-unrestricted coupled-cluster ROHF-UCCSD-R12 level. For comparison, the conventional coupled-cluster calculations in the cc-pVnZ basis sets on this system are carried out similarly, that is, using the ROHF-UCCSD(T) method for the open shells. The CCSD-R12 calculations are carried out in the 19s14p8d6f4g3h basis (9s6p4d3f for H).[193] The perturbative triples are taken from the conventional coupled-cluster approach.

Reaction rates

For the calculation of reaction rate constants, simple transition state theory is used. Observed rates are of course dependent on the whole potential energy surface and not just the reactants and the transition state, but it would be computationally too expensive to use some of the methodologies employed here for that purpose. The well-known expression for the reaction rate constant of a bimolecular reaction $X + Y \rightarrow XY^{\ddagger}$ is:

$$k = \kappa V_m \sigma_{TOT} \frac{k_B T}{h} \frac{q^{\ddagger}}{q_X q_Y} \exp\left(\frac{-\Delta E_{B,0}}{RT}\right) \tag{6.1}$$

where $q^{\ddagger}$, q_X and q_Y are the dimensionless partition functions (including translational, vibrational and rotational contributions) of the transition state and the reactants, respectively, calculated using the module FREEH of TURBOMOLE (using the harmonic oscillator, rigid rotor approximation and correcting for internal hindered rotations). R is the gas constant, k_B the Boltzmann constant, h the Planck constant and V_m the molar volume of an ideal gas at temperature T, which varied from 600 to 1,300 K in the present work. σ_{TOT} is the total symmetry factor. $\Delta E_{B,0}$ is the electronic barrier height $\Delta E_{B,e}$ plus the zero-point vibrational energy (ZPVE). The ZPVE is computed at the B3LYP/def2-TZVP level and is included for all the methods under study. κ is the transmission coefficient accounting for tunneling effects, computed from the well-known Wigner formula:

$$\kappa = 1 - \frac{1}{24}\left(\frac{h\nu}{k_B T}\right)^2 \left(1 + \frac{RT}{\Delta E_{B,0}}\right) \tag{6.2}$$

Only the imaginary frequency, ν, associated with the reaction coordinate and the reaction barrier $\Delta E_{B,0}$ are required to calculate κ. For the temperature range of interest here, the Wigner formula does not yield transmission coefficients significantly different from the Eckart formula nor from the approach proposed by Skodje and Truhlar.[36] For example, for a prototypical system with $\nu = 1650i$ cm^{-1} and $\Delta E_{B,0} = 90$ kJ mol^{-1}, which represents our systems well, Truhlar's approach and the Eckart formula give identical results in the temperature range 700–1,300 K and are not more than 15% larger than the Wigner transmission coefficient. At 1,300 K, $\kappa_{\text{Wigner}} = 1.16$ and $\kappa_{\text{Eckart}} = 1.15$, whereas at 700 K, $\kappa_{\text{Wigner}} = 1.51$ and $\kappa_{\text{Eckart}} = 1.71$, and only at lower temperatures the differences become more pronounced, for example at 600 K, $\kappa_{\text{Wigner}} = 1.69$ and $\kappa_{\text{Eckart}} = 2.16$.

Corrections to account for hindered rotations are included and will be explained in detail in 6.4, where the results obtained are shown.

Arrhenius-like expressions of the form:

$$k = AT^n \exp\left(\frac{-E_A}{RT}\right) \tag{6.3}$$

are fitted to the computed rate constants at temperatures 600 to 1,300 K (in 100 K intervals); A, n and E_A are treated as fitting parameters. We fit the above

expression to rate constants computed from the B3LYP/def2-TZVP partition functions (corrected for hindered rotations) with the best estimates of the reaction barriers $\Delta E_{B,0}$ obtained at the coupled-cluster level of theory (*vide infra*). Note that these best estimates are used not only in the exponential but also in the Wigner formula for the transmission coefficient κ.

In this section, we have shown the procedure used to calculate the rate constants. It mimics the one employed by Carstensen *et al.* except that we have used alternative methods to compute the reaction barrier. This allows us to focus on the differences arising from these contrasting approaches. Note that the consequences of using B3LYP geometries, albeit with different basis functions, which both Carstensen *et al.* and ourselves employ, are difficult to predict. To improve on this one could optimize all of the geometries at the coupled-cluster level of theory, but even then, the overall accuracy will remain difficult to assess due to the approximations in the TST treatment.

6.3   Benchmarking

Before presenting and discussing the results for all the reactions, let us first have a close look at the barrier for the reaction:

$$CH_4 + HO_2^{\bullet} \rightarrow TS^{\ddagger} \rightarrow CH_3^{\bullet} + H_2O_2$$

For this reaction we calculate the optimized geometries at the B3LYP/def2-TZVP level for the two reactants, the two products and the transition state $TS^{\ddagger}$. The geometry of the latter can be seen in Fig. 6.2.

We can compare the $C \cdots H$ distance in the $TS^{\ddagger}$, 1.430 , with the same distance found in the CH_4 minimum, 1.090 . The $H \cdots O$ distance is 1.124 for the $TS^{\ddagger}$ and 0.968 for the H_2O_2 minimum. This indicates a $TS^{\ddagger}$ very close to the products, $CH_3^{\bullet} + H_2O_2$, and agrees with Hammond's postulate[194] with respect to the endothermic character of the reaction under study. The electronic energies are obtained at the level of ROHF-UCCSD-R12 theory. This theory uses electronic wave functions that depend explicitly on all of the electron-electron distances and is capable of yielding results close to those that would be obtained in a complete basis set of atomic orbitals — if it were possible to use such a basis. To the CCSD-R12 energies, we add the perturbative (T) correction for connected triples
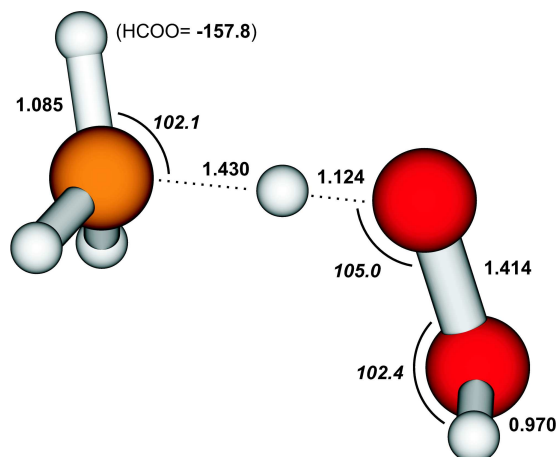
Figure 6.2: Geometry of the transition state of the $CH_4 + HO_2^{\bullet}$ reaction. Distances in angstroms and angles in degrees

computed in the cc-pV5Z basis, and we shall refer to the corresponding energies as CCSD(T)-R12 in short. Table 6.1 shows the electronic atomization energies for the five species involved in the above reaction, computed at this CCSD(T)-R12 level.

Table 6.1: Electronic Atomization Energies / kJ mol^{-1}.

System	Experiment[a]	Calculation[b]
CH_4	1755.4	1752.5
$HO_2^{\bullet}$	732.5	729.9
$TS^{\ddagger}$	$\cdots$	2372.6
$CH_3^{\bullet}$	1285.7	1283.0
H_2O_2	1122.1	1122.3

[a]Experimental atomization enthalpy at 0 K and experimental zero-point vibrational energy from [Ref. 195].
[b]Obtained by adding the (T) triples correction from cc-pV5Z basis to the ROHF-UCCSD(T)-R12 energies.

The CCSD(T)-R12 results agree to within 3 kJ mol^{-1} with well known experimental data, and we expect that the atomization energy of $TS^{\ddagger}$, and thus the barrier height, is similarly accurate. This assumption is based both in previ-

ous work on the explicitly-correlated methods and the low multireference character of the system; the latter was observed as we performed a multireference study (CASSCF) on the transition state TS‡, and found that the wavefunction is dominated by a single determinant. The agreement with experiment is very satisfactory. We should note that the seemingly extreme accuracy for H_2O_2 is a coincidence, since several corrections have been omitted. To obtain a better founded agreement it would be necessary to include higher excitations into the coupled-cluster treatment (full triples as well as quadruples and quintuples), to include core orbitals into the correlation treatment, and to correct for relativistic and non-Born-Oppenheimer effects,[196,197] but due to the amount of computational time required they are beyond the scope of this work.

The electronic reaction energy $\Delta E_{R,e}$ and the electronic barrier height $\Delta E_{B,e}$ can be calculated from the CCSD(T)-R12 data displayed in Table 6.1. We compare the CCSD(T)-R12 data with the results obtained from conventional CCSD(T) theory using the standard cc-pVnZ basis sets. Table 6.2 shows the computed data ($\Delta E_{R,e}$ and $\Delta E_{B,e}$) obtained with the conventional CCSD(T) method in the cc-pVnZ basis sets. The results show clearly that CCSD(T) calculations in small basis sets such as cc-pVDZ and cc-pVTZ are not accurate enough for our purposes. The deviations from the CCSD(T)-R12 values are 14–17 and 4–5 kJ mol^{-1}, respectively. Only in the case of the cc-pVQZ basis is the error below 3 kJ mol^{-1}.

Since the convergence of the computed data with the size of the atomic basis set is slow but systematic, it is possible to extrapolate the results to the limit of a complete basis (cc-pV∞Z) using the cc-pVQZ and cc-pV5Z values;[10] such an extrapolation yields energies that are only 0.2-0.3 kJ mol^{-1} away from the CCSD(T)-R12 data. This is a strong indication that both methods are accurate to within 1 kJ mol^{-1} of the basis-set limit of CCSD(T) theory.

6.4   Results

Reaction barriers

At present, it is possible to perform frozen-core CCSD-R12 calculations on the transition state of the reaction of CH_4 with the $HO_2^{\bullet}$ radical in the large 19s14p8d6f4g3h basis (9s6p4d3f for H), but similar calculations on the transition

Table 6.2: Reaction Energy, $\Delta E_{R,e}$, and Reaction Barrier, $\Delta E_{B,e}$, for $CH_4 + HO_2^{\bullet}$ $\rightarrow CH_3^{\bullet} + H_2O_2$ / kJ mol^{-1}.

Basis	$\Delta E_{R,e}$	$\Delta E_{B,e}$
cc-pVDZ	94.5	124.0
cc-pVTZ	81.9	113.5
cc-pVQZ	79.1	111.5
cc-pV5Z	77.9	110.5
cc-pV(Q5)Z[a]	77.0	109.6
CCSD(T)-R12	77.2	109.9

[a]Extrapolated from the cc-pVQZ and cc-pV5Z basis sets using the n^{-3} formula of Helgaker *et al.*[10]

states for the reactions with the larger hydrocarbons are technically not feasible. Therefore, we have calculated the electronic barrier heights for all the reactions in the def2-TZVP basis using various functionals and in the cc-pVTZ basis set using frozen-core RCCSD(T) theory.

For the reaction of the hydroperoxyl radical with methane, the B3LYP/def2-TZVP ZPVE correction to the barrier (applied to all the methods) amounts to -9.8 kJ mol^{-1}. Adding this contribution to the ROHF-UCCSD(T)/cc-pVTZ and CCSD(T)-R12 electronic barriers (*cf.* Table 6.2) yields $\Delta E_{B,0} = 103.7$ kJ mol^{-1} and $\Delta E_{B,0} = 100.1$ kJ mol^{-1}, respectively. Thus, the CCSD(T)/cc-pVTZ value appears to slightly overestimate the $CH_4 + HO_2^{\bullet}$ barrier height. This can be easily corrected by scaling the electron-correlation contribution to the electronic barrier $\Delta E_{B,e}$ by a factor of 1.053. This factor is the ratio between the correlation contribution in the R12 and cc-pVTZ basis sets. Note that the electron-correlation contribution to the barrier is negative. We adopt this scaling factor of 1.053 to obtain the best estimates of the barrier heights for all the reactions under study. Note also that since the factor applies only to the correlation contribution, $\Delta E_{B,e}$ using CCSD(T)-R12 is not equal to the best estimate (100.1 *versus* 100.4 kJ mol^{-1}) due to the different basis set used in the non-correlation contribution, but allows us to be consistent in the treatment of all the reactions under

study. So all of them are computed at the same level. The results are presented in Table 6.3, with the best estimates given in the last row.

Table 6.3: Reaction Barriers $\Delta E_{B,0}$, for the Reactions of the Hydrocarbons with the Hydroperoxyl Radical / kJ mol^{-1}.

Method[a]	$CH_3^\bullet$	$C_2H_5^\bullet$	$n\text{-}C_3H_7^\bullet$	$i\text{-}C_3H_7^\bullet$	$p\text{-}C_4H_9^\bullet$	$s\text{-}C_4H_9^\bullet$	$i\text{-}C_4H_9^\bullet$	$t\text{-}C_4H_9^\bullet$
B3LYP[b]	97.6	78.2	79.5	64.5	78.9	64.3	79.2	54.3
BP86	75.0	53.6	55.9	39.0	55.2	38.9	55.7	28.5
TPSS	86.2	65.5	66.7	50.8	65.6	51.0	66.2	39.9
TPSSh	94.9	75.4	76.3	61.4	75.4	61.7	76.0	51.4
BMK	112.4	92.1	95.5	80.2	92.9	78.9	92.8	69.8
B97K	114.7	96.2	97.5	82.9	97.0	82.6	96.3	72.7
CBS-QB3	92.6	74.0	71.4	59.4	71.0	57.2	72.2	48.5
CBS-APNO	98.5	79.0	76.3	64.1	75.6	61.9	77.2	53.8
RCCSD(T)[c]	104.0	86.0	86.4	72.3	85.9	69.6	83.6	62.6
Best estimate[d]	100.4	81.6	82.0	67.3	81.4	64.4	79.0	57.2

[a]All methods include B3LYP ZPVE.
[b]All DFT data are obtained in the def2-TZVP basis.
[c]Frozen-core CCSD(T)/cc-pVTZ value.
[d]Best estimate of the barrier height $\Delta E_{B,0}$ obtained by scaling the frozen-core CCSD(T)/cc-pVTZ electron-correlation contributions to $\Delta E_{B,e}$ by the factor 1.053 (see text).

In comparison with the DFT results obtained with various functionals, we find that the B3LYP values are very close to the best estimates. On average, the B3LYP barriers are only 3 kJ mol^{-1} below the best estimates. The TPSSh functional yields values that in turn are circa 3 kJ mol^{-1} below the B3LYP barriers. Furthermore, the BMK and B97K functionals yield barriers that are too high in comparison with the best estimates derived from CCSD(T) calculations. These functionals overestimate the barriers by more than 10 kJ mol^{-1}.

The results (using the B3LYP values) show, not unexpectedly, that the reaction barriers for the abstraction of a primary hydrogen cluster around 79 kJ mol^{-1}, abstraction of a secondary hydrogen is lower at about 64 kJ mol^{-1} and finally a tertiary hydrogen lower again at 54 kJ mol^{-1} — reflecting of course the decrease in the C-H bond dissociation energies from primary to tertiary.[198]

A more detailed look should be taken to the results of the compound methods CBS-QB3 and CBS-APNO. As can be extracted from Table 6.3 the standard deviation of the CBS-QB3 method is more than 8 kJ mol^{-1}. Taking into account

that this is the difference to the coupled-cluster basis-set limit, and as we pointed out earlier this has an error against experiment of at least 3 kJ mol^{-1}, it would potentially lead to an error of more than 10 kJ mol^{-1}. As is perhaps to be expected, the CBS-APNO method performs very close to our best estimates because of the additional corrections that embodies over those in CBS-QB3 and which therefore bring it nearer to the CCSD(T) basis set limit.

Preliminary work on H-abstraction from n-butanol by HO$_2^\bullet$ may be compared to our results for n-butane. The barrier heights evaluated at the CBS-QB3 and CBS-APNO levels of theory for abstraction from the terminal or δ-carbon in the alcohol (70.3 and 75.0 kJ mol^{-1}, respectively) are very close to those reported here for abstraction of the primary hydrogens in n-butane (Table 3). This is not unexpected, given the diminishing influence of the hydroxyl group along the lengthening carbon chain. The influence of the -OH group becomes evident on comparison of the barrier heights for abstraction of a secondary H from n-butane and a secondary H from the γ position in n-butanol, which might be expected to be sufficiently far from the -OH group to behave similarly to its alkane equivalent. However, the difference in this case between the barrier heights for n-butanol and n-butane is noticeable, though small (ca. 4 kJ mol^{-1} lower for n-butanol, with CBS-QB3 and CBS-APNO barriers of 53.5 and 58.4 kJ mol^{-1}, respectively) and is attributable to a stabilization of the transition state due to a H-bonding interaction between the H of the -OH group and the terminal O of HO$_2^\bullet$.

Hindered rotations

Corrections to account for hindered rotations are included for all rotations about the C-C and O-O bonds as well as for rotations about the reaction co-ordinate C$\cdots$H$\cdots$O. Following Vansteenkiste et $al.$,[34] instead of removing the harmonic vibrational modes from the partition function, we correct it by multiplying with the ratio q_{hr}/q_{v-1D}. To obtain q_{hr}, potential energy curves are computed for the rotations about the above mentioned bonds using discrete steps of five degrees, thereby allowing for a geometry relaxation of all the other internal coordinates (for the transition state, the difference between the C$\cdots$H and H$\cdots$O distances is kept fixed since otherwise the geometry relaxation would lead to either the reactants or the products), as long as the modes uncopled. This is clearly an approximation, but allows us to treat every rotation individually.
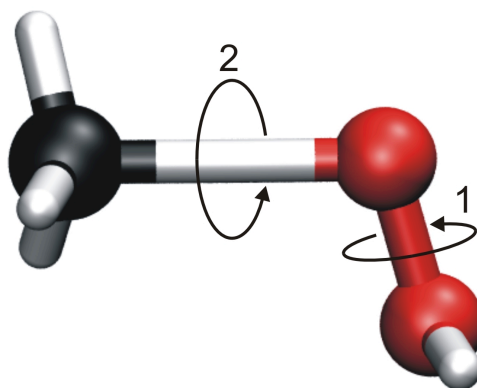
Figure 6.3: Rotations analyzed for the CH_4O_2H transition state.
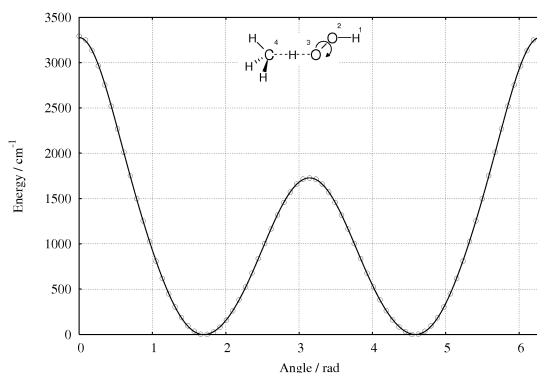
Figure 6.4: Angle 1 (HOOC)
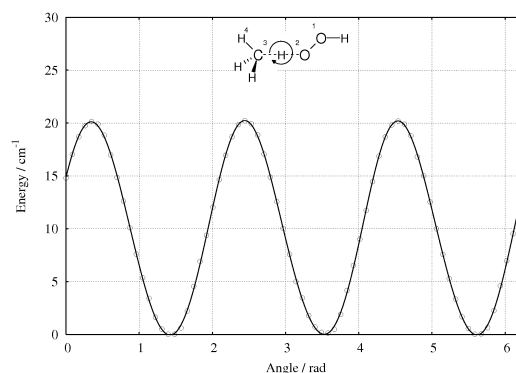
Figure 6.5: Angle 2 (OOCH)

A one-dimensional Schrödinger equation is solved to obtain the eigenstates needed to compute the partition function q_{hr}. q_{v-1D} is the harmonic oscillator value obtained from these one-dimensional curves. The reactants and transition states have several conformations, which are all accounted for by computing the hindered-rotor partition function with respect to rotation about 360°. This procedure for example yields a factor of two for the rotation about the O-O bond for the two conformations that cannot be superimposed by rotation.[199]

Symmetry numbers are included in the hindered-rotor partition functions for symmetric groups such as -CH_3 but most of these factors cancel between reactant and transition state. In the reactions producing the radicals n-$C_3H_7^{\bullet}$, p-$C_4H_9^{\bullet}$ and i-$C_4H_9^{\bullet}$, however, the lower symmetry of the hindered rotation about one of the C-C bonds in the transition state adds a factor of three to the reaction

Table 6.4: Detailed composition of the symmetry numbers applied.

Radical	σ_{R}	σ_{TS}	$\sigma_{\mathrm{R,HR}}$	$\sigma_{\mathrm{TS,HR}}$	Chirality	σ_{TOT}
$CH_3^\bullet$	12	1	1	3	1	$1\times(12\times 1)/(1\times 3) = 4$
$C_2H_5^\bullet$	6	1	3	3	1	$1\times(6\times 3)/(1\times 3) = 6$
$n\text{-}C_3H_7^\bullet$	2	1	9	3	1	$1\times(2\times 9)/(1\times 3) = 6$
$i\text{-}C_3H_7^\bullet$	2	1	9	9	1	$1\times(2\times 9)/(1\times 9) = 2$
$p\text{-}C_4H_9^\bullet$	2	1	9	3	1	$1\times(2\times 9)/(1\times 3) = 6$
$s\text{-}C_4H_9^\bullet$	2	1	9	9	2	$2\times(2\times 9)/(1\times 9) = 4$
$i\text{-}C_4H_9^\bullet$	3	1	27	9	1	$1\times(3\times27)/(1\times 9) = 9$
$t\text{-}C_4H_9^\bullet$	3	1	27	81	1	$1\times(3\times27)/(1\times81) = 1$

rate. Similarly, in the reactions yielding the $CH_3^\bullet$ and $t\text{-}C_4H_9^\bullet$ radicals, symmetry numbers for the rotations of the methyl and tertiary-butyl groups in the transition state are not compensated by a corresponding symmetry number in the reactant.
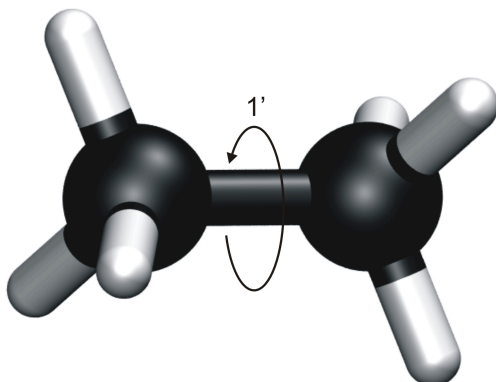
Figure 6.6: Rotation analyzed for the C_2H_6 molecule.

Moreover, a factor of two is included for the reaction producing $s\text{-}C_4H_9^\bullet$, because a chiral transition state is involved.[199]

A summary of the different symmetry factors that have been taken into account are shown in Table 6.4. σ_{R} is the symmetry factor for the reactants, σ_{TS} for the transition states (all one in this case, since no symmetry is present). $\sigma_{\mathrm{R,HR}}$ and $\sigma_{\mathrm{TS,HR}}$ are, respectively, the factors corresponding to the hindered rotations present.

As a byproduct, the scanning procedure confirmed that the energy calculations were done for the lowest-energy conformers.
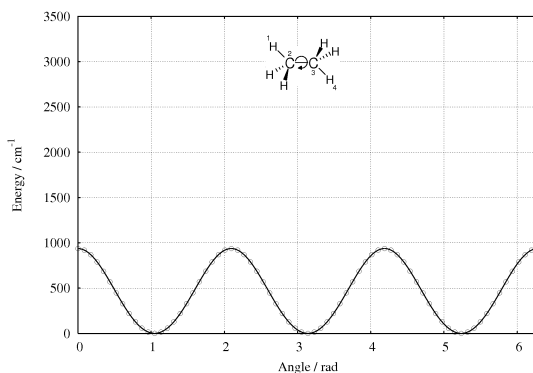
Figure 6.7: Angle 1' (HCCH)
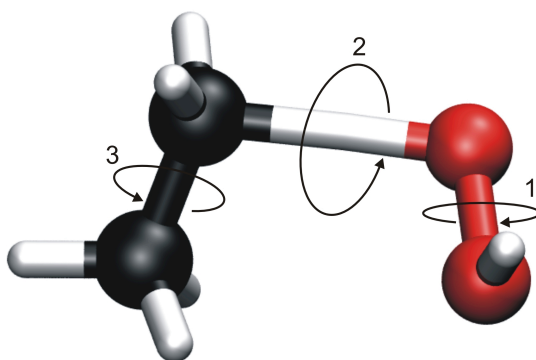
Figure 6.8: Rotations analyzed for the $C_2H_6O_2H$ transition state.
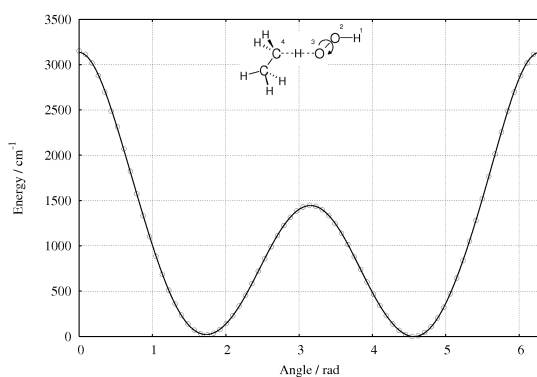
Figure 6.9: Angle 1 (HOOC)
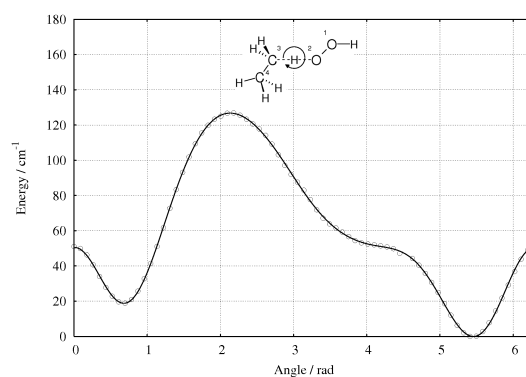
Figure 6.10: Angle 2 (OOCC)

The function used to fit the data points that describe the potential surface follow the equation:
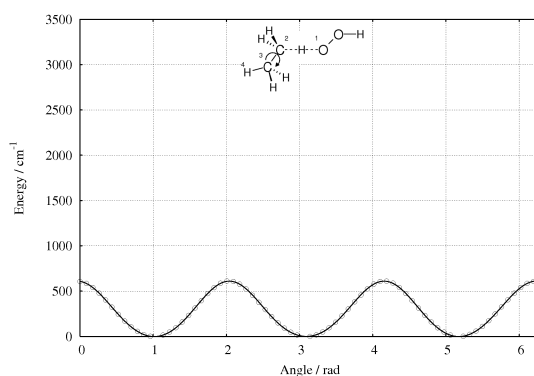
Figure 6.11: Angle 3 (OCCH)
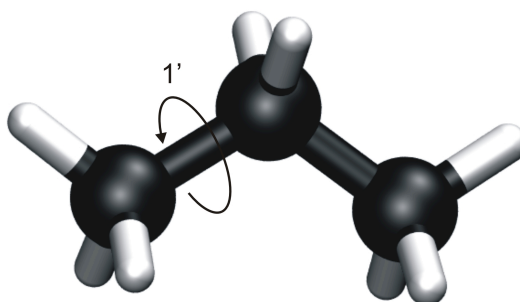
Figure 6.12: Rotation analyzed for the C₃H₈ molecule.
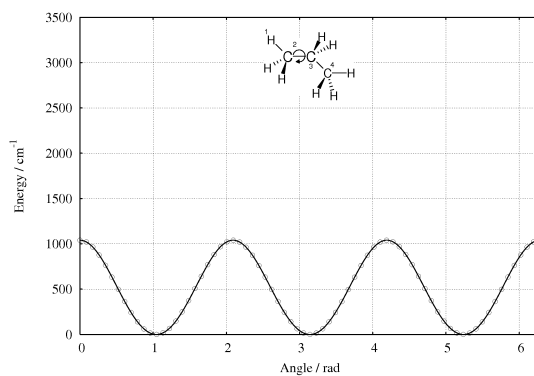
Figure 6.13: Angle 1' (HCCC)

$$V(\phi) = a + \sum_{i=1}^{7} b_i \cdot \sin(i \cdot \phi) + \sum_{j=1}^{7} c_j \cdot \cos(j \cdot \phi) \qquad (6.4)$$

And from there we can obtain the different states. It is important to note

that the global minimum of the potential surface must be shifted to 0 in order to obtain the right result.
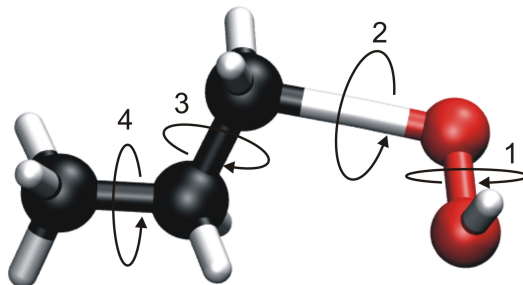
Figure 6.14: Rotations analyzed for the n-$C_3H_8O_2H$ transition state.
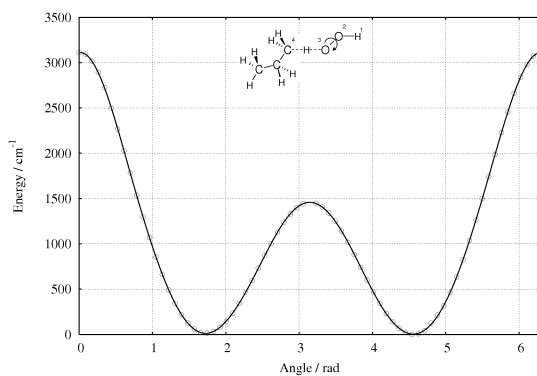
Figure 6.15: Angle 1 (HOOC)
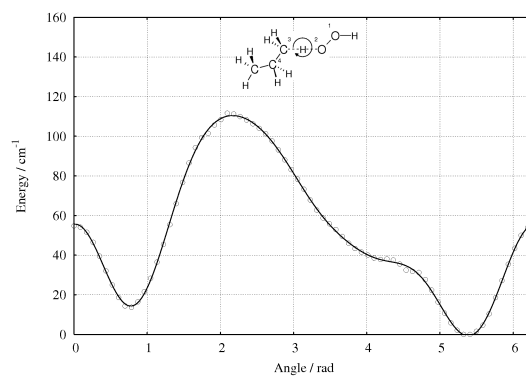
Figure 6.16: Angle 2 (OOCC)
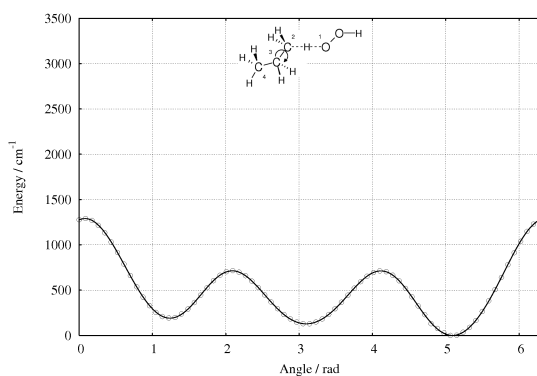
Figure 6.17: Angle 3 (OCCC)
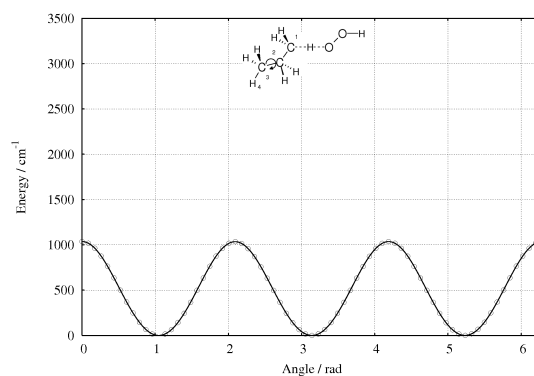
Figure 6.18: Angle 4 (CCCH)

Once that we have the states and the function $V(i)$ we can compute the two

quantities that are needed to solve Eq. (3.22), $q_{j,harm\ 1-D}$ and $q_{j,HIR}$. The former is obtained with

$$q_{j,harm\ 1-D} = \frac{1}{1 - \exp(-\hbar\omega/k_B T)} \tag{6.5}$$

with

$$\omega = \sqrt{\frac{V''(\phi_{min})}{I_{red}}} \tag{6.6}$$

being $V''(\phi_{min})$ the second derivative of the fitting function at the global minimum.
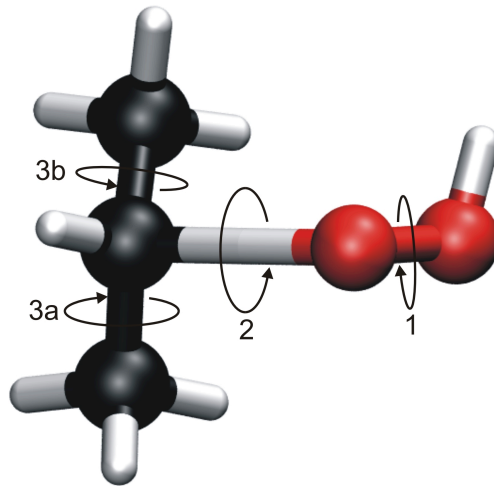
Figure 6.19: Rotations analyzed for the i-$C_3H_8O_2H$ transition state.
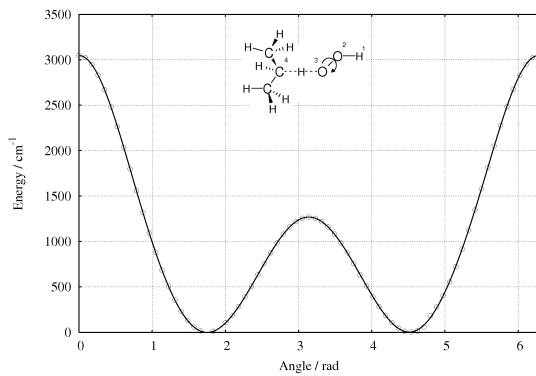
Figure 6.20: Angle 1 (HOOC)
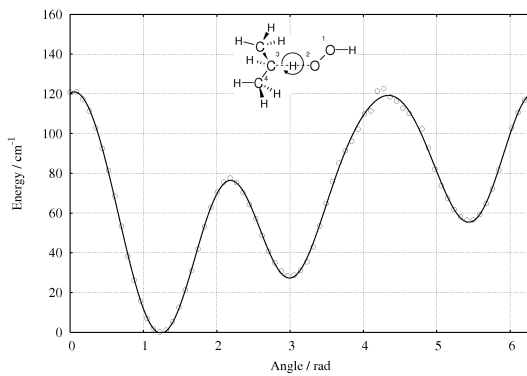
Figure 6.21: Angle 2 (OOCC)
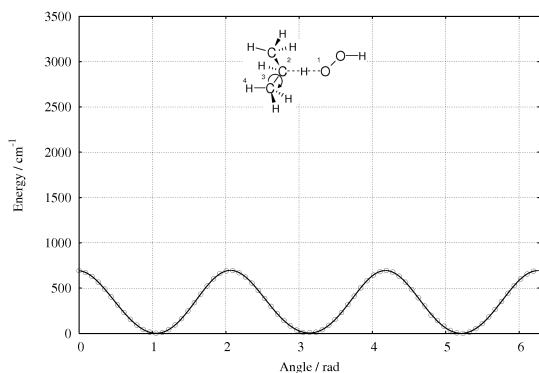
Figure 6.22: Angle 3a (OCCH)
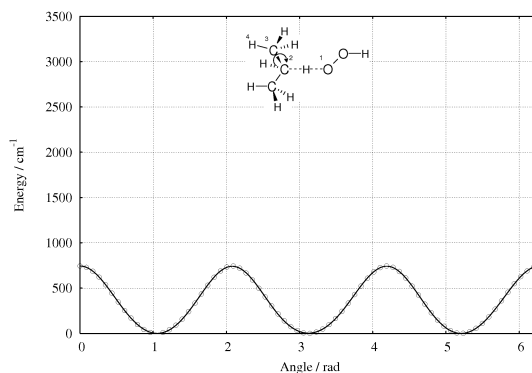
Figure 6.23: Angle 3b (OCCH)

The second quantity needed, $q_{j,HIR}$ is easily obtained once that we have obtained the different states. Then we only have to apply

$$q_{j,HIR} = \sum_{k=1}^{m} \exp\left(\frac{hc(\varepsilon_K - \varepsilon_1)}{k_B T}\right) \tag{6.7}$$
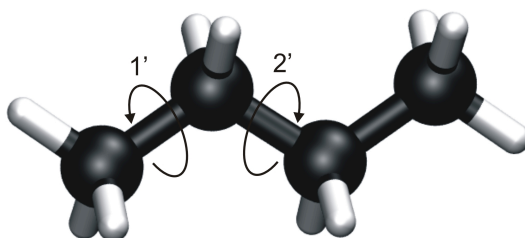
Figure 6.24: Rotations analyzed for the n-C$_4$H$_{10}$ molecule.
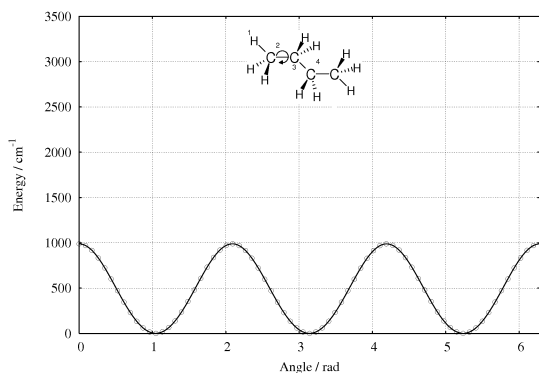
Figure 6.25: Angle 1' (HCCC)
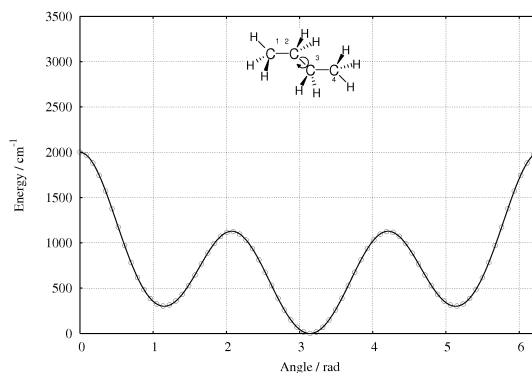
Figure 6.26: Angle 2' (CCCC)
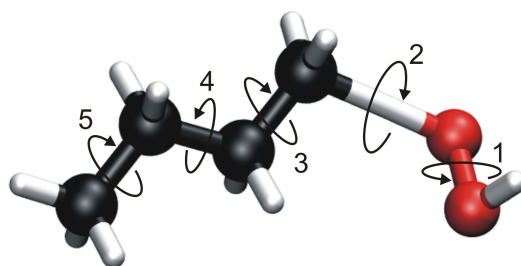
Figure 6.27: Rotations analyzed for the p-$C_4H_{10}O_2H$ transition state.
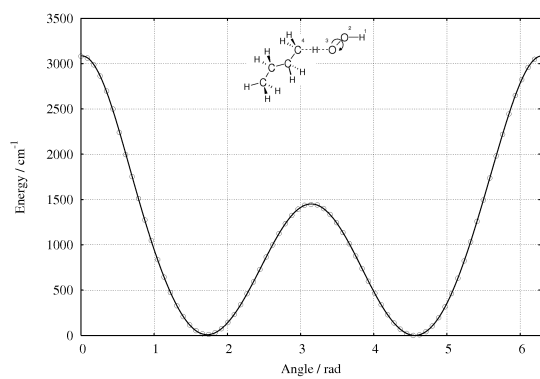
Figure 6.28: Angle 1 (HOOC)
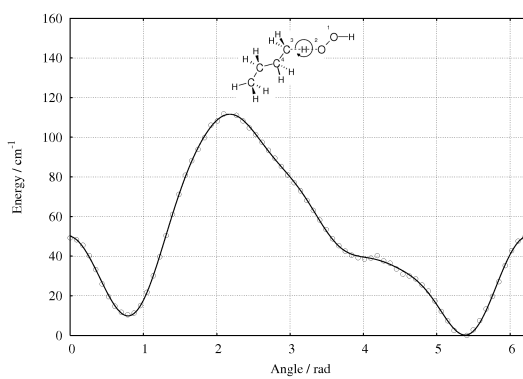
Figure 6.29: Angle 2 (OOCC)
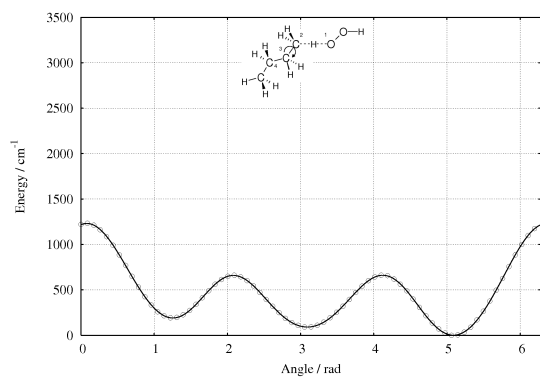
Figure 6.30: Angle 3 (OCCC)
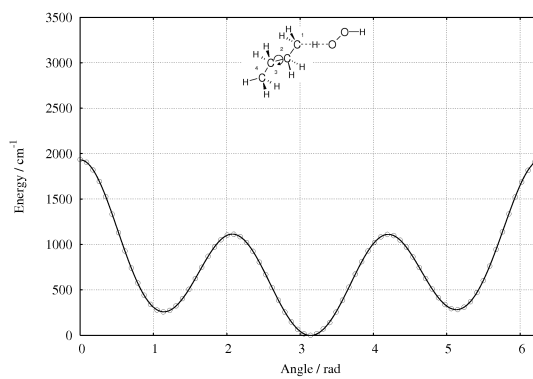
Figure 6.31: Angle 4 (CCCC)
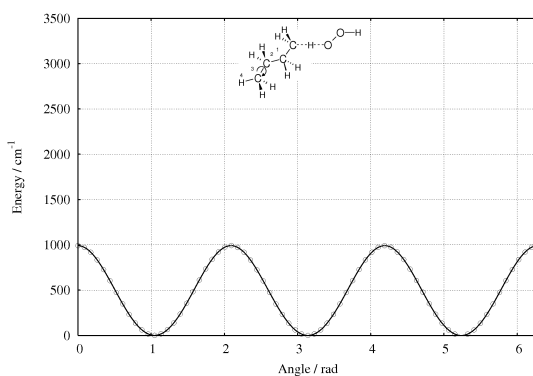
Figure 6.32: Angle 5 (CCCH)
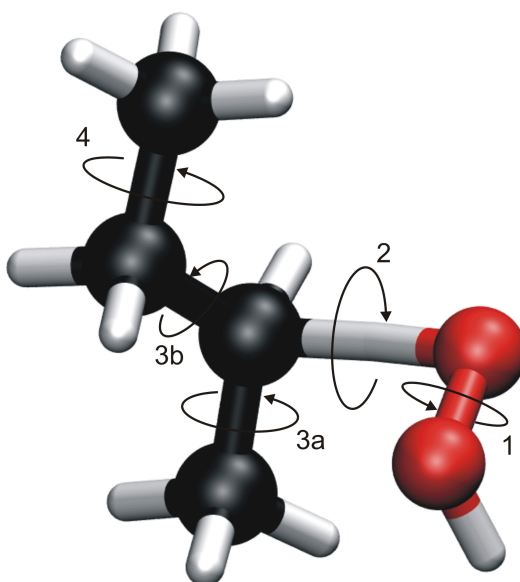
Figure 6.33: Rotations analyzed for the s-$C_4H_{10}O_2H$ transition state.
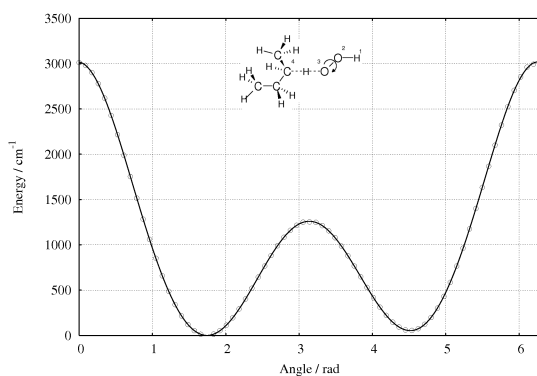
Figure 6.34: Angle 1 (HOOC)
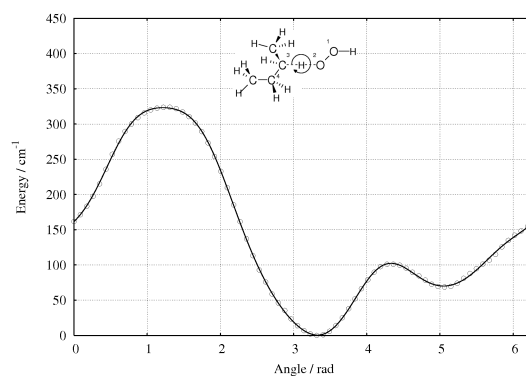
Figure 6.35: Angle 2 (OOCC)
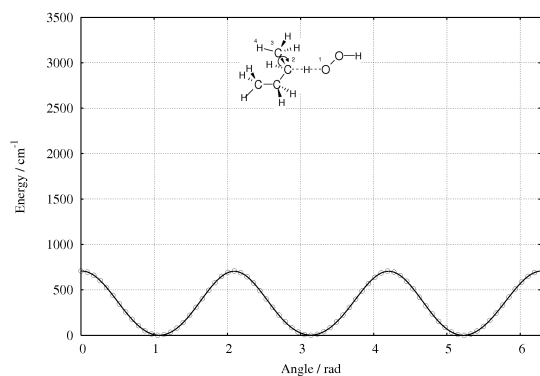
Figure 6.36: Angle 3a (OCCH)
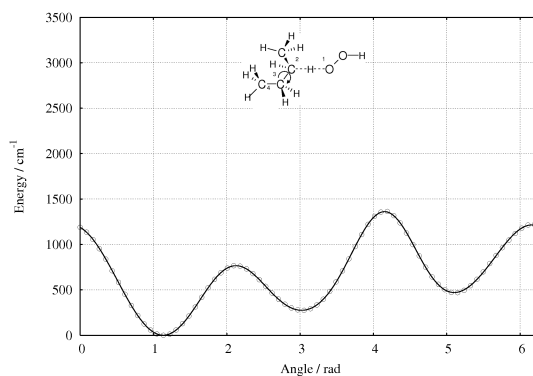
Figure 6.37: Angle 3b (OCCC)
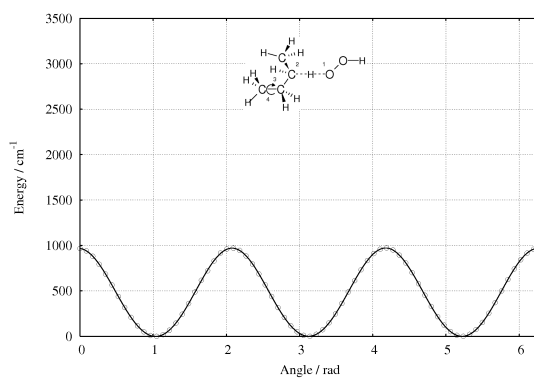
Figure 6.38: Angle 4 (CCCH)
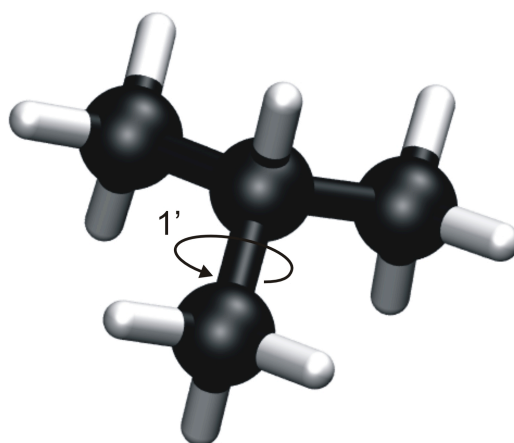
Figure 6.39: Rotations analyzed for the i-C$_4$H$_{10}$ molecule.
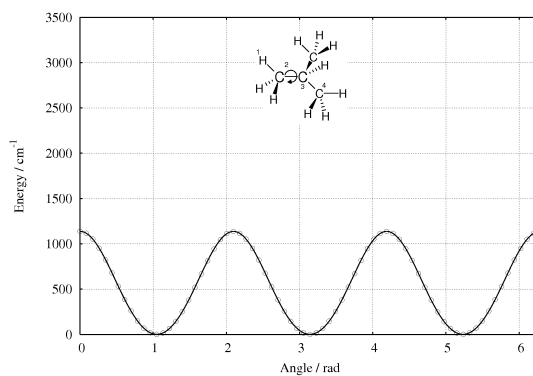
Figure 6.40: Angle 1' (HCCC)
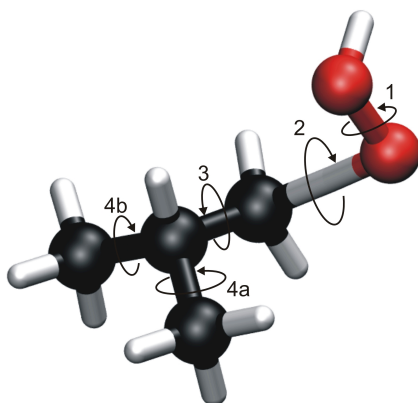
Figure 6.41: Rotations analyzed for the i-$C_4H_{10}O_2H$ transition state.
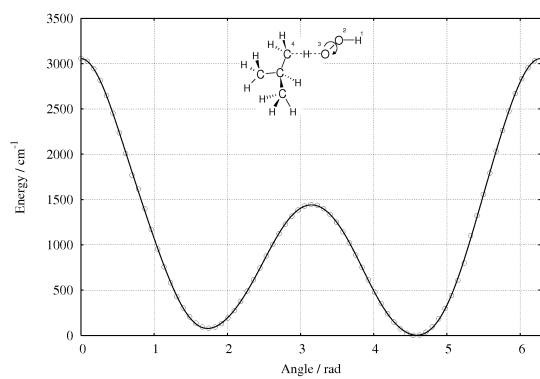
Figure 6.42: Angle 1 (HOOC)
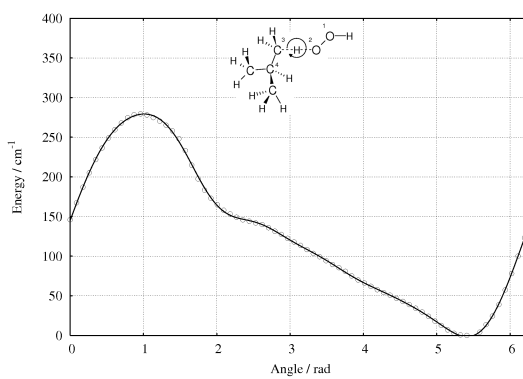
Figure 6.43: Angle 2 (OOCC)
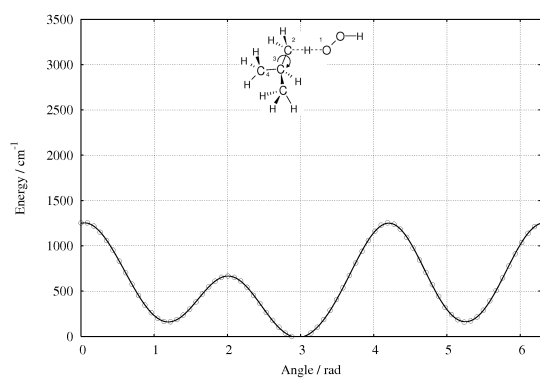
Figure 6.44: Angle 3 (OCCC)
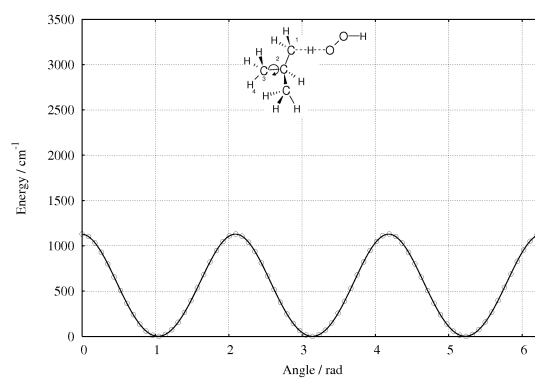
Figure 6.45: Angle 4a (CCCH)
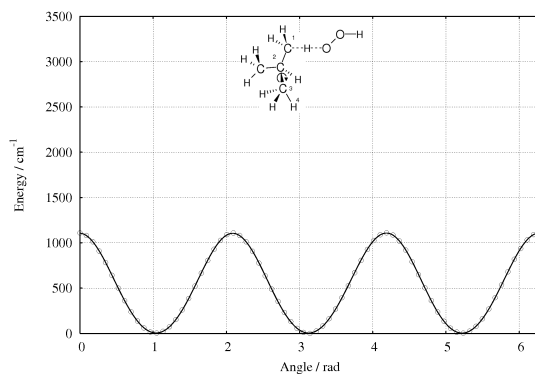
Figure 6.46: Angle 4b (CCCH)
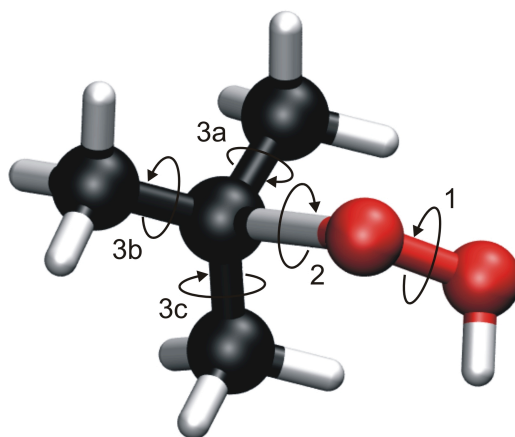
Figure 6.47: Rotations analyzed for the t-C$_4$H$_{10}$O$_2$H transition state.
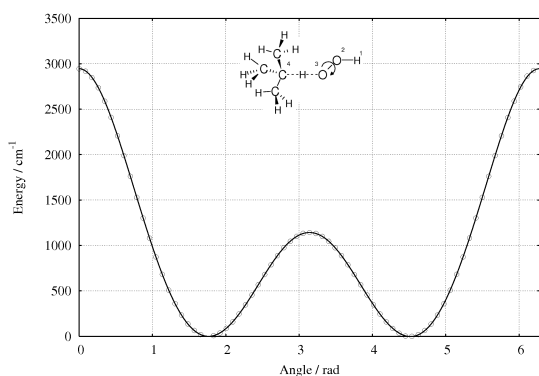
Figure 6.48: Angle 1 (HOOC)
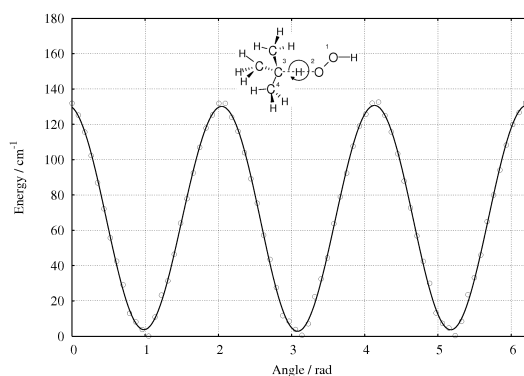
Figure 6.49: Angle 2 (OOCC)
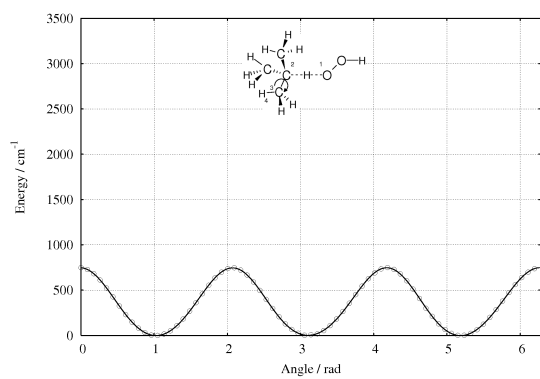
Figure 6.50: Angle 3a (OCCH)
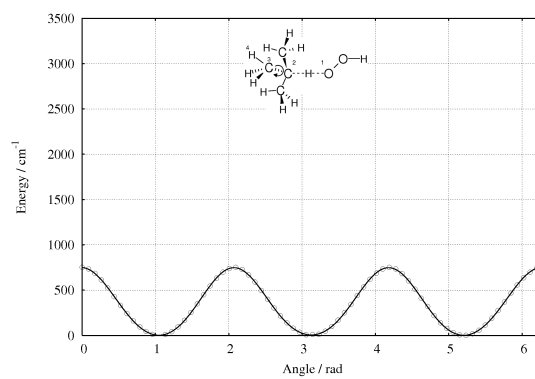
Figure 6.51: Angle 3b (OCCH)
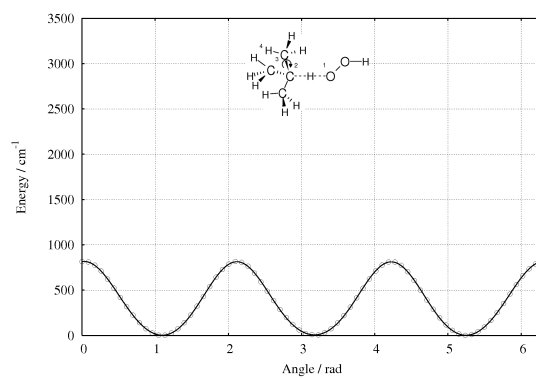
Figure 6.52: Angle 3c (OCCH)

Reaction rates

The final kinetic results are collected in Table 6.5 where we present the TST rate constants k calculated from the fitting using the B3LYP/def2-TZVP partition functions in conjunction with the best estimates of $\Delta E_{B,0}$. The fit parameters A, n and E_A needed to represent the rate constants by an Arrhenius-like expression are also given in Table 6.5. Note that the activation energy E_A given in the table is the fit parameter, not the best estimate $\Delta E_{B,0}$. In fact, the fitted E_A values are about 7 to 14 kJ mol^{-1} *lower* than the best estimates.

Table 6.5: Calculated TST Rate Constants / cm^3 mol^{-1} s^{-1} Coming from the Fit Parameters A / cm^3 mol^{-1} s^{-1}, n, E_A / kJ mol^{-1} and Imaginary 'frequency' ν / cm^{-1}.

Radical	600 K	800 K	1000 K	1200 K	A	n	E_A	ν
CH$_3^\bullet$	6.16E+03	1.48E+06	4.79E+07	5.52E+08	11.3	3.74	87.9	1539i
C$_2$H$_5^\bullet$	2.54E+05	2.49E+07	4.69E+08	3.75E+09	34.6	3.41	70.8	1661i
n-C$_3$H$_7^\bullet$	6.48E+04	7.00E+06	1.40E+08	1.18E+09	4.5	3.75	71.9	1656i
i-C$_3$H$_7^\bullet$	1.15E+06	5.59E+07	6.83E+08	4.05E+09	58.1	3.37	58.2	1684i
p-C$_4$H$_9^\bullet$	7.12E+04	7.48E+06	1.46E+08	1.18E+09	34.0	3.48	72.9	1657i
s-C$_4$H$_9^\bullet$	1.79E+06	8.21E+07	9.66E+08	5.60E+09	65.6	3.38	56.9	1677i
i-C$_4$H$_9^\bullet$	9.79E+04	1.00E+07	1.92E+08	1.54E+09	38.8	3.49	72.3	1648i
t-C$_4$H$_9^\bullet$	5.89E+06	1.78E+08	1.59E+09	7.57E+09	650.4	3.01	50.6	1658i

6.5   Comparison with previous work

In this section we compare the rate constants obtained in the present work with those obtained in previous studies. We can divide these works in three categories:

- Purely theoretical work. This includes our work and the one done by Carstensen *et al.*[182] The approaches differ drastically in the computation of the reaction barrier. Carstensen *et al.*[182] provide reaction rates using the CBS-QB3 method. The reaction barriers are not explicitly shown in the cited reference so we compute the CBS-QB3 values in our study. In Table 6.3 we can see that our best estimate is always higher than that obtained with CBS-QB3. This means that we expect our rate constant to be always

slower. Since the reaction barrier appears in $\exp\left(-\Delta E_{B,0}/RT\right)$ the effect of the difference in reaction barrier on the reaction rates will be significant at low and medium temperatures (where the reactions under study play a key role), and less important at high temperatures. For example, if the difference in the calculated reaction barriers is 10 kJ mol^{-1}, at 530 K the difference in the reaction rate coming from the exponential part is of an order of magnitude, at 1760 K, only a factor of 2. We confirm these effects through all the figures in this section.

- Literature review. We include here the extensive literature reviews of Tsang *et al.*[176,177] and that of Orme *et al.*[178] which was carried out in order to construct detailed chemical kinetic models.

- Experimental work. There are no direct measurements of the reactions involved. The work done by Baldwin *et al.*[169,170,173,175] is based on the measurement of relative reaction rates of the reaction in question by the use of a reference reaction.

Methane

Our values are in excellent agreement with the relative rate measurements (based on $HO_2^\bullet + HO_2^\bullet \rightarrow H_2O_2 + O_2$) of Baldwin *et al.*[170] and the recommendation of Baulch *et al.*[174] However, our values are between five times (at 600 K) and three times (at 1,500 K) slower compared to that of Carstensen *et al.*[182] (Fig. 6.53).

Ethane

Our rate constants are two times slower than the relative rate measurements of Baldwin *et al.*[169] and show a stronger temperature curvature compared to the previous recommendations of Scott and Walker[172] and the review of Tsang *et al.*[176] and thus are considerably faster at temperatures above 600 K. Our rate constant is four times slower than that calculated by Carstensen *et al.*[182] at 600 K and is twice as slow at 1,500 K (Fig. 6.54).
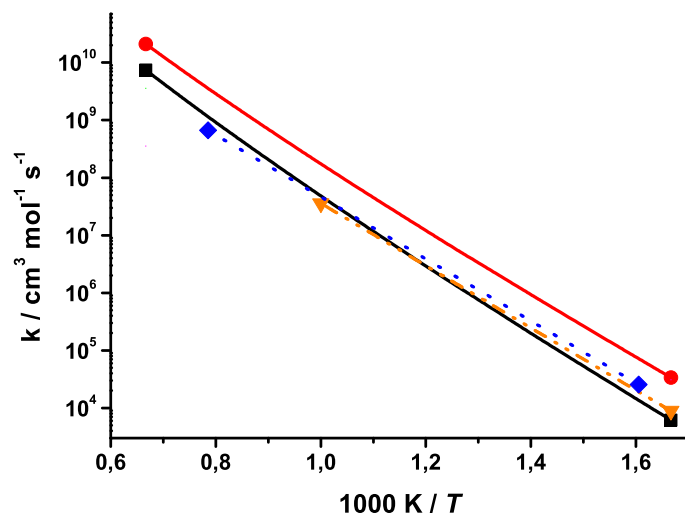
Figure 6.53: $k(CH_4 + HO_2^\bullet \rightarrow CH_3^\bullet + H_2O_2)$. This work (——■——), Carstensen[182] (——●——), Baulch[174] ($- \cdot \cdot \blacktriangledown \cdot \cdot -$), Baldwin[170] ($\cdots \blacklozenge \cdots$).
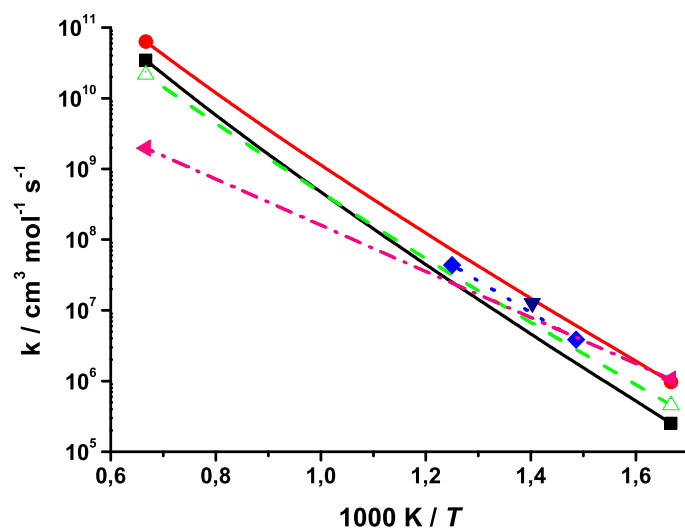
Figure 6.54: $k(C_2H_6 + HO_2^\bullet \rightarrow C_2H_5^\bullet + H_2O_2)$. This work (——■——), Carstensen[182] (——●——), Scott[172] ($--\triangle--$), Baldwin[169] ($\cdots \blacklozenge \cdots$), Baldwin[173] ($\blacktriangledown$), Tsang[176] ($-\cdot \blacktriangleleft -$).

Propane

In the case of propane there are two distinct abstractable hydrogen atoms leading to either n-propyl (Fig. 6.55) , or iso-propyl (Fig. 6.56) radicals.

Baldwin *et al.*[175] performed a relative rate measurement at 773 K and found a relative rate of 0.03 for the production of the n-propyl radical relative to the reaction $CH_2O + HO_2^{\bullet} \rightarrow HCO^{\bullet} + H_2O_2$. All other rate constants presented in Fig. 6.55 are either calculations or estimates. The rate constant calculated in *this study* is in very good agreement with all other estimations, slightly slower at 600 K. The value calculated by Carstensen *et al.*[182] is more than five times faster at 600 K but very similar at 1,500 K.
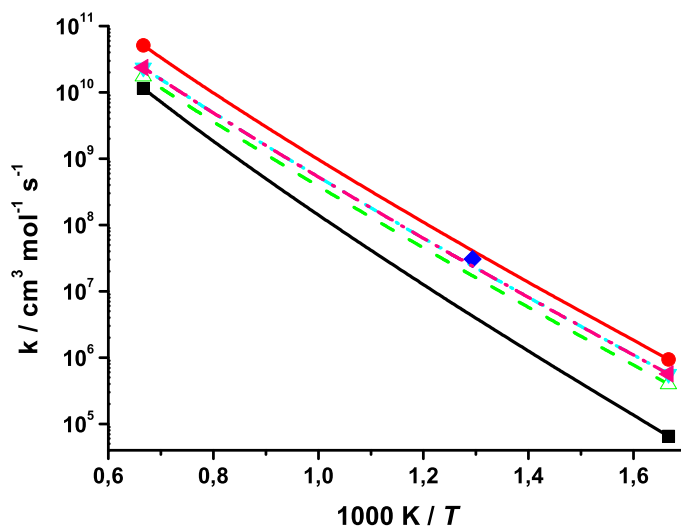
Figure 6.55: $k(C_3H_8 + HO_2^{\bullet} \rightarrow n\text{-}C_3H_7^{\bullet} + H_2O_2)$. This work (—■—), Carstensen[182] (—●—), Scott[172] (– –△– –), Orme[178] (– ·· ▽ – ··), Baldwin[175] (◆).

Baldwin *et al.*[175] also carried out a relative rate measurement for the production of the iso-propyl radical at 773 K and found a relative rate of 0.048 relative to the reaction $CH_2O + HO_2^{\bullet} \rightarrow HCO^{\bullet} + H_2O_2$. All other rate constants presented in Fig. 6.56 are also either calculations or estimates. The rate constant calculated in the present study is in very good agreement with the determination of Baldwin *et al.* and with the recommendations of Scott and Walker,[172] and Orme *et al.*[178] However, our calculation is significantly slower than that computed by

Carstensen *et al.*[182]
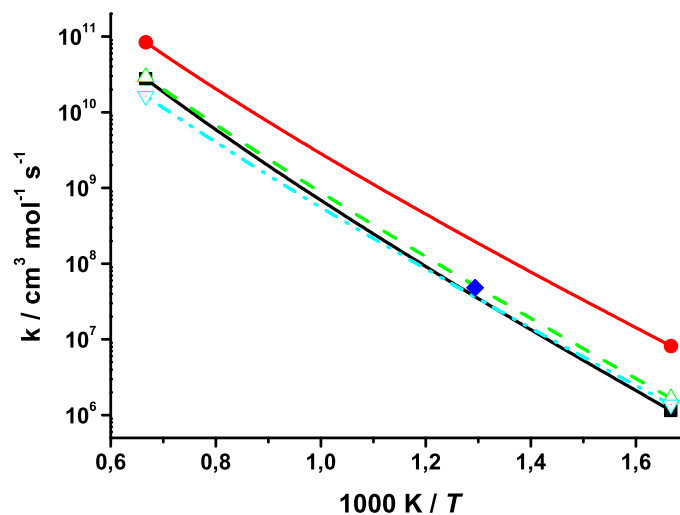
Figure 6.56: $k(C_3H_8 + HO_2^\bullet \rightarrow i\text{-}C_3H_7^\bullet + H_2O_2)$. This work (—■—), Carstensen[182] (—●—), Scott[172] (--△--), Orme[178] (–··▽–··), Baldwin[175] (♦).

n-Butane

In the case of n-butane, both primary or secondary radicals can be generated (Fig. 6.57 and Fig. 6.58).

There have been no measurements of the rate constant for hydrogen atom abstraction by the hydroperoxyl radical from n-butane. The rate constant calculated in our study is again in very good agreement with all other estimations, consistent with the result for abstraction of a primary hydrogen atom from propane. The rate constant calculated by Carstensen *et al.*[182] is five times faster at 600 K but very close at 1,500 K.

For secondary hydrogen atom abstraction from butane, our calculations are two times faster than the recommendations of Scott and Walker. The rate constant calculated by Carstensen *et al.*[182] is between seven times (600 K) and three times (1,500 K) faster than our calculation.
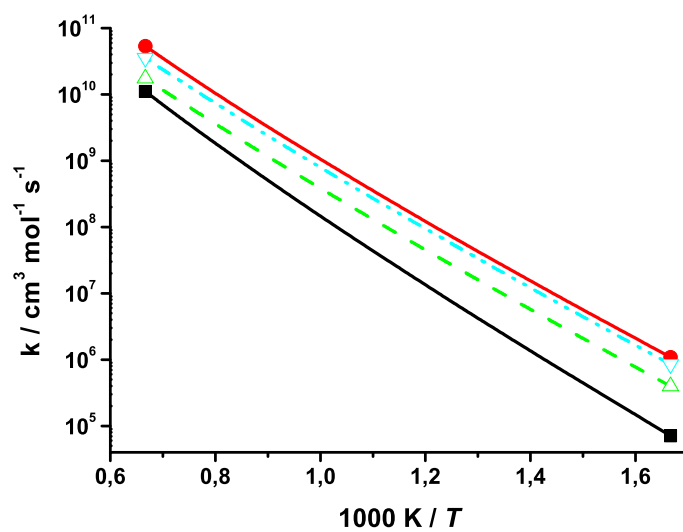
Figure 6.57: $k(n\text{-}C_4H_{10} + HO_2^\bullet \rightarrow p\text{-}C_4H_9^\bullet + H_2O_2)$. This work (—■—), Carstensen[182] (—●—), Scott[172] (--△--), Orme[178] ($-\cdots\triangledown-\cdots$).
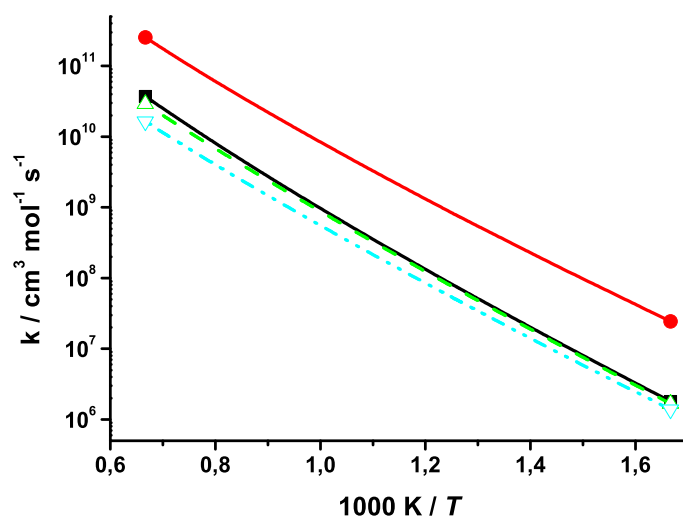
Figure 6.58: $k(n\text{-}C_4H_{10} + HO_2^\bullet \rightarrow s\text{-}C_4H_9^\bullet + H_2O_2)$. This work (—■—), Carstensen[182] (—●—), Scott[172] (--△--), Orme[178] ($-\cdots\triangledown-\cdots$)

iso-Butane

For iso-butane, both iso-butyl (Fig. 6.59) and tertiary-butyl (Fig. 6.60) radicals are formed. Baldwin *et al.*[175] performed a relative measurement at 773 K and found a relative rate of 0.133 for the production of iso-butyl radicals relative to the reaction $CH_2O + HO_2^{\bullet} \rightarrow HCO^{\bullet} + H_2O_2$. Recommendations of Scott and Walker,[172] Orme *et al.*,[178] Tsang[177] and the calculations of Carstensen *et al.*[182] are in reasonable agreement with this rate constant. Our calculation is 2–3 times slower than the value derived by Baldwin *et al.*[175] at 773 K.
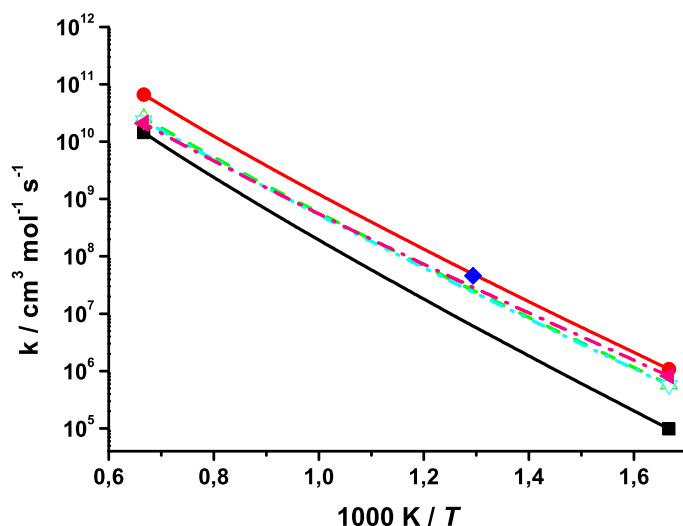
Figure 6.59: $k(i\text{-}C_4H_{10} + HO_2^{\bullet} \rightarrow i\text{-}C_4H_9^{\bullet} + H_2O_2)$. This work (—■—), Carstensen[182] (—●—), Scott[172] (––△––), Orme[178] (–··▽–··), Baldwin[175] (♦), Tsang[177] (–·◄·–).

Fig. 6.60 depicts rate constants for the abstraction of the tertiary hydrogen atom from iso-butane. Baldwin *et al.*[175] performed measurements at 773 K and found a relative rate of 0.045 for the production of tert-butyl radicals relative to $CH_2O + HO_2^{\bullet} \rightarrow HCO^{\bullet} + H_2O_2$. Recommendations of Scott and Walker,[172] Orme *et al.*,[178] Tsang[177] are in reasonable agreement with this rate constant. Our calculation is in excellent agreement with that of Baldwin *et al.*[175] At the same temperature, the value suggested by Carstensen *et al.*[182] is five times faster than that of Baldwin *et al.*[175]
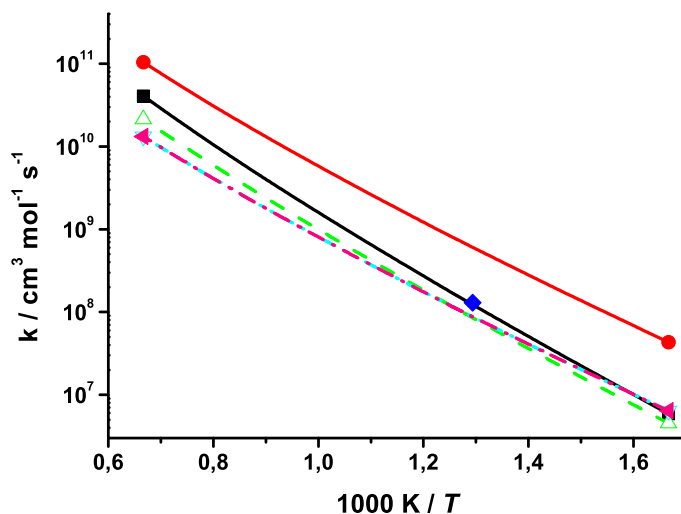
Figure 6.60: $k(i\text{-}C_4H_{10} + HO_2^\bullet \rightarrow t\text{-}C_4H_9^\bullet + H_2O_2)$. This work (—■—), Carstensen[182] (—●—), Scott[172] (--△--), Orme[178] ($-\cdot\cdot\nabla-\cdot\cdot$), Baldwin[175] (♦), Tsang[177] ($-\cdot◄\cdot-$).

Recommended rate constants

Using the data obtained in the previous section, we suggest values for the rate constants which depend upon the local environment of the hydrogen being abstracted — that is, whether from a primary, secondary or tertiary carbon.

In Fig. 6.61, the rate constants for primary carbons are plotted separately, together with the resulting average. The same procedure is shown in Fig. 6.62, in this case for the secondary carbons. Note that these are rate constants on a per hydrogen atom basis with the final suggested values summarized in Table 6.6.

6.6   Conclusions

We have computed the reaction barrier for the $CH_4 + HO_2^\bullet$ reaction within chemical accuracy using R12 methodology. Comparisons with results obtained with compound methods revealed that CBS-QB3 may be insufficient to achieve the same goal. Methods higher in the CBS hierarchy such as CBS-APNO should be used for high accuracy. We have computed the rate constants for the reactions under study and we have used them to recommend values for various substitu-
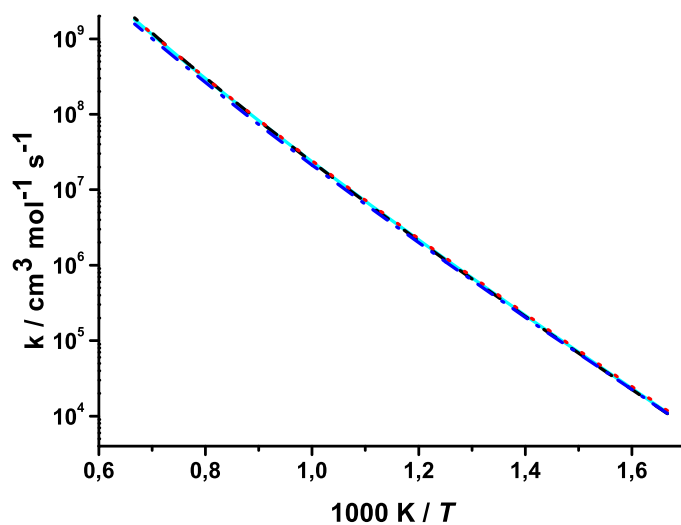
Figure 6.61: k for primary carbon on a per H-atom basis. $C_2H_5^{\bullet}$ ($-\cdot-$), $n\text{-}C_3H_7^{\bullet}$ ($---$), $p\text{-}C_4H_9^{\bullet}$ ($\cdots$), $i\text{-}C_4H_9^{\bullet}$ ($--\cdots$), average (—).
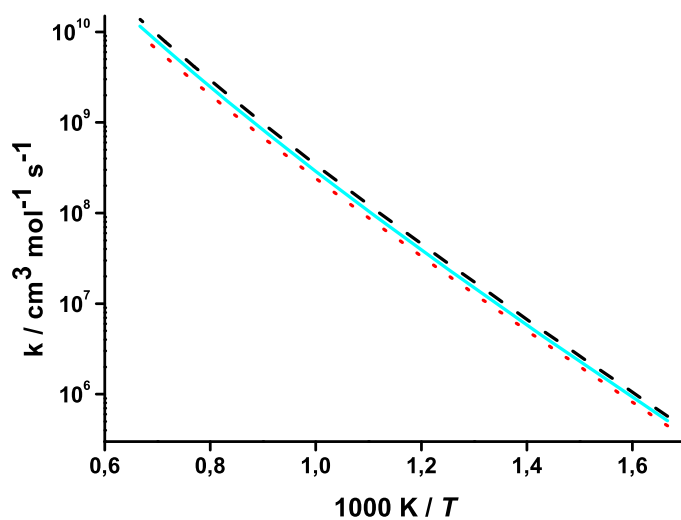
Figure 6.62: k for secondary carbon on a per H-atom basis. $i\text{-}C_3H_7^{\bullet}$ ($---$), $s\text{-}C_4H_9^{\bullet}$ ($\cdots$), average (—).

Table 6.6: Fit Parameters A / cm^3 mol^{-1} s^{-1}, n, E_A / kJ mol^{-1} per Hydrogen Atom According to Carbon Type.

Carbon	A	n	E_A
$CH_3^\bullet$	2.8	3.74	87.9
$C_2H_5^\bullet$	5.8	3.61	70.8
primary	10.7	3.40	73.8
secondary	10.6	3.47	56.9
tertiary	650.4	3.01	50.6

tions of the carbon involved in the reaction. We have compared the constants computed in the present work with available experimental data and found a reasonable agreement for methane, primary, secondary and tertiary carbons. In the comparison with previous theoretical work we have found for all the molecules in the study lower reaction rates, what is a reasonable consequence of our higher reaction barriers.

Summary

A small set of conclusions have been extracted for every individual chapter, we will now try to summarize the global conclusions of this work.

It is clear that the complexity of the study of hydrocarbon chemistry makes a homogeneous approach an impossible task. The full problem must be reduced to smaller ones that can be solved, at this respect the introduction of combustion modeling with a closed (but always increasing) number of reactions has been a big step forward. Since not every reaction can be carefully investigated the sensitivity analysis as a way to decide the most important paths is very helpful. Using this knowledge we have proposed detailed mechanisms for the formation of naphthalene and phenanthrene. It has been shown that these reactions are far from straightforward, and every step has been characterized. Kinetic data in form of reaction rates was extracted and included in the modeling, showing the power of this carefully selected reaction study. The flexibility and speed of DFT fits well to obtain a reasonable result when scanning a big sample of molecules. Interesting four-membered ring intermediates have been found, that allow lower energy pathways, altering drastically previous data available.

We have shown that sometimes DFT results are not accurate enough to obtain the required result. In the example of hydroperoxyl radical reactions even a low level coupled-cluster calculation was clearly not reaching the desired accuracy. A mixed approach has been carried out successfully with a geometry and thermodynamic DFT calculation combined with a explicitly-correlated coupled-cluster calculation of the reaction barrier (obtaining chemical accuracy) for an improvement in all the hydrogen abstractions from hydrocarbons analyzed. In contrast to our first example, this methodology cannot be used as a blind scanning method, but once that the reactions involved are clear the accuracy is much improved.

We have also tested the limits of the accuracy in the context of hydrocar-

bon research. Coupled-cluster geometry optimization together with explicitly-correlated coupled-cluster energy calculations, with addition of several corrections have been performed successfully determining atomization energies with high accuracy. This work is relevant, not only in the hydrocarbon research context, but also in the development and assessment of explicitly-correlated techniques.

Overall, we face a very complex problem and a set of tools are required and available to provide answers.

Zusammenfassung

Die Kohlenwasserstoffchemie, durch ihre Komplexität kann verständlicherweise nicht in einem homogenen Ansatz betrachtet werden, sondern das komplette Problem muss vielmehr zu Kleineren, lösbaren reduziert werden. An dieser Stelle stellte die Einführung der Verbrennungsmodellierung, mit einer begrenzten (aber stetig zunehmender) Anzahl von Reaktionen einen großen Fortschritt dar. Da nicht jede einzelne Reaktion sorgfältig untersucht werden konnte, war die Sensitivitätsanalyse ein gutes Kriterium für die Auswahl der wichtigsten Reaktionspfade. Mit dieser Kenntnis wurden detaillierte Mechanismen für die Bildung von Naphtalin und Phenanthren vorgeschlagen. Es konnte gezeigt werden, dass diese Reaktionen kein vorhersehbares Verhalten aufwiesen, ebenso konnte jeder einzelner Schritt bestimmt werden. Kinetische Daten in Form von Reaktionsraten wurden aus den jeweiligen Reaktionen extrahiert und in die Modellierung mit eingebunden. Damit konnte die Güte, der mit Sorgfalt ausgewählten Reaktionsuntersuchungen gezeigt werden. Die Flexibilität und Schnelligkeit von DFT ist oftmals ausreichend gut für das Erzielen sinnvoller Ergebnisse, wenn große Mengen an Beispielmolekülen gescannt werden. Interessante Vierring-Zwischenprodukte, die niedrige Reaktionspfade zulassen wurden gefunden. Dadurch wurden vorhandene Erkenntnisse drastisch verändert.

Es konnte gezeigt werden, dass DFT Ergebnisse mitunter die erforderlichen Ergebnisse nicht ausreichend genau bestimmen konnte. Für das Beispiel der Hydroperoxylreaktionen wurde sogar mit Rechnungen auf low-level Coupled-Cluster Niveau nicht die gewünschte Genauigkeit erreicht. An dieser Stelle wurde ein gemischter Ansatz zur Verbesserung aller untersuchten Wasserstoffreaktionen an Kohlewasserstoffen erfolgreich durchgeführt. Dafür wurden DFT Rechnungen für die Geometrie und Thermodynamik mit explizit korrelierten Coupled-Cluster Rechnungen für die Reaktionsbarriere (hier konnte chemische Genauigkeit

erzielt werden) kombiniert. Im Gegensatz zu dem ersten Beispiel, konnte diese Methodik nicht als blindes Scanverfahren eingesetzt werden, dennoch konnte die Genauigkeit deutlich verbessert werden wenn die involvierten Reaktionen eindeutig definiert sind. Im Rahmen der Kohlenstoffwasserforschung wurden ebenso die Grenzen der Genauigkeit überprüft. Es konnten Coupled-Cluster Geometrieoptimierungen, zusammen mit explizit korrelierten Coupled-Cluster Energieberechnungen mit mehreren zusätzlichen Korrekturen erfolgreich durchgeführt werden und damit die Atomisierungsenergien mit hoher Genauigkeit bestimmt werden. Diese Arbeit ist nicht nur im Kontext der Kohlewasserstoffforschung von Bedeutung, sondern auch durch die Entwicklung und Berechnung der explizit korrelierten Techniken. Zusammenfassend lässt sich sagen dass hier eine sehr komplexe Fragestellung behandelt wurde, jedoch sind die notwendigen Instrumente, die zum Beantworten der Fragestellung benötigt wurden, vorhanden.

Bibliography

[1] E. Schrödinger, *Ann. Physik*, 1926, **79**, 361.

[2] B. T. Sutcliffe, *Adv. Quantum Chem.*, 1997, **28**, 65.

[3] D. R. Hartree, *Proc. Cambridge Phil. Soc.*, 1928, **24**, 89.

[4] V. Fock, *Z. Physik*, 1930, **61**, 126.

[5] A. Szabo and N. S. Ostlund, *Modern Quantum Chemistry, Introduction to Advanced Electronic Structure Theory.*, Dover Publications, INC., Mineola, New York, 1982.

[6] P. E. M. Siegbahn, *Lecture notes in Quantum chemistry, European Summerschool in Quantum Chemistry, Vol. 1, pp. 243-284*, B. O. Roos (Ed.), Lund, 2000.

[7] R. J. Bartlett, *Modern Electronic Structure Theory, pp. 1047-1130*, World Scientific Publishing Co. Ltd., Singapore, 1995.

[8] K. Raghavachari, G. W. Trucks, J. A. Pople, and M. Head-Gordon, *Chem. Phys. Lett.*, 1989, **157**, 479.

[9] T. H. Dunning, Jr., *J. Chem. Phys.*, 1989, **90**, 1007.

[10] T. Helgaker, W. Klopper, H. Koch, and J. Noga, *Chem. Phys.*, 1997, **106**, 9639.

[11] A. Halkier, T. Helgaker, P. Jørgensen, W. Klopper, H. Koch, J. Olsen, and A. K. Wilson, *Chem. Phys. Lett.*, 1998, **286**, 553.

[12] E. A. Hylleraas, *Z. Phys.*, 1929, **54**, 347.

[13] W. Kutzelnigg, *Theor. Chim. Acta*, 1985, **68**, 445.

[14] W. Klopper and W. Kutzelnigg, *Chem. Phys. Lett.*, 1987, **134**, 17.

[15] W. Klopper, *The Encyclopedia of Computational Chemistry, Vol. 4, pp. 2351-2375*, John Wiley & Sons, Ltd., Chichester, New York, 1998.

[16] J. Noga, W. Klopper, and W. Kutzelnigg, *Recent Advances in Computational Chemistry*, Vol. 3, World Scientific, Singapore, 1997.

[17] J. Noga and P. Valiron, *Chem. Phys. Lett.*, 2000, **324**, 166.

[18] E. Fermi, *Rend. Accad. Lincei*, 1927, **6**, 602.

[19] L. H. Thomas, *Proc. Cambridge Phil. Soc.*, 1927, **23**, 542.

[20] P. Hohenberg and W. Hohn, *Phys. Rev.*, 1964, **136**, B864.

[21] W. Kohn and L. J. Sham, *Phys. Rev.*, 1965, **140**, A1133.

[22] Turbomole; cosmologic gmbh & co.; leverkusen, germany, 2005. www.turbomole.com.

[23] J. F. Stanton, J. Gauss, J. D. Watts, P. G. Szalay, R. J. Bartlett, A. A. Auer, D. B. Bernholdt, O. Christiansen, M. E. Harding, M. Heckert, O. Heun, C. Huber, D. Jonsson, J. Juselius, W. J. Lauderdale, T. Metzroth, C. Michauk, D. P. O'Neill, D. R. Price, K. Ruud, F. Schiffmann, A. Tajti, M. E. Varner, , and J. Vázquez, Aces II, (Mainz–Austin–Budapest version), a Quantum Chemical Program Package for High-Level Calculations of Energies and Properties, containing the integral packages Molecule (J. Almlöf and P. R. Taylor), Props (P. R. Taylor) and Abacus (T. Helgaker, H. J. Aa. Jensen, P. Jørgensen, and J. Olsen). For the current version, see http://www.aces2.de.

[24] H.-J. Werner, P. J. Knowles, R. Lindh, F. R. Manby, M. Schütz, P. Celani, T. Korona, G. Rauhut, R. D. Amos, A. Bernhardsson, A. Berning, D. L. Cooper, M. J. O. Deegan, J. Dobbyn, F. Eckert, C. Hampel, G. Hetzer, A. W. Lloyd, S. J. McNicholas, W. Meyer, M. E. Mura, A. Nicklass, P. Palmieri, R. Pitzer, U. Schumann, H. Stoll, A. J. Stone, R. Tarroni, and T. Thorsteinsson, Molpro 2006.1, Cardiff, UK, 2006, www.molpro.net.

[25] J. Noga, W. Klopper, T. Helgaker, and P. Valiron, DIRCCR12-OS, a direct CCSD(T)-R12 program.

[26] M. J. Frisch, G. W. Trucks, H. B. Schlegel, G. E. Scuseria, M. A. Robb, J. R. Cheeseman, V. G. Zakrzewski, J. A. Montgomery, Jr., R. E. Stratmann, J. C. Burant, S. Dapprich, J. M. Millam, A. D. Daniels, K. N. Kudin, M. C. Strain, O. Farkas, J. Tomasi, V. Barone, M. Cossi, R. Cammi, B. Mennucci, C. Pomelli, C. Adamo, S. Clifford, J. Ochterski, G. A. Petersson, P. Y. Ayala, Q. Cui, K. Morokuma, D. K. Malick, A. D. Rabuck, K. Raghavachari, J. B. Foresman, J. Cioslowski, J. V. Ortiz, A. G. Baboul, B. B. Stefanov, G. Liu, A. Liashenko, P. Piskorz, I. Komaromi, R. Gomperts, R. L. Martin, D. J. Fox, T. Keith, M. A. Al-Laham, C. Y. Peng, A. Nanayakkara, C. Gonzalez, M. Challacombe, P. M. W. Gill, B. G. Johnson, W. Chen, M. W. Wong, J. L. Andres, M. Head-Gordon, E. S. Replogle, and J. A. Pople, GAUSSIAN 98 (Revision A.7), Gaussian, Inc., Pittsburgh PA, 1998.

[27] C. M. Smith, *Theor. Chim. Acta*, 1988, **74**, 85.

[28] T. Helgaker, *Chem. Phys. Lett.*, 1991, **182**, 503.

[29] H. Eyring and M. Polanyi, *Z. Phys. Chem. B*, 1931, **12**, 279.

[30] H. Eyring, *J. Chem. Phys.*, 1935, **3**, 107.

[31] E. P. Wigner, *J. Chem. Phys.*, 1937, **5**, 720.

[32] D. G. Truhlar and A. Kuppermann, *J. Am. Chem. Soc.*, 1971, **93**, 1840.

[33] D. G. Truhlar, A. D. Isaacson, and B. C. Garrett, *Generalized Transition State Theory*, CRC Press, Boca Raton, Florida, 1985.

[34] P. Vansteenkiste, D. van Neck, V. Van Speybroeck, and M. Waroquier, *J. Chem. Phys.*, 2006, **124**, 044314.

[35] J. I. Steinfeld, J. S. Francisco, and W. L. Hase, Prentice-Hall, 1999.

[36] R. T. Skodje and D. G. Truhlar, *J. Phys. Chem.*, 1981, **85**, 624.

[37] A. Fernández-Ramos, B. A. Ellingson, B. C. Garrett, and D. G. Truhlar, *Variational Transition State Thory with Multidimensional Tunneling*, Wiley-VCH, Hoboken, NJ, 2006.

[38] K. J. Hüttinger, *Chem. Vap. Dep.*, 1998, **4**, 151.

[39] K. J. Hüttinger, *Fibers and Composites*, Vol. 75, Taylor & Francis, 2003.

[40] A. Becker and K. J. Hüttinger, *Carbon*, 1998, **36**, 177.

[41] K. Norinaga, O. Deutschmann, and K. J. Hüttinger, *Carbon*, 2006, **44**, 1790.

[42] M. Frenklach, *Phys. Chem. Chem. Phys.*, 2002, **4**, 2028.

[43] H. Richter and J. B. Howard, *Phys. Chem. Chem. Phys.*, 2002, **4**, 2038.

[44] S. J. Klippenstein and J. A. Miller, *J. Phys. Chem. A*, 2005, **109**, 4285.

[45] K. Norinaga and O. Deutschmann, *Ind. Eng. Chem. Res.*, 2007, **46**, 3547.

[46] J. Appel, H. Bockhorn, and M. Frenklach, *Combust. Flame*, 2000, **121**, 122.

[47] N. W. Moriarty and M. Frenklach, *Proc. Combust. Inst.*, 2000, **28**, 2563.

[48] C. W. Bauschlicher, Jr. and A. Ricca, *Chem. Phys. Lett.*, 2000, **326**, 283.

[49] M. Frenklach and H. Wang, *Proc. Combust. Inst.*, 1991, **23**, 1559.

[50] V. V. Kislov, A. M. Mebel, and S. H. Lin, *J. Phys. Chem.*, 2002, **106**, 6171.

[51] K. Norinaga and O. Deutschmann Vol. 2005-09, p. 348, 2005.

[52] R. Ahlrichs, M. Bär, M. Häser, H. H., and C. Kölmel, *Chem. Phys. Lett.*, 1989, **162**, 165.

[53] M. Häser and R. Ahlrichs, *J. Comput. Chem.*, 1989, **10**, 104.

[54] O. Treutler and R. Ahlrichs, *J. Chem. Phys.*, 1995, **102**, 346.

[55] A. Schäfer, H. Horn, and R. Ahlrichs, *J. Chem. Phys.*, 1992, **97**, 2571.

[56] S. H. Vosko, L. Wilk, and M. Nusair, *Can. J. Phys.*, 1980, **59**, 1200.

[57] A. D. Becke, *Phys. Rev. A: At., Mol., Opt. Phys.*, 1988, **38**, 3098.

[58] J. P. Perdew, *Phys. Rev. B: Condens. Matter Mater. Phys.*, 1986, **33**, 8822.

[59] K. Eichkorn, O. Treutler, H. Öhm, M. Häser, and R. Ahlrichs, *Chem. Phys. Lett.*, 1995, **240**, 283.

[60] K. Eichkorn, O. Treutler, H. Öhm, M. Häser, and R. Ahlrichs, *Chem. Phys. Lett.*, 1995, **242**, 625.

[61] A. Schäfer, C. Huber, and R. Ahlrichs, *J. Chem. Phys.*, 1994, **100**, 5829.

[62] A. D. Becke, *J. Chem. Phys.*, 1993, **98**, 5648.

[63] C. Lee, W. Yang, and R. G. Parr, *Phys. Rev. B: Condens. Matter Mater. Phys.*, 1988, **37**, 785.

[64] A. D. Boese and J. M. L. Martin, *J. Chem. Phys.*, 2004, **121**, 3405.

[65] P. Deglmann, F. Furche, and R. Ahlrichs, *Chem. Phys. Lett.*, 2002, **362**, 511.

[66] P. Deglmann and F. Furche, *J. Chem. Phys.*, 2002, **117**, 9535.

[67] J. P. Perdew and Y. Wang, *Phys. Rev. B: Condens. Matter Mater. Phys.*, 1992, **45**, 13244.

[68] J. Tao, J. P. Perdew, V. N. Staroverov, and G. E. Scuseria, *Phys. Rev. Lett.*, 2003, **91**, 146401.

[69] V. N. Staroverov, G. E. Scuseria, J. P. Perdew, and J. Tao, *J. Chem. Phys.*, 2003, **119**, 12129.

[70] F. Weigend and M. Häser, *Theor. Chem. Acc.*, 1997, **97**, 331.

[71] C. Hättig and F. Weigend, *J. Chem. Phys.*, 2000, **113**, 5154.

[72] P. J. Knowles, C. Hampel, and H.-J. Werner, *J. Chem. Phys.*, 1993, **99**, 5219.

[73] P. J. Knowles, C. Hampel, and H.-J. Werner, *J. Chem. Phys.*, 2000, **112**, 3106.

[74] J. D. Watts, J. Gauss, and R. J. Bartlett, *J. Chem. Phys.*, 1993, **98**, 8718.

[75] H. Richter and J. B. Howard, *Prog. Energy Combust. Sci.*, 2000, **26**, 565.

[76] J. A. Miller, M. J. Pilling, and J. Troe, *Proc. Combust. Inst.*, 2005, **30**, 43.

[77] C. A. Taatjes, S. J. Klippenstein, N. Hansen, J. A. Miller, T. A. Cool, J. Wang, M. E. Law, and P. R. Westmoreland, *Phys. Chem. Chem. Phys.*, 2005, **7**, 806.

[78] Y. Georgievskii, J. A. Miller, and S. J. Klippenstein, *Phys. Chem. Chem. Phys.*, 2007, **9**, 4259.

[79] S. E. Wheeler, K. A. Robertson, W. D. Allen, H. F. Schaefer, III, Y. J. Bomble, and J. F. Stanton, *J. Phys. Chem. A*, 2007, **111**, 3819.

[80] L. Vereecken, J. Peeters, H. F. Bettinger, R. I. Kaiser, P. v. R. Schleyer, and H. F. Schaefer, III, *J. Am. Chem. Soc.*, 2002, **124**, 2781.

[81] J. Aguilera-Iparraguirre and W. Klopper, *J. Chem. Theor. Comp.*, 2007, **3**, 139.

[82] L. M. Ziurys, *Proc. Nat. Acad. Sci.*, 2006, **103**, 12274.

[83] K. W. Hinkle, J. J. Keady, and P. F. Bernath, *Science*, 1988, **241**, 1319.

[84] W. M. Irvine, P. Friberg, A. Hjalmarson, L. E. B. Johansson, P. Thaddeus, R. D. Brown, and P. D. Godfrey, *Bull. Am. Astron. Soc.*, 1984, **16**, 877.

[85] J. G. Mangum and A. Wootten, *Astron. Astrophys.*, 1990, **239**, 319.

[86] D. Fossé, J. Cernicharo, M. Gerin, and P. Cox, *Astrophys. J.*, 2001, **552**, 168.

[87] A. Fuente, S. García-Burillo, M. Gerin, D. Teyssier, A. Usero, J. R. Rizzo, and P. de Vicente, *Astrophys. J.*, 2006, **619**, L155.

[88] G. D. Purvis, III and R. J. Bartlett, *J. Chem. Phys.*, 1982, **76**, 1910.

[89] J. F. Stanton, J. Gauss, J. D. Watts, and R. J. Bartlett, *J. Chem. Phys.*, 1991, **949**, 4334.

[90] R. J. Bartlett, J. D. Watts, S. A. Kucharski, and J. Noga, *Chem. Phys. Lett.*, 1990, **165**, 513.

[91] J. F. Stanton, *Chem. Phys. Lett.*, 1997, **281**, 130.

[92] J. D. Watts, J. Gauss, and R. J. Bartlett, *Chem. Phys. Lett.*, 1992, **200**, 1.

[93] E. B. Jochnowitz, X. Zhang, M. R. Nimlos, M. E. Varner, J. F. Stanton, and G. B. Ellison, *J. Phys. Chem. A*, 2005, **109**, 3812.

[94] P. Botschwina, *Mol. Phys.*, 2005, **103**, 1441.

[95] P. Botschwina, *Phys. Chem. Chem. Phys.*, 2003, **5**, 3337.

[96] P. Botschwina, R. Oswald, J. Flügge, and M. Horn, *Z. Phys. Chem.*, 1995, **188**, 29.

[97] L. Vereecken, K. Pierloot, and J. Peeters, *J. Chem. Phys.*, 1998, **108**, 1068.

[98] A. D. Boese, M. Oren, O. Atasoylu, J. M. L. Martin, M. Kállay, and J. Gauss, *J. Chem. Phys.*, 2004, **120**, 4129.

[99] A. Karton, E. Rabinovich, J. M. L. Martin, and B. Ruscic, *J. Chem. Phys.*, 2006, **125**, 144108.

[100] J. Noga and P. Valiron, *Computational Chemistry: Reviews of Current Trends*, Vol. 7, World Scientific, Singapore, 2002.

[101] W. Klopper and J. Noga, *ChemPhysChem*, 2003, **4**, 32.

[102] A. L. L. East and W. D. Allen, *J. Chem. Phys.*, 1993, **99**, 4638.

[103] A. G. Császár, W. D. Allen, and H. F. Schaefer, III, *J. Chem. Phys*, 1998, **108**, 9751.

[104] Y. J. Bomble, J. F. Stanton, M. Kállay, and J. Gauss, *J. Chem. Phys.*, 2005, **123**, 054101.

[105] W. Klopper, R. Röhse, and W. Kutzelnigg, *Chem. Phys. Lett.*, 1991, **178**, 455.

[106] J. Noga, W. Klopper, and W. Kutzelnigg, *Chem. Phys. Lett.*, 1992, **199**, 497.

[107] J. Noga and W. Kutzelnigg, *J. Chem. Phys.*, 1994, **101**, 7738.

[108] J. Noga, D. Tunega, W. Klopper, and W. Kutzelnigg, *J. Chem. Phys.*, 1995, **103**, 309.

[109] W. Klopper and J. Noga, *J. Chem. Phys.*, 1995, **103**, 6127.

[110] D. E. Woon and T. H. Dunning, Jr., *J. Chem. Phys.*, 1995, **103**, 4572.

[111] J. Gauss and J. F. Stanton, *J. Mol. Struct.*, 1999, **485-486**, 43.

[112] W. Klopper, *Mol. Phys.*, 2001, **99**, 481.

[113] J. Noga and P. Valiron, *Mol. Phys.*, 2005, **103**, 2123.

[114] J. Gauss and J. F. Stanton, *Chem. Phys. Lett.*, 1997, **276**, 70.

[115] P. G. Szalay, J. Gauss, and J. F. Stanton, *Theor. Chim. Acta*, 1998, **100**, 5.

[116] W. Schneider and W. Thiel, *Chem. Phys. Lett.*, 1989, **157**, 367.

[117] R. D. Amos, I. L. Alberts, J. S. Andrews, S. M. Colwell, N. C. Handy, D. Jayatikala, P. J. Knowles, R. Kobayashi, K. E. Laidig, G. Laming, A. M. Lee, P. E. Maslen, C. W. Murray, P. Palmieri, J. E. Rice, E. D. Simandiras, A. J. Stone, M.-D. Su, , and D. J. Tozer, Cambridge Analytic Derivatives Package (CADPAC), Issue 6.5, University Chemical Laboratory, Cambridge, UK, 1998.

[118] A. D. Boese, W. Klopper, and J. M. L. Martin, *Mol. Phys.*, 2005, **103**, 863.

[119] A. D. Boese, W. Klopper, and J. M. L. Martin, *Int. J. Quantum Chem.*, 2005, **104**, 830.

[120] F. A. Hamprecht, A. J. Cohen, D. J. Tozer, and N. C. Handy, *J. Chem. Phys.*, 1998, **109**, 6264.

[121] D. J. Tozer and N. C. Handy, *J. Chem. Phys.*, 1998, **108**, 2545.

[122] T. H. Dunning, Jr., *J. Chem. Phys.*, 1971, **55**, 716.

[123] J. F. Gaw, A. Willets, W. H. Green, and N. C. Handy, *Advances in Molecular Vibration and Collision Dynamics*, JAI Press, Greenwich, CT, 1990.

[124] J. M. L. Martin, POLYAD: a vibrational perturbation theory program including arbitrary resonance matrices, Weizmann Institute of Science, Rehovot (1997).

[125] J. F. Stanton, J. Gauss, J. D. Watts, W. J. Lauderdale, and R. J. Bartlett, *Int. J. Quantum Chem. Symp.*, 1992, **26**, 879.

[126] B. Ruscic, R. E. Pinzon, M. L. Morton, G. von Laszewski, S. Bittner, S. G. Nijsure, K. A. Amin, M. Minkoff, and A. F. Wagner, *J. Phys. Chem. A.*, 2004, **108**, 9979.

[127] B. Ruscic, R. E. Pinzon, G. von Laszewski, D. Kodeboyina, A. Burcat, D. Leahy, D. Montoya, and A. F. Wagner, *J. Phys. Conf. Ser.*, 2005, **16**, 561.

[128] B. Ruscic, R. E. Pinzon, M. L. Morton, N. K. Srinivasan, M.-C. Su, J. W. Sutherland, and J. V. Michael, *J. Phys. Chem.*, 2006, **110**, 6592.

[129] A. G. Császár, P. G. Szalay, and M. L. Leininger, *Mol. Phys.*, 2002, **100**, 3879.

[130] A. G. Császár, M. L. Leininger, and P. G. Szalay, *J. Chem. Phys.*, 2003, **118**, 10631.

[131] K. L. Bak, P. Jørgensen, J. Olsen, T. Helgaker, and W. Klopper, *J. Chem. Phys.*, 2000, **112**, 9229.

[132] M. W. Chase, Jr., *NIST–JANAF thermochemical tables, 4$^{\text{th}}$ edition*, ACS and AIP, 1998.

[133] D. Feller and K. A. Peterson, *J. Chem. Phys.*, 2007, **126**, 114105.

[134] P. G. Szalay, A. Tajti, and J. F. Stanton, *Mol. Phys.*, 2005, **103**, 2159.

[135] D. D. Wagman, W. H. Evans, V. B. Parker, R. H. Schumm, I. Halow, S. M. Bailey, K. L. Churney, and R. L. Nuttall, *J. Phys. Chem. Ref. Data*, 1982, **11**, Suppl. 2.

[136] J. D. Cox and G. Pilcher, *Thermochemistry of Organic and Organometallic Compounds*, Academic Press, London, 1970.

[137] J. L. Dunham, *Phys. Rev.*, 1932, **41**, 721.

[138] G. Herzberg, *Molecular Spectra and Molecular Structure. I. Spectra of Diatomic Molecules, 2nd ed.*, Van Nostrand, Princeton, NJ, 1950.

[139] J. M. L. Martin, Private communication of a post-W4 result, see also [Ref. 99].

[140] L. J. Chyall and R. R. Squires, *Int. J. Mass Spectrom. Ion Processes*, 1995, **149–150**, 257.

[141] M. Mladenović, S. Schmatz, and P. Botschwina, *J. Chem. Phys.*, 1994, **101**, 5891.

[142] A. M. Mebel, W. M. Jackson, A. H. H. Chang, and S. H. Lin, *J. Am. Chem. Soc.*, 1998, **120**, 5751.

[143] R. I. Kaiser, A. M. Mebel, and Y. T. Lee, *J. Chem. Phys.*, 2001, **114**, 231.

[144] P. Botschwina, *Theor. Chem. Acc.*, 2000, **104**, 160.

[145] S. Yamamoto and S. Saito, *J. Chem. Phys.*, 1994, **101**, 5484.

[146] R. S. Mulliken, *J. Chem. Phys.*, 1955, **23**, 1997.

[147] J. F. Stanton, *Chem. Phys. Lett.*, 1995, **237**, 20.

[148] T. L. Nguyen, A. M. Mebel, and R. I. Kaiser, *J. Phys. Chem. A*, 2001, **105**, 3284.

[149] C. Ochsenfeld, R. I. Kaiser, Y. T. Lee, A. G. Suits, and M. Head-Gordon, *J. Chem. Phys.*, 1997, **106**, 4141.

[150] J. Takahashi and K. Yamashita, *J. Chem. Phys.*, 1996, **104**, 6613.

[151] C. D. Sherill, C. G. Brandow, W. D. Allen, and H. F. Schaefer, III, *J. Am. Chem. Soc.*, 1996, **118**, 7158.

[152] R. A. Seburg, E. V. Patterson, J. F. Stanton, and R. J. McMahon, *J. Am. Chem. Soc.*, 1997, **119**, 5847.

[153] H. Clauberg, D. W. Minsek, and P. Chen, *J. Am. Chem. Soc.*, 1992, **114**, 99.

[154] V. Jonas, M. Bohme, and G. Frenking, *J. Phys. Chem.*, 1992, **96**, 1640.

[155] C. A. Gottlieb, T. C. Killian, P. Thaddeus, P. Botschwina, J. Flügge, and M. Oswald, *J. Chem. Phys.*, 1993, **98**, 4478.

[156] M. Rubio, J. Stålring, A. Bernhardsson, R. Lindh, and B. O. Roos, *Theor. Chem. Acc.*, 2000, **105**, 15.

[157] M. S. Robinson, M. L. Polak, V. M. Bierbaum, C. H. DePuy, and W. C. Lineberger, *J. Am. Chem. Soc.*, 1995, **117**, 6766.

[158] J. F. Stanton and K. S. Byun, *Mol. Phys.*, 1999, **96**, 505.

[159] R. Walsh, *Trans. Faraday Soc.*, 1971, **67**, 2085.

[160] J. A. W. Harkless and W. A. Lester, Jr., *J. Chem. Phys.*, 2000, **113**, 2680.

[161] T. N. Le, H. Lee, A. M. Mebel, and R. I. Kaiser, *J. Phys. Chem. A*, 2001, **105**, 1847.

[162] S. Ten-no, *Chem. Phys. Lett.*, 2004, **398**, 56.

[163] D. P. Tew, W. Klopper, M. Heckert, and J. Gauss, *J. Phys. Chem. A*, 2007, **111**, 11242.

[164] T. B. Adler, G. Knizia, and H.-J. Werner, *J. Chem. Phys.*, 2007, **127**, 22110.

[165] J. M. Simmie, *Prog. Energy Combust. Sci.*, 2003, **29**, 599.

[166] H. J. Curran, P. Gaffuri, W. J. Pitz, and C. K. Westbrook, *Combust. Flame*, 1998, **114**, 149.

[167] H. J. Curran, P. Gaffuri, W. J. Pitz, and C. K. Westbrook, *Combust. Flame*, 2002, **129**, 253.

[168] C. K. Westbrook, *Proc. Combust. Inst.*, 2000, **28**, 1563.

[169] R. R. Baldwin, C. E. Dean, M. R. Honeyman, and R. W. Walker, *J. Chem. Soc. Farad. Trans.*, 1986, **1**, 89.

[170] R. R. Baldwin, P. N. Jones, and R. W. Walker, *J. Chem. Soc. Farad. Trans.*, 1988, **2**, 199.

[171] S. M. Handford-Styring and R. W. Walker, *Phys. Chem. Chem. Phys.*, 2001, **3**, 2043.

[172] M. Scott and R. W. Walker, *Combust. Flame*, 2002, **129**, 365.

[173] R. R. Baldwin and R. W. Walker, *Symp. Int. Combust. Proc.*, 1979, **17**, 525.

[174] D. L. Baulch, C. J. Cobos, R. A. Cox, C. Esser, P. Frank, T. Just, J. A. Kerr, M. J. Pilling, J. Troe, R. W. Walker, and J. Warnatz, *J. Phys. Chem. Ref. Data*, 1992, **21**, 411.

[175] R. R. Baldwin, A. R. Fuller, D. Longthorn, and R. W. Walker, *Combust. Inst. European Symp.*, 1973, **1**, 70.

[176] W. Tsang and R. F. Hampson, *J. Phys. Chem. Ref. Data*, 1986, **15**, 1087.

[177] W. Tsang, *J. Phys. Chem. Ref. Data*, 1990, **19**, 1.

[178] J. P. Orme, H. J. Curran, and J. M. Simmie, *J. Phys. Chem. A*, 2006, **110**, 114.

[179] S. F. Sousa, P. A. Fernandes, and M. J. Ramos, *J. Phys. Chem. A*, 2007, **111**, 10439.

[180] A. G. Vandeputte, M. K. Sabbe, M.-F. Reyniers, V. Van Speybroeck, M. Waroquier, and G. B. Marin, *J. Phys. Chem. A*, 2007, **111**, 11771.

[181] J. A. Montgomery, Jr., J. W. Ochterski, and G. A. Peterson, *J. Chem. Phys.*, 1994, **101**, 5900.

[182] H.-H. Carstensen, A. M. Dean, and O. Deutschmann, *Proc. Combust. Inst.*, 2007, **31**, 149.

[183] W. Klopper and J. Noga, *Explicitly Correlated Wave Functions in Chemistry and Physics*, Kluwer, Dordrecht, 2003.

[184] J. Noga, P. Valiron, and W. Klopper, *J. Chem. Phys.*, 2001, **115**, 2022.

[185] M. Heckert, M. Kállay, D. P. Tew, W. Klopper, and J. Gauss, *J. Chem. Phys.*, 2006, **125**, 044108.

[186] J. Aguilera-Iparraguirre, A. D. Boese, W. Klopper, and B. Ruscic, *Chem. Phys.*, 2008, **346**, 56.

[187] P. J. Stephens, F. J. Devlin, C. F. Chabalowski, and M. J. Frisch, *J. Phys. Chem.*, 1994, **98**, 11623.

[188] F. Weigend and R. Ahlrichs, *Phys. Chem. Chem. Phys.*, 2005, **7**, 3297.

[189] B. V. Unterreiner, M. Sierka, and R. Ahlrichs, *Phys. Chem. Chem. Phys.*, 2004, **6**, 4377.

[190] J. W. Ochterski, G. A. Peterson, and J. A. Montgomery, Jr., *J. Chem. Phys.*, 1996, **104**, 2598.

[191] C. Hampel, K. A. Peterson, and H.-J. Werner, *Chem. Phys. Lett.*, 1992, **190**, 1.

[192] M. J. O. Deegan and P. J. Knowles, *Chem. Phys. Lett.*, 1994, **227**, 321.

[193] W. Klopper and C. C. M. Samson, *J. Chem. Phys.*, 2002, **116**, 6397.

[194] G. S. Hammond, *J. Am. Chem. Soc.*, 1955, **77**, 334.

[195] Computational chemistry comparison and benchmark data base http://srdata.nist.gov/cccbdb/.

[196] A. Karton, P. R. Taylor, and J. M. L. Martin, *J. Chem. Phys.*, 2007, **127**, 064104.

[197] Y. J. Bomble, J. Vázquez, M. Kállay, C. Michauk, P. G. Szalay, A. G. Császár, J. Gauss, and J. F. Stanton, *J. Chem. Phys.*, 2006, **125**, 064108.

[198] Y.-R. Luo, *Comprehensive Handbook of Chemical Bond Energies*, CRC Press, Boca Raton, 2007.

[199] A. Fernández-Ramos, B. A. Ellingson, R. Meana-Pañeda, J. M. C. Marques, and D. G. Truhlar, *Theor. Chem. Acc.*, 2007, **118**, 813.

List of publications

1. J. Aguilera-Iparraguirre, H. J. Curran, W. Klopper, and J. M. Simmie, *Accurate benchmark calculation of the reaction barrier height for hydrogen abstraction by the hydroperoxyl radical from methane; implications for* C_nH_{2n+2} *where* n $= 2 - 4$, Chem. Phys. 346, 56-58 (2008)

2. J. Aguilera-Iparraguirre, A. Daniel Boese, W. Klopper and Branko Ruscic, *Accurate ab-initio computation of thermochemical data for* C_3H_x *(x $= 0, \dots, 4$) species*, Chem. Phys. 346, 56-58 (2008)

3. J. Aguilera-Iparraguirre and W. Klopper, *Density functional theory study of the formation of naphthalene and phenanthrene from reactions of phenyl with vinyl- and phenylacetylene*, J. Chem. Theor. Comp. 3, 139-145 (2007)

Curriculum Vitae

Name:	Jorge Aguilera Iparraguirre
Date of birth:	14.07.1978
Place of birth:	Zaragoza (Spain)
Nationality:	Spanish
Marital status:	Single
Primary school	1984-1992 Colegio de Primaria Lestonnac (Zaragoza)
Secondary school	1992-1996 I.E.S. Blecua (Zaragoza)
	08.1996 Selectividad
University	1996-2001 Study of the 'Licenciatura en ciencias quimicas' at the University of Zaragoza
	2001-2003 'Diploma de Estudios Avanzados (D.E.A.)' in the Organic Chemistry department at the University of Zaragoza, Subject: 'Application of theoretical tools to the study of hetero-Diels-Alder reactions with dithioesters'
	Since 2004 Scientific employee in the Institute of Physical Chemistry, Chair of Theoretical Chemistry, University of Karlsruhe

Acknowledgments

Janet, Robin, Ago, Nehika, Patrice and Christian. A la tropa goofy, por mantener los lazos con ZGZ en la distancia. *To Liz, Darren, Susand, Vincent, Henry, John and Miss B., for showing me that to judge how warm a country is, you have to check much more than the temperature.*

To Dave, Sheetala and Joel, with love. *"Differences of habit and language are nothing at all if our aims are identical and our hearts are open" (Albus Dumbledore).*

A la gente del Limonar, especialmente a Tere (madre no hay más que una), por seguir llamando a pesar de los gruñidos al otro lado de la línea.